Phase-modulating Spatial Light Modulators

M. J. Ranshaw

Ph.D.
University of Edinburgh
1988

Acknowledgements

It would not be possible to thank properly everyone who has helped me during the course of this work. I wish to express my special thanks to those who have been most closely involved, in particular to my supervisors, David Vass and Dick Sillitto, and the other members of staff of the Applied Optics group, for their encouragement and the benefit of their wide scientific experience. I appreciate the friendship of my fellow research students which made the hard times bearable and the good times great fun. The technical assistance of Jim Stevens, Andy Garrie, Eric Davidson, and the staffs of the Physics department mechanical workshop and of the Edinburgh Microfabrication Facility was indispensible. The integrated circuit which is the basis of much of the experimental work contained in the thesis was designed by Ian Underwood to whom I am indebted. I am grateful to the Science and Engineering Research Council for the provision of financial support during the project.

Without the encouragement of my family – my parents and my sister – I would not have been able to complete this work and it is to them that I dedicate this thesis.

Declaration

I declare that the composition of this thesis, and all of the work described within it, was carried out by me, except where otherwise acknowledged.

to Mum, Dad and Gill

Abstract

Coherent optical information processing is widely recognised as an important complement to digital electronic signal processing. Spatial Light Modulators, devices for impressing information onto optical wavefronts, are essential components of any real time optical processing system. In particular, there are great increases in processing power to be gained when the device can be used to act upon the phase, as opposed to the amplitude, of the coherent light.

This thesis describes the development of two phase modulating spatial light modulators. Both are electronically addressed, binary devices consisting of a square array of 16x16 pixels. One uses the deformable mirror principle to acheive the light modulation. In the other, the birefringence of a liquid crystal is the modulating mechanism.

The various stages in the development of the two devices are described from the initial assessment and selection of the modulation effects, through the device construction, to the evaluation of completed spatial light modulators.

The behaviour of phase modulating spatial light modulators in coherent optical systems is investigated both experimentally, using the liquid crystal device, and theoretically.

Chapter 1

Optical Information Processing and Spatial Light Modulators

1.1. The general characteristics of spatial light modulators.

A Spatial Light Modulator (or SLM) is any device which impresses information onto an optical wavefront. These devices can range in simplicity from a photographic transparency through to the many real-time programmable SLMs being currently developed and applied in information processing. In this first section it is intended to discuss SLMs in very general terms to set the scene for the examination of specific devices and applications later in the chapter.

While treating the SLM in this way three matters will be discussed: the types of modulation that the light beam can carry, the ways in which the information is input to the device, and the response characteristics of SLMs which will govern their performance in practice.

1.1.1. The Modulation of Light

Consider illuminating a black and white slide with a beam of light in a slide projector. In normal use, where the illumination is uniform, the information encoded as a transmittance pattern on the slide is impressed on the light beam and can be seen projected on a remote screen. Mathematically this process can be described as multiplying the intensity distribution of the illumination by the transmittance distribution of the slide.In general, the transmitted light has an intensity distribution which is described by this

product of the illumination and the transmittance. The slide, which is a medium that carries a distribution of information in a way that can alter the properties of transmitted light, is a *spatial light modulator.*

The action of the modulator is described by the equation

$$I_{out}(x,y) = T(x,y) \cdot I_{in}(x,y) \qquad (1.1)$$

Where $I_{out}(x,y)$ and $I_{in}(x,y)$ describe the intensity distributions across the light beam before and after modulation and $T(x,y)$ describes the transmittance.

As the modulator changes the intensity of the light it is known as an *intensity modulator.* In this example the intensity has an initial value which is positive and which is multiplied, in the modulation process, by a value between zero and one. As the intensity modulation involves multiplication only by positive values, it is referred to as a *unipolar* operation.

If the illumination is coherent light, such as that produced by a laser, the light is described by its complex amplitude instead of its intensity and information can be encoded in a different way. It can be carried in the *phase* of this amplitude as well as its modulus. To make full use of coherent light therefore requires a more versatile spatial light modulator which can alter the relative phase and amplitude of regions of the wave-front. For example, changing the phase by π radians of a real amplitude distribution changes the sign of the information and so *bipolar* operations can be carried out.

In this case the incident beam of light is described by $A(x,y)e^{i\phi(x,y)}$ where $A(x,y)$ describes its amplitude distribution and $\phi(x,y)$ describes its phase. The complex transmittance function of the SLM can be written as $T(x,y)e^{i\tau(x,y)}$ where $T(x,y)$ describes the attenuation of the amplitude of the transmitted light and $\tau(x,y)$ describes the relative phase change.

The light transmitted by the modulator is described by the product of the incident amplitude distribution and the complex transmittance as

$$A_{out}(x,y)\exp[i\phi_{out}(x,y)]$$

$$= T(x,y)e^{i\tau(x,y)} \cdot A(x,y)e^{i\phi(x,y)}$$

$$= T(x,y) \cdot A(x,y) \cdot e^{i[\tau(x,y) + \phi(x,y)]} \qquad (1.2)$$

Note that the description of the action of the modulus of the complex transmittance on the incident amplitude has the same form as the description of the intensity modulator.

The practical problems of constructing a device to independently modulate both the amplitude and phase of coherent illumination are very great. Generally an amplitude modulator as previously described could be used together with a pure phase modulator to realise any general complex transmittance distribution.

The slide considered above as an example of an SLM has a fixed transmittance but an SLM is most generally useful if the phase or amplitude modulation pattern can be altered to suit a particular purpose. From here on, the term SLM will usually be taken to refer specifically to these adaptive devices.

1.1.2. The addressing of SLMs

The manner in which the modulation pattern is input into a programmable SLM, that is the manner in which it is *addressed*, is one of its major distinguishing features. This largely determines the part that it will play in a processing system. SLMs can be either optically addressed or electronically addressed.

Optically Addressed SLMs

The basic function of an optically addressed SLM is illustrated in Fig. 1.1(a). The input to such a device is an image (the "write image") projected onto the photosensitive *detector layer* of the SLM. The function of the SLM is to alter the optical properties of the *modulator layer* so that its amplitude or phase transmittance depends at each point on the write image intensity.

The "read image" projected onto the modulator is multiplied by this transmittance and so the "output image" is a product of the read and write

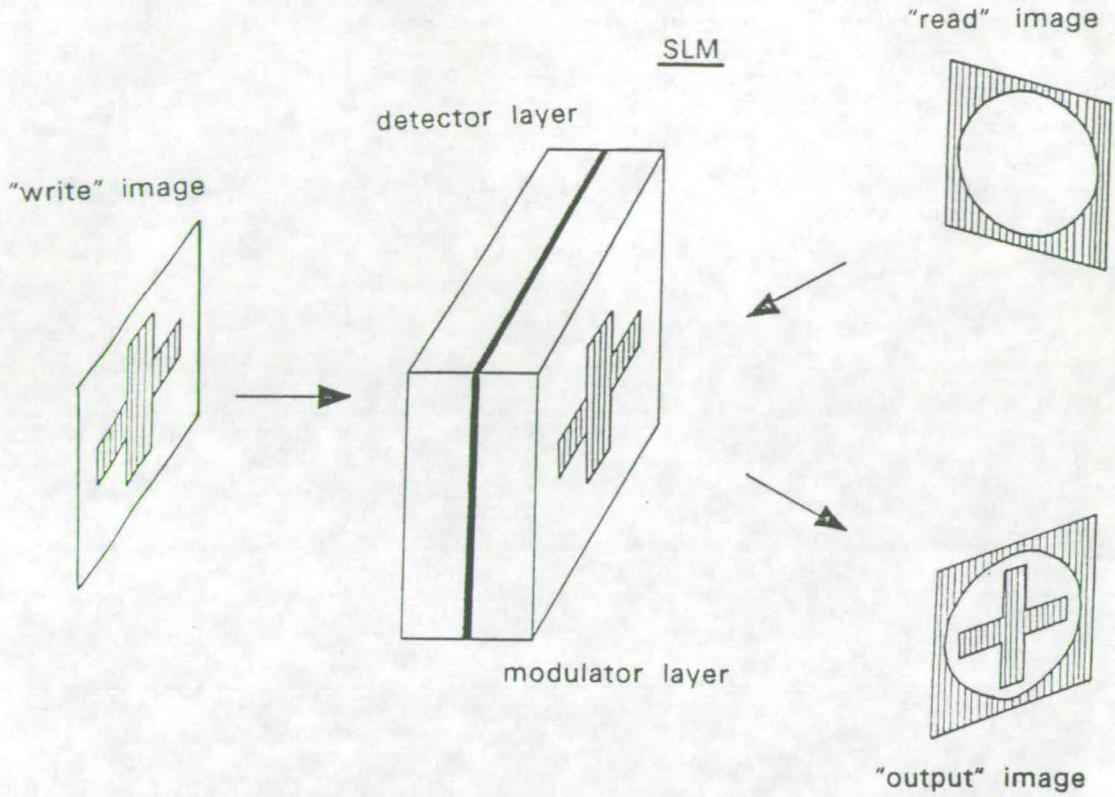

Fig 1.1 (a) An optically addressed SLM

Fig 1.1 (b) An electronically addressed SLM

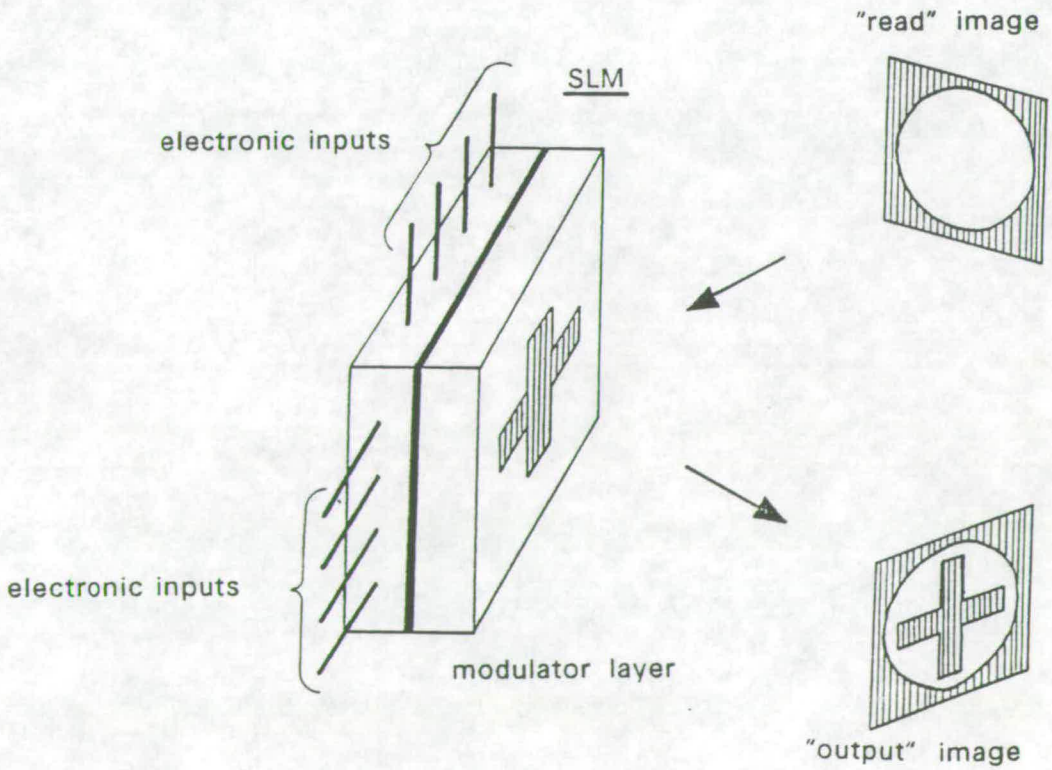

beams. This is analogous to the modulation processes described in section 1.1.1. By such mechanisms, the SLM can be used to control the interactions between more than one image in the processing system.

One special case of this deserves particular attention. If the read beam is spatially uniform then the output beam is a direct analogue of the write image and the SLM acts as an image transducer or buffer. In this particular use, the SLM operates as an interface to the processing system from the "outside world". This will be discussed further as image conversion in section 1.2.

Electronically Addressed SLMs.

Electronically addressed SLMs are used as interface devices between electronic and optical processing systems. Their function is similar to their optically addressed counterparts with an incident read image being multiplied by an effective transmittance to produce an output image. The transmittance in this case is a function of an electronically input field of information as opposed to an optical image. This is illustrated in Fig. 1.1(b). The input is usually either from an array of electrodes or from a scanning electron beam.

1.1.3. Performance Factors of SLMs.

There are a large number of characteristics of SLMs which are likely to determine their relevance for a particular application. Casasent [1977] lists the following characteristics as important.

Fig. 1.2

SLM Performance Factors.

Type of addressing	Erase mechanism
Type of modulation	Storage capability
Diffraction efficiency	Response & cycle time
Resolution & contrast	Lifetime
Sensitivity	Nondestructive readout
Linearity	Ease of fabrication
Grey scale	Complexity
Optical quality	Special features

The importance and relevance of many of these factors will be readily apparent. However several comments are worth making. High resolution and contrast are desirable features for many applications but cannot always be achieved together. The total number of resolution elements, or *pixels*, on a device may be a more relevant figure than the absolute resolution. For optically addressed SLMs, the spectral sensitivity is of as much importance as the absolute sensitivity. Some devices may be operated at low light levels by using long exposure times. A high degree of linearity may not be important. For an image transducer, a monotonic input/output characteristic is the major requirement. Some of the more powerful SLMs, such as the PEMLM and MSLM described in section 1.2, make active use of non-linear response to acheive special processing operations. The matter of optical quality is of great importance in coherent applications where sub-wavelength tolerances are often encountered to avoid spurious phase modulation. In addition, Fisher [1985] stresses the importance of such special features as cost,size, portability, simple peripherals, reliability and ease of use.

1.2. Applications of Spatial Light Modulators.

There are a great many applications of SLMs which are discussed in detail in such review papers as that by Fisher and Lee [1986]. A number of these applications are briefly described in this section. Of these, some have been selected purely for completeness and for illustrative purposes, but many are encountered later in the thesis as possible areas of research.

1.2.1. Coherent Optical Processing

The development of SLMs in the Applied Optics group at Edinburgh university is aimed primarily at this application. As suggested in the first section of the thesis, phase modulating devices are essential if the full potential of coherent systems is to be realised. The theory of phase modulators is considered in some detail in chapter two. The following is simply a brief, qualitative introduction to the subject of coherent optical processing.

The physical basis of this subject is the existence, under coherent

illumination, of a two-dimensional Fourier Transform relationship between the complex amplitude distributions in the front and back focal planes of a spherical lens.

This is illustrated in its practical context in Fig. 1.3. The laser, pinhole and collimating lens serve to produce a parallel, coherent, monochromatic beam of light . This illuminates the object O whose transmittance may of course be real or complex.

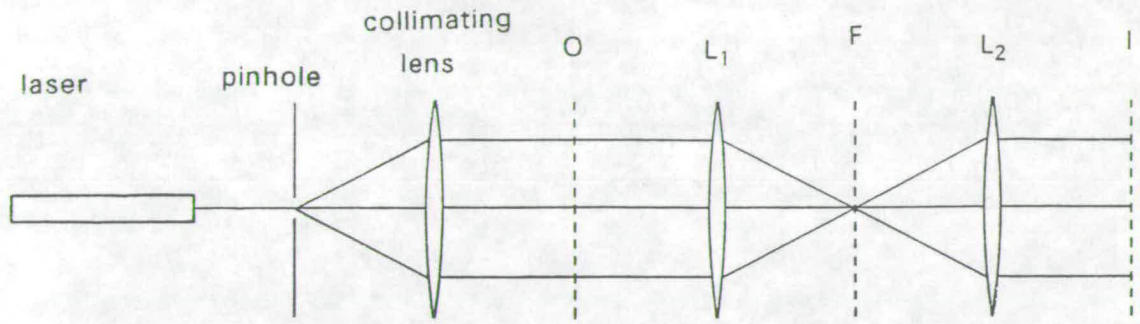

Fig 1.3 The "6-f" optical system

The planes O and F are the two focal planes of the lens L_1 and thus we form in F the two-dimensional Fourier Transform of O. (Strictly speaking we observe the squared modulus of this.) This means that we see a spatial-frequency decomposition of the information in O with the lowest frequencies at the centre of F.

The second lens L_2 performs a second Fourier Transform operation on F to yield an image I. From the properties of the Fourier Transform, we know that two forward FTs are equivalent to a simple coordinate inversion. Thus I is an

inverted, unmagnified image of O, a result which is compatible with geometrical considerations of the system.

Binary Spatial Filtering

The plane F is referred to as the Fourier plane. The inclusion of a spatial filter in the Fourier plane permits the selective alteration of the frequency spectrum of the object. This results in a processed image with certain features and traits being enhanced or suppressed.

Binary amplitude filtering is a very simple but useful technique, often realised by using a high contrast photographic transparency as the spatial filter.

The technique is illustrated by the process of enhancing the edges of the equilateral triangle shown in Fig. 1.4 (a). Fig. 1.4 (b) shows the distribution observed in the Fourier transform plane. The third photograph shows the spatial filtering process. The central part of the Fourier transform, which corresponds to the low spatial frequency information, has been removed by the spatial filter. Fig. 1.4 (d) shows the image obtained by retransforming the modified frequency spectrum containing only the high frequency edge information.

Many image modifications can be acheived using suitable binary spatial filters. These include the suppression of superfluous structure such as scan lines or half-tone dots, and the enhancement of features with certain prominent directions or sizes.

Matched Filtering

There exist more advanced techniques such as matched filtering. This technique compares the FT of a "target" object with that of a general object and registers the positions of coincidences in the output. Thus it is a pattern recognition application.

There are major practical problems in constructing the matched filter. The

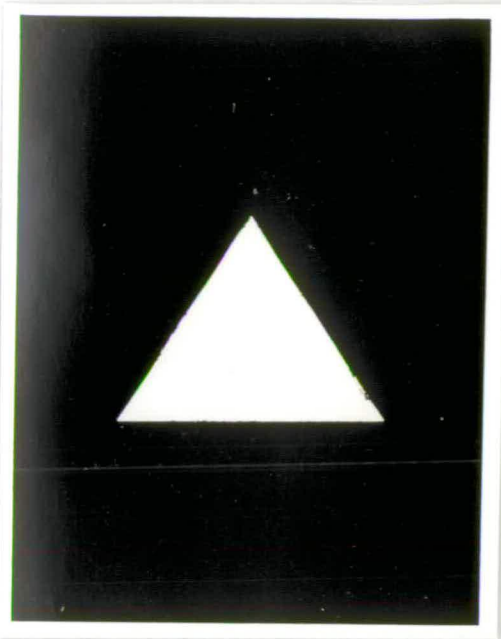

(a) Object

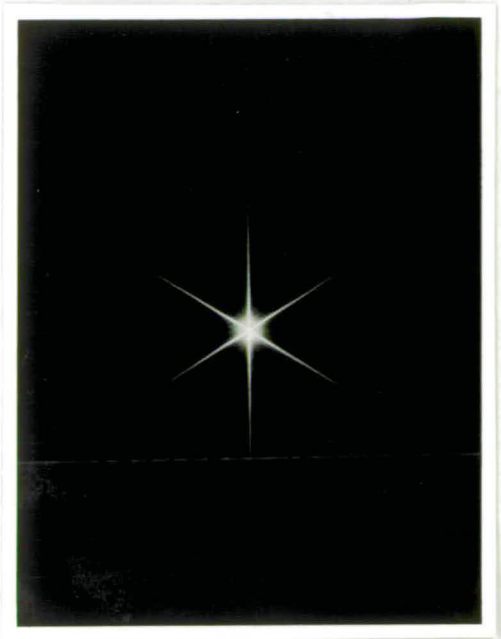

(b) Fourier transform

(c) Filtered Fourier transform

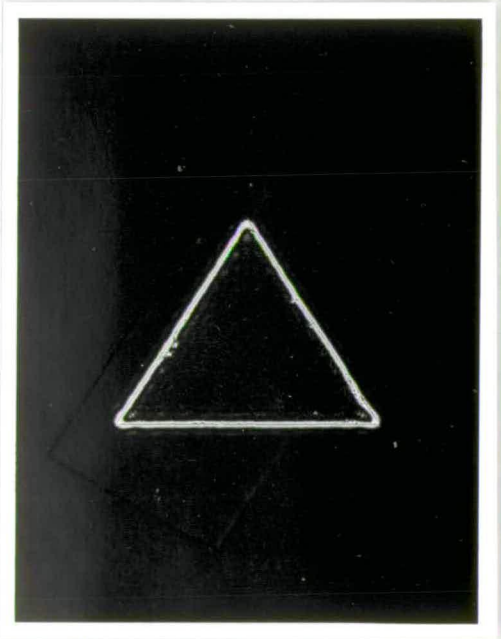

(d) Filtered image

Fig 1.4 Spatial filtering

classical matched filter is the *Vander Lugt* filter, described by Vander Lugt [1974], in which the phase and amplitude information of the "test" Fourier Transform are retained by recording the superposition of the FT and a coherent reference beam as a hologram on very high resolution film. After processing this must be precisely replaced in the Fourier plane.

When used in practice, the Fourier plane contains the product of the matched filter and the FT of the general object. In the image plane by the convolution theorem we observe the convolution of the general object with the FT of the matched filter (target object). Amongst other things this includes the cross-correlation of the two objects, with peaks of intensity at positions of coincidence

Phase only correlator filters.

Many variations of the basic Vander Lugt filter have been proposed. Because this thesis is concerned with phase modulating SLMs, one particular group of filters is of particular interest. The *phase-only filter* is formed by discarding the amplitude information in the FT of the target object. The amplitude transmittance of the filter is uniform, while its phase transmittance is the phase of the target FT. Horner and Bartelt [1985] discuss this method in detail. They show that the performance of these filters in the Fourier plane of pattern recognition systems is greatly superior to that of the conventional matched filter. This can be explained by considering the discarding of the amplitude information as a multiplication by a filter whose transmittance is the reciprocal of the amplitude. As most spatial frequency spectra are peaked in the low frequency regime, this is equivalent to applying a high pass filtering operation. As was illustrated earlier in Fig. 1.4, this does an edge-enhancement to the object. It is well known that using edge-enhanced versions of objects leads to more efficient correlation. In the correlator system described by Gibson et al. [1984], an amplitude modulating filter is in fact used to carry out this step, but using a phase only filter is a much more efficient alternative approach.

Coherent Optical Processing is a very specialised but highly powerful image processing technique. However its very fast, parallel processing potential is lost in the time lag of producing transparencies for the input and Fourier planes. Spatial Light Modulators can be used to overcome this problem.

Both optically and electronically addressed SLMs find applications in coherent processing systems. For all devices it is important to ensure a high optical quality to prevent the introduction of random phase terms.

Electronically addressed devices are used as real-time Fourier plane filters, or as a means of generating a library of test objects in the input plane of a correlator system.

Optically addressed SLMs can be used, given high enough resolution, as a real time substitute for film in the Fourier plane of a correlator. Alternatively they can be used in the input plane for incoherent-to-coherent conversion. In this application, the modulating layer of the SLM replaces the photographic transparency in the object plane. As explained before, the transmittance of this layer depends on the level of illumination of the detector layer of the device. Therefore by imaging onto this plane using the ambient light reflected from the scene or object of interest, the information is impressed directly onto the coherent illumination for processing. The main advantage of this is the bypassing of the film processing stage. With such a device, rapid processing of the input images at TV frame rates becomes possible.

1.2.2. Other applications of SLMs

The applications discussed in this section are included to illustrate some of the many subsidiary areas in which high optical quality devices can be used.

Image Conversion and Projection.

This subset of applications is conceptually simple, perhaps to the point of appearing trivial. However it has been included because it illustrates the basic functions of SLMs in all applications. Although information display is very important in its own right it is not intended as a main objective in this project. Devices developed in this project are intended for more sophisticated uses in information processing. In particular it should be clear that phase modulating devices are not directly applicable to display applications.

Wavelength conversion and intensity enhancement are two applications of optically addressed SLMs used as simple image transducers. In both applications the SLM produces a visible analogue of an image which would otherwise be invisible to the human eye; at a wavelength in the IR, UV or X-ray part of the spectrum for the former or at very low intensity for the latter. The spatially uniform read light is at a wavelength and intensity easily seen by the observer. For wavelength conversion the detector plane of the SLM must have a spectral sensitivity appropriate to the application intended. For intensity enhancement it must have a very high absolute sensitivity. In both cases good optical isolation must be ensured to prevent the read and write beams from corrupting one another.

The light from a television screen may be used as the input to an optically addressed device to acheive large screen TV projection. With suitable optics and a sufficiently intense read beam, a real magnified image of the TV picture may be obtained.

Electronically addressed SLMs are also widely used in such applications. In these cases the information to be displayed is input from a computer but the light modulation and projection stages remain basically the same. SLMs are in wide use as passive (light modulating) displays. These are generally more versatile then active (light emitting) devices, whose output light has fixed properties such as low intensity, incoherence and restricted wavelength spectrum. Passive displays have the further advantage that less power is generally required to modulate light than to produce it.

Optical logic

There is much interest in development of digital optical computing systems. These attempt to improve upon conventional electronic computers by exploiting the speed and inherent parallelism of optics. There is a bottle-neck imposed upon electronic computers by the topology of interconnecting processing elements on a two dimensional surface (that is, a silicon chip). However, as two beams of light can pass through each other without any cross talk, optical systems have great potential once the fundamental processing operations have been realised. It is interesting to observe that it is this absense of interaction that necessitates SLMs in these systems.

The basic elements of an electronic computer are logic gates. These are combined in VLSI arrays to form gate arrays. In an optical computing system, SLMs are used in a similar way to gate arrays. There are numerous ways of arranging that the output of an optical system corresponds to the result of applying a Boolean logic operation (AND, OR, NOT etc.) to the patterns on input SLMs. In other words the optical computer can perform SIMD (single-instruction multiple-data) operations between two-dimensional arrays of data. Some of the implementations of optical logic use incoherent illumination such as the shadow-casting system described by Tanida and Ichioka [1983]. Other approaches use coherent light and encode logic levels as particular spatial frequencies in the input. Weigelt [1987] encodes the input images as diffraction gratings at different angles. Logic is implemented by using specially chosen Fourier plane filters. A different approach to these logic operations is discussed in section 1.3.1 in connection with photoemitter addressed SLMs in which an extremely non-linear response allows the logical combination of input images to be determined by the SLM itself.

In the near future, it is unlikely that all-optical computing systems will be developed beyond the laboratory prototype stage. Hybrid systems using electronic processing elements with optical interconnection are however receiving a great deal of attention. In this approach, communication between chips is done optically to reduce crosstalk and increase parallelism, and processing is done conventionally using electronics. SLMs are important components of many such systems where they are used, often in conjunction

with holographic elements, to route time-modulated optical data signals to the processors. Neff [1987] considers in detail the issues involved in developing these systems.

Optical associative memory

The neural network models described by Hopfield [1982] have the property of being content-addressable memories. The networks store a number of images and will converge from an arbitrary input to the nearest stored image. They therefore have important pattern recognition applications. Other operations such as image-noise suppression and super-resolution can also be carried out. A great deal of theoretical work has been done using large electronic computers in this subject.

Central to the method are vector-matrix multiplication, thresholding and feedback operations which can all be acheived by suitable use of SLMs. Farhat et al. [1985] discuss an optical implementation of the Hopfield neural net model where the vector-matrix multiplication operation central to the model is done optically. Psaltis and Farhat [1985] discuss a number of arrangements for optical neural network systems. In particular they point out the value of using bipolar vectors and matrices in the system. This can be implemented by using incoherent light but given a phase modulator of suitable quality this could be done in coherent light also. Wallace [1987] quantifies the improvement from using a bipolar system as an increase by a factor of about two in the number of distinguishable patterns can be stored in a network of a given size.

An interesting hybrid of the matched filter and the neural network types of pattern recognition systems is described in the paper by Paek and Psaltis [1987]. In this system the FTs of all of the stored images are superimposed on a hologram, each with a carrier wave of a different spatial frequency. For an arbitrary input, the image plane consists of the cross correlation of each stored image with the input. These are spatially seperated because of their different carrier frequencies. These correlations are each imaged onto a pinhole array used as an array of point sources whose intensity depends on the strength of the correlation between the input and the stored image. These

sources illuminate a second hologram to reconstruct a superposition of stored images weighted by the strength of the correlation. This image is detected by an optically addressed SLM. The light reflected from the SLM modulator layer now forms the input to the system and the whole process is repeated. Over a number of iterations, the image converges towards the stored image most similar to the input. Although this application is not suited to phase modulators, except perhaps to produce high efficiency holographic filters as described earlier, it has been included as a final example to show the great potential of optical information processing.

1.3. Types of Spatial Light Modulator

There are a great number of modulation effects and address mechanisms which have been combined to produce working SLMs. A general overview of these is best gained from one of the many review papers such as those by Casasent [1977], Thompson [1977] and Fisher and Lee [1986]. All SLMs have their relative strengths and weaknesses, their real worth being dependent on the intended application. In this section, effects and devices with features of direct relevance to this project will be briefly considered.

The first group of devices discussed are the deformable mirror devices. These are all by definition phase modulators. A variety of liquid crystal (LC) devices are considered. It will be seen that most, if not all, liquid crystal SLMs have been used as amplitude modulators. However liquid crystals are birefringent and LC technology is highly advanced therefore development of a phase modulator may be worthwhile. Finally, a variety of other phase modulating devices using the Pockels effect or the Faraday effect are briefly examined.

1.3.1. Deformable mirror devices

<u>The Gamma-Ruticon</u>

The Ruticon family of SLMs is discussed in detail in the papers by Sheridon [1972] and Sheridon and Berkovitz [1975]. The only one of these to have

found practical use is the γ-ruticon illustrated in Fig. 1.5.

The device has a sandwich structure: a glass substrate with a transparent electrode, a 5μm thick photoconducting layer, a 5μm thick elastomer (synthetic rubber) layer, and a thin, flexible, conducting and reflecting metal layer. A dc voltage (typically 100V) is applied between the transparent electrode and the metal layer while the input image is made on the photoconductor. Photogenerated charge carriers are trapped at the elastomer-photocathode interface. The forces due to the charge distribution cause the elastomer and flexible metal layer to deform into a surface relief pattern corresponding to the input image. Read-out light reflected by the deformed mirror is phase modulated. Detailed practical and theoretical studies of the operation of the γ-ruticon have been carried out by Lakatos [1974].

All SLMs with continuous deformable modulators are characterised by a band-pass spatial frequency response. In this case, it is peaked at 10 to 100 lines per mm. For image conversion applications, a grating ruled at the peaked spatial frequency is placed on the conducting substrate. This introduces a spatial carrier frequency allowing large area features to be properly imaged. Without the grating, as the device has no pixelation, there is a response at very high spatial frequencies (up to 500 lines per mm) making it suitable for recording of holographic matched filters.

One major problem reported in ruticons is a relatively short device lifetime. The optical quality of the devices makes them more suited to non-coherent applications, though Sheridon and Berkovitz [1975] demonstrate that it is possible to fabricate devices adequate for coherent optical processing.

The Deformable Mirror Device (DMD)

The deformable mirror device (DMD) reported by Pape and Hornbeck [1983] is an important example of the class of devices with pixelated mirrors. It consists of a metalised nitrocellulose mirror approximately 120nm thick which is stretched over a silicon chip. The chip has an array of 128x128 electrodes around each of which is a raised spacer to support the mirror. A fixed voltage of typically 20V is applied to the mirror, the underlying electrodes being at the

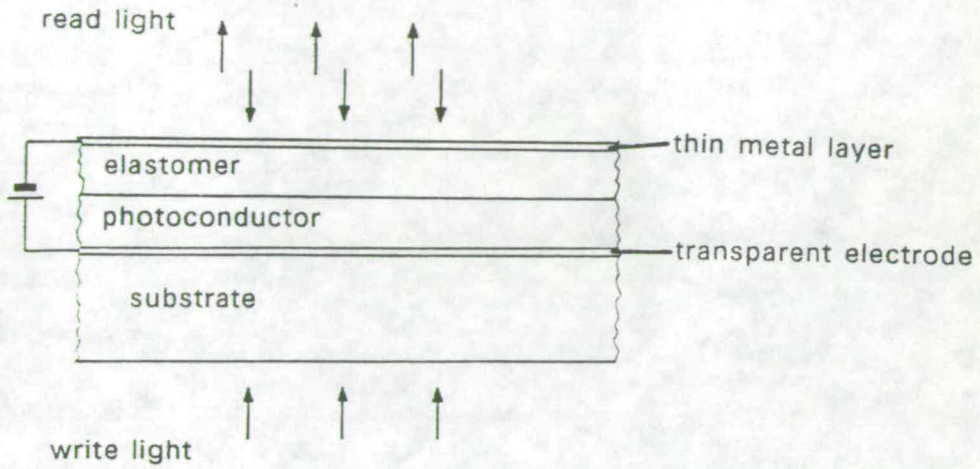

Fig 1.5 The γ-ruticon

Fig 1.6 The deformable mirror device (DMD)

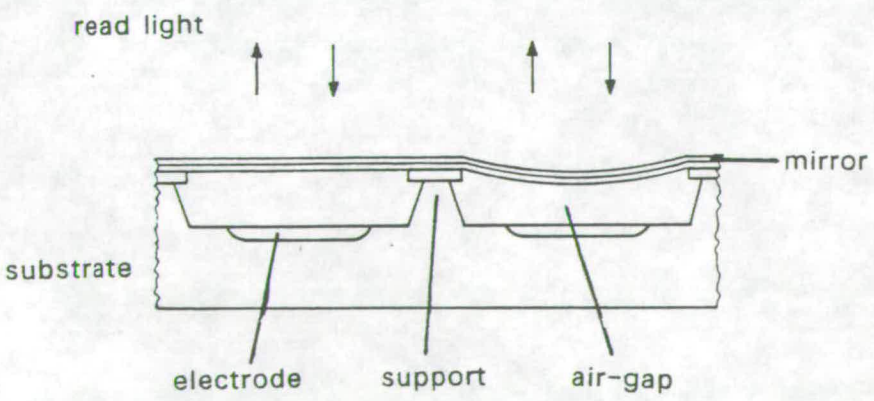

signal voltages. The voltage difference between the electrode and mirror in each pixel determines the corresponding deflection of the mirror into the air gap. The structure and operation of the DMD are illustrated in Fig. 1.6.

Pape [1984] describes an optically addressed device with the same structure. The writing is done using green light for which the mirror has a high transmission. Photogenerated charge in the silicon layer discharges the air-gap capacitor causing image-wise deformation. The device is read in the near infra-red at which wavelength the mirror is reflecting.

The Photo-Emitter Membrane Light Modulator (PEMLM)

The PEMLM under development at the Naval Research Laboratory, Washington D.C. described by Fisher et al. [1984] and [1986] deserves particular attention.

The light sensor of the device is a photocathode as illustrated in Fig. 1.7. The "electron image" this creates is amplified by a microchannel plate (MCP) and deposited onto an array of reflecting, electrically insulating membranes, formed by stretching a metalised nitrocellulose film over the end of the MCP. The electric field between the grid and the conducting window deforms the membrane elements by an amount depending on the charge they carry. These devices have resolutions of the order of 100 lines per mm.

The SLM can be used at very low light levels due both to its ability to integrate charge over long exposure times and to the amplification of the MCP.

The grid is of particular importance to the device. It serves to control the energy of the electrons reaching the deformable mirror, and collects any secondary electrons emitted by the membrane. The secondary emission process is responsible for image erasure in the device and is the key to the important non-linear response mentioned in the following paragraph. It would be inappropriate to enter into detail on this secondary emission which is described adequately in the original papers.

Many applications of optically addressed SLMs rely on a near linear response of the device to produce an output in direct correspondance to the

Fig 1.7 Photoemitter membrane light modulator (PEMLM)

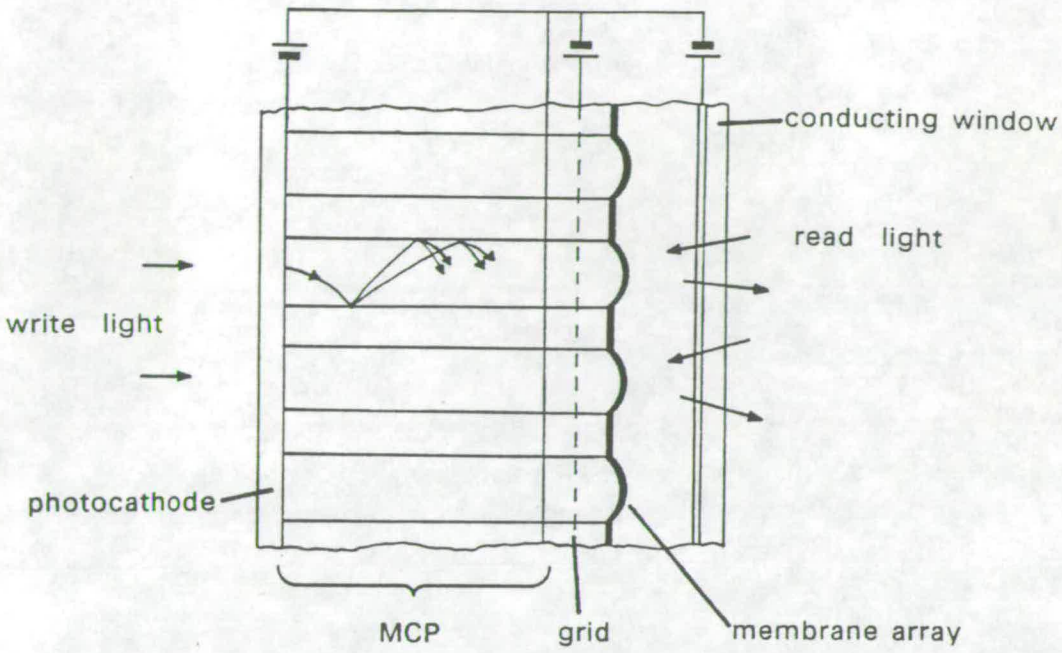

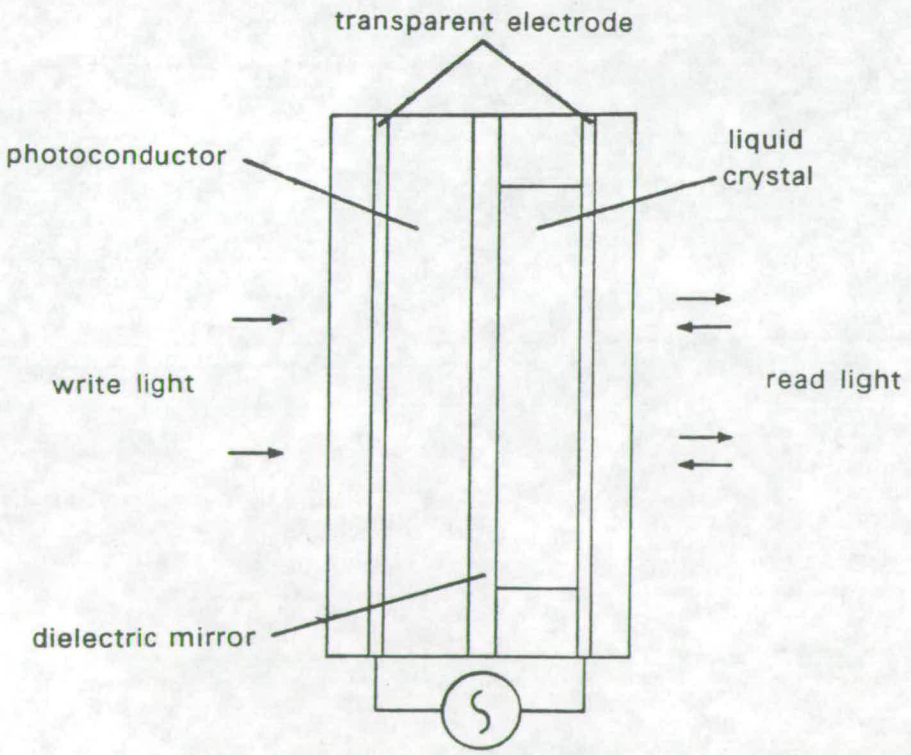

Fig 1.8 The liquid crystal light valve (LCLV)

write image. The PEMLM can be operated with a highly nonlinear response which leads to a large variety of special processing operations. These include arithmetic and boolean logic operations between images. The thresholding, hard-clipping or contrast enhancement of a single image form another class of operations.

It should be noted that until recently the device used the input electrode of the MCP as a UV sensitive photocathode. Rolsma et al. [1988] have now reported the advances made by incorporating a visible spectrum photocathode into the device.

1.3.2. Liquid crystal SLMs

Liquid crystals are particularly widely used in many light modulation applications. The modulating mechanisms are considered in detail in chapter four. They all exploit changes in orientation of the LC molecules on the application of an electric field. The molecules are characterised by large optical anisotropies so the bulk liquid crystal will absorb or change the polarisation of the transmitted light. Many SLMs have been developed using LCs. The principles of the devices are illustrated by the examples below.

The Liquid-crystal light valve

The device was developed at Hughes research laboratories by Grinberg et al. [1975]. and is optically addressed using cadmium sulphide (CdS) as the photosensitive detector. The principle of operation of the device is illustrated in Fig. 1.8. This shows the sandwich structure of layers of photoconductor, dielectric mirror and liquid crystal between a pair of transparent electrodes. An ac bias voltage is applied across the device and is divided between the CdS and LC layers in a manner depending on the level of illumination of the photoconductor. For low intensity illumination, most of the drive voltage is dropped across the high impedance CdS layer and the LC has a low transmittance. For higher intensities, the CdS impedance decreases and the LC voltage increases making the LC layer transmit more light. The LC uses the Hybrid Field Effect described in section 4.1.3.

This device is the fore-runner of a whole generation of SLMs. These include other devices from Hughes such as that described by Efron et al. [1985] in which a photodiode array replaces the photoconductor to improve speed. Latham and Owen [1986] describe a version of this device developed at the Marconi Research Centre. The paper by Baillie [1987] reports on the work done at British Aerospace on devices using Bismuth Silicon Oxide (BSO) as a photoconductor.

Electronically addressed LC SLMs

Electronically addressed SLMs using liquid crystal have often been founded upon the technologies of the LC display industry. The special demands on optical quality imposed by coherent applications have required significant improvements to these devices.

Underwood [1987] reports on the work done in Edinburgh University on guest-host liquid crystal devices addressed by silicon arrays. These devices form the background for much of the work conducted during this project. The guest host effect is described in section 4.1.3 and the operation of the silicon backplane is described in appendix two of this thesis.

An electronically addressed version of the LCLV developed by Hughes using an array of CCDs to drive the liquid crystal is described by Welkovsky et al. [1987]. The major reason cited against liquid crystal SLMs in the past has been their relatively slow speed. Nematic LCs, which are by far the most commonly used (see chapter four), have switching times of the order of several milliseconds. This compares poorly with times of microseconds for deformable mirrors and of picoseconds for electro-optic crystals. However there has been much recent interest in ferro-electric LCs which include sub-microsecond switching speeds among their useful properties. Thus although a relatively small amount of work has been done to date on electronically addressed LC SLMs, this is one of the areas in which immediate advances are to be expected.

Some attention has however been given recently to the possibility of improving low optical quality displays such as LC televisions for coherent

applications by incorporating a liquid gate or phase-compensating filter. (see Young [1986])

1.3.3. Other phase-modulating SLMs

Pockels effect SLMs

The Pockels effect, or linear longitudinal electro-optic effect has been used quite widely in SLMs, usually in optically addressed devices. Birefringence is induced in a crystal in proportion to an applied electric field. This allows modulation of the phase or amplitude of transmitted light by appropriate arrangements of polaroids. Note that as the birefringence is proportional to the field then phase differences induced are proportional to the voltage across the crystal independent of thickness. One disadvantage of using this effect is that the voltage required for a π phase change, the half-wave voltage, is typically hundreds or thousands of volts. This is the major reason why electronically addressed SLMs using electro-optic crystals are uncommon.

The PROM described by Vohl et al. [1973] is an optically addressed device which uses BSO as the electro-optic modulator. As remarked in the previous section, BSO is photoconductive so the light detection and modulation are carried out in the same component. The crystal is charged up to the half-wave voltage and then is discharged in correspondence to the input image information. The device is read using light of a wavelength to which the BSO is not photo-sensitive.

The MSLM described by Warde and Thackara [1983] is most similar to the PEMLM except that it uses the Pockels effect in an electro-optic crystal ($LiNbO_3$) in place of the deformable mirror. This device is capable of the same sort of processing operations as the PEMLM. Warde et al. [1981] give a particularly good description of the special non-linear operations performable by the MSLM (and PEMLM).

Magneto-optic SLMs

Magneto-optic effects have been used with some success in SLM

development recently in the Light mod device described by Ross et al.[1983]. The principle which this uses is light modulation by the Faraday effect. In suitable materials the plane of polarisation of transmitted light is rotated by application of a magnetic field. In the SLMs, the effect of currents in the intersections of an network of addressing lines alters the magnetisation, and optical properties of the pixel at the intersection. The devices are binary and can be configured as amplitude or phase modulators by suitable polariser arrangemements. These devices are commercially available in array sizes of up to 128x128 pixels and are frequently being used in research work.

1.4. Objectives of this project

This chapter has reviewed the present state of spatial light modulator technology. To complete this introduction to the project, it is now planned to present its objectives in the context of the other work on optical information processing being done at Edinburgh.

SLM research at Edinburgh

In the Applied Optics group of Edinburgh University, a hybrid electronic and coherent-optical processing system is under development. Work being done includes digital image processing, optical system design and spatial light modulator research.

Ths SLM development so far has concentrated on producing electronically addressed, amplitude modulating liquid crystal devices for Fourier plane filtering. The prototype nMOS addressed SLM developed by Ian Underwood has already been discussed. Modifications being made in future devices are larger arrays, other electronic drive systems and different liquid crystals.

This Project

The project will examine phase-modulating SLMs in a programme of research complementary to the binary amplitude modulator work conducted

until now. The fabrication of phase modulators will be investigated relying where possible on the silicon drive circuitry and other expertise currently in the group. Initial assessments would suggest that phase modulation by the Pockels effect on a silicon drive circuit is not feasible due to the large voltages required. The use of the Faraday effect must also be excluded on the grounds of unsuitability of the drive circuitry. Liquid crystals have been used in the SLMs for amplitude modulation and have the potential for phase modulation by birefringence. The experience in this medium and the fact that the chip was designed specifically for this modulation medium make the investigation of LCs for phase modulation an important objective. The striking appropriateness of the chip for a device based on the principle of the DMD described earlier make this another possible area of investigation. A potentially useful property of deformable mirrors is that they produce a pure phase modulation, there is no intrinsic mechanism which can modulate the amplitude of light.

The objectives of the project are listed below:

1. To investigate the possibilities of constructing deformable mirror SLMs, with an emphasis on the pixelated mirror type.

2. To investigate the possibilities of using liquid crystals in phase-modulating SLMs.

3. To compare the strengths and weaknesses of these modulation effects and assess the direction of future work in this field.

4. To demonstrate the use of phase-modulating SLMs in optical processing systems and gain a deeper understanding of the difference between them and amplitude modulators in such systems.

The following chapter of the thesis will examine coherent processing in more detail and, in particular, the way in which phase modulators are used. Chapter three will describe the work done in assessing deformable mirror structures and in producing deformable mirror SLMs. Chapter four discusses liquid crystals and demonstrates a SLM using LC birefringence as a phase modulator. In chapter five the emphasis is moved from device development back to optics. The use of phase modulating SLMs is examined experimentally

showing some processing operations unique to these devices. This chapter links up with the theories discussed in chapter two. Finally the two device technologies are compared in chapter six with regard both to their present status and ultimate performance and conclusions are reached about possible areas of future research.

Chapter 2

Pixelated Filters in Coherent Optical Processors

2.1. The Fourier Transform of a phase SLM

The subject of this thesis is phase modulating spatial light modulators with particular emphasis on their application in coherent optical processing systems. The texts by Cathey [1974] and Goodman [1968] provide a very thorough foundation in the subject of Fourier optics.

The particular strength of these systems is the existance of two-dimensional Fourier Transform (FT) relationships between certain pairs of planes in the system, which allows powerful spatial frequency filtering and image convolution operations to be performed. The basic concept is described in section 1.2.1 and illustrated in Fig. 1.3 for the standard "6-F" system, although any imaging system can be used as a coherent processor. It is relevant to briefly repeat the description of basic Fourier optics before it is enlarged upon in the remainder of the chapter.

The object O, which may be a photographic transparency or a SLM, is illuminated by a parallel monochromatic coherent beam of light. The angular spectrum of the light diffracted by the object is a two-dimensional FT of the spatial information of the object. Each component of the angular spectrum, being a plane wave, is imaged as a point in the back focal plane F of the lens L_1. The amplitude distribution in the back focal plane would thus be a FT of the amplitude distribution in the object plane.

The plane F, which is called the Fourier plane, is in general that plane

which is conjugate to the point source P. The lens L_2 performs a second FT to give the amplitude distribution in plane I. As the resultant of two successive FT operations is a simple spatial inversion, this plane I contains an image of O of magnification −1 as would be expected from applying geometrical optics to the system.

Image processing is carried out using a spatial filter in the Fourier plane to alter the magnitude and phase of the spatial frequency spectrum components. Alternatively the filtering operation can be described as the convolution of the object with the FT of the filter (or more strictly, with the Point Spread function of the imaging system).

To use a SLM in such processing systems it is therefore necessary to understand what the FT of the SLM is for a given programmed pattern. For amplitude modulating devices, the theory of this is well understood. However for phase modulating filters the theory is not as well developed. Therefore we examine this in the following section. The theory used to describe amplitude modulators will be briefly described. A comparison of amplitude and phase diffration gratings will show why the theory can not be readily applied to phase modulators. Finally some theories used to treat phase modulators will be described and some improvement of these will be made. This will allow a more deep understanding of the devices described later in the thesis.

2.1.1. The Fourier Transform of an amplitude modulator

Let us assume that the SLM is an array of pixels. Assume that the transmission of each pixel is the product of a constant transmission and a function describing the transmission distribution within the pixel. The transmission of the filter can then be described as

$$t(x,y) = [\, f(x,y) \,.\, array(x,y) \,] * pixel(x,y) \qquad (2.1)$$

where f(x,y) describes the *information* impressed on the SLM. Its value at each array point determines the transmission of the pixel at that location.

array(x,y) is an array of dirac delta functions which describe the locations of the pixels on the SLM. The array *samples* and thus band-limits the

information function.

pixel(x,y) describes the transmission distribution of a pixel. The "*" symbol denotes a convolution. Thus in the whole expression, the pixel appears at each instance of the array with a constant multiplier as determined by the local value of the information function.

The array function in many practical cases is a "bed of nails" function, or a two dimensional comb function. This means that the pixels are repeated on a regular square array.

As a final simplification, this can be rewritten in one dimension as

$$t(x) = [\, f(x) \,.\, comb(x/a) \,] * pixel(x) \qquad (2.2)$$

The FT of t(x), which is the amplitude in the Fourier plane for the SLM illuminated by a uniform plane wave of unit amplitude, is T(ω). Using the symbol $\mathcal{F}$ to denote the FT operation,

$$T(\omega) = \mathcal{F}(t(x)) = [\, F(\omega) * comb(a\omega) \,] \,.\, \mathcal{F}(pixel(x)) \qquad (2.3)$$

where $F(\omega) = \mathcal{F}(f(x))$ and assuming the FT pair $\mathcal{F}(comb(x/a)) = comb(\omega a)$.

This means that the FT spectrum of the information function F(ω) is *replicated* on an array , and is modulated by an envelope that depends on the form of the transmission of an individual pixel. In the commonly occuring case of pixels with the same transmission at every point of their active area the pixel function is rect(x/L) which has a value of 1 inside the region $-L/2 < x < L/2$ and zero elsewhere. In this case the modulating envelope is described by

$$\mathcal{F}(rect(x/L)) = sinc(\omega L) = \sin(\pi\omega L)/\pi\omega L. \qquad (2.4)$$

Thus we have a representation of the FT of a pixelated amplitude filter and this is the usual starting point for considering the filter in a processing system. It should be remembered that all of the information function f(x) is encoded within each spectrum. The replication of the spectra and the modulating envelope are only artefacts of the pixelation of the filter.

Object plane SLMs

In some applications the SLM is used to input an image to a processing system for spatial filtering. As shown above, for a pixelated filter, this gives rise to replication of the spatial frequency spectrum in the Fourier plane.

There are two approaches to spatially filtering this. The first is to use a filter which conducts the same filtering operation on each spectrum. However there are practical difficulties in constructing such a filter on a transparency and to use a SLM would be wasteful of the limited number of pixels it has. Generally this approach is pointless as all of the information is contained in each individual spectrum. If however several replicas are used then the effect of the pixelation is retained in the image and a "harder" contrast may be observed. These matters could be relevant if the image is to be processed further by an electronic computer.

In most cases the sensible approach is to block all replicas but one. This will often be the zero-order for reasons of symmetry and high intensity of this order. This single spectrum can then be filtered by conventional techniques to process the image.

Using pixelated amplitude objects in a processing system is considered experimentally in section 2.2.1.

Fourier plane SLMs

An object, which need not be pixelated, can be described in one dimension by g(x) and can be Fourier transformed in a coherent processing system. Let G(ω) represent the FT of g(x). This spectrum can be spatially filtered by a Fourier-plane SLM carrying an information function (or filter function) F(ω).

The SLM transmission can be represented by

$$T(\omega) = [\, F(\omega) \,.\, \mathrm{comb}(\omega/a) \,] * \mathrm{rect}(\omega/L) \qquad (2.5)$$

The amplitude distribution leaving the SLM in the Fourier plane can then be

described by the product of G(ω) and T(ω). In the image plane the FT of this is observed, which by the convolution theorem is

$$I(x) = g(x) * t(x)$$

$$= g(x) * [(f(x) * comb(ax)) . sinc(xL)] \qquad (2.6)$$

This can be interpreted as a replication of the convolution of the object g(x) with the FT of the filter function f(x) (and modulated by the envelope of the sinc function). Each replica of the image is thus what would be observed by filtering g(x) with an *unpixelated* filter function F(ω).

Summary

It has been shown that there is a simple way to consider amplitude modulating filters in a coherent processing system. The Fourier transform of such a filter carrying an information function f(x) is essentially a replication of the FT of f(x) on an array.

This is an introduction to considering in the following sections whether a similar approach can be used for a general phase modulating filter. In the next section we shall compare simple amplitude and phase diffraction gratings to highlight some important differences, and examine SLMs whose optical transmission is that of a modulated phase grating.

2.1.2. Diffraction gratings

The transmission of a simple one-dimensional, amplitude modulating, diffraction grating is given by

$$t_A(x) = A \cos(2\pi\omega_o x). \qquad (2.7)$$

$T_A(\omega)$, the FT of $t_A(x)$ is the even impulse pair

$$T_A(\omega) = A/2 [\delta(\omega+\omega_o) + \delta(\omega-\omega_o)]. \qquad (2.8)$$

The analogous phase grating has a complex transmittance given by

$$t_P(x) = \exp [\ iA \cos(2\pi\omega_o x)\ ]. \tag{2.9}$$

The FT of $t_P(x)$ is given by the Jacobi-Anger identity to be

$$T_P(\omega) = \sum_{n=-\infty}^{\infty} i^n\ J_n(A)\ \delta(\omega+n\omega_o) \tag{2.10}$$

as is explained below.

The Jacobi-Anger identity

The mathematics of the Bessel functions of the first kind of integral order n, $J_n(x)$, can be derived from the starting point of a generating function

$$g(x,t) = \exp[\ (x/2)\ .\ (t-1/t)\ ] = \sum_{n=-\infty}^{\infty} J_n(x)\ t^n \tag{2.11}$$

as described by Arfken [1970].

Making the substitution $t = i\ \exp[\ i\theta\ ]$ gives

$$\exp[\ ix\cos\theta\ ] = \sum_{n=-\infty}^{\infty} i^n\ J_n(x)\ \exp[\ in\theta\ ]. \tag{2.12}$$

Alternatively, substituting $t = \exp[\ i\theta\ ]$ gives

$$\exp[\ ix\sin\theta\ ] = \sum_{n=-\infty}^{\infty} J_n(x)\ \exp[\ in\theta\ ]. \tag{2.13}$$

These two results are known as the Jacobi-Anger expansion and can be interpreted as the representation of a simple harmonic phase modulation as a superposition of harmonic plane waves. Thus the phase grating has been Fourier-transformed:

$$t_P(x) = \exp[\ iA\ \cos2\pi x\ ] = \sum_{n=-\infty}^{\infty} i^n\ J_n(A)\ \exp[\ i2\pi nx\ ]. \tag{2.14}$$

Therefore

$$T_P(\omega) = \sum_{n=-\infty}^{\infty} i^n J_n(A)\ \delta(\omega+n\omega_o). \qquad (2.15)$$

While the amplitude grating has only two Fourier components, the corresponding phase grating has an infinite number of components whose amplitudes are given by the Bessel function terms.

It is interesting and reassuring to note that the general relations between the symmetry properties of a function and its FT are satisfied here. These properties are listed in full by Bracewell [1978] p14. An even function such as exp[ixcosθ] has an even FT. It is easy to show that $i^n J_n(x) = i^{-n} J_{-n}(x)$. A hermitean function (even real part and odd imaginary part) such as exp[ixsinθ] has a real asymmetrical FT. This is also easily verified. It is also interesting to note that as exp[ixcosθ] and exp[ixsinθ] are related by a shift of $\theta = \pi/2$, so their FTs are related by a multiplicative phase gradient of $\exp[in\pi/2] = i^n$. This is expected from the convolution theorem.

Modulated phase gratings in SLMs

In some SLMs such as the Ruticon described in chapter 1, the phase modulation is applied as a one-dimensional periodic deformation of a mirror surface whose local amplitude depends on the magnitude of the local input stimulus. Symbolically the surface deformation s(x,y) has the form

$$s(x,y) = f(x,y)\ .\ \cos\ 2\pi\omega_o x \qquad (2.16)$$

The function f(x,y) is the analogue of the information function of section 2.1.1. The cos term is the spatial carrier wave. The phase modulation applied to reflected light is therefore a multiplicative factor of

$$\phi(x,y) = \exp[\ i2k\ .\ f(x,y)\ .\ \cos\ 2\pi\omega_o x\ ] \qquad (2.17)$$

Where k is the wavenumber of the illumination. The similarities between this and the phase grating described earlier should be obvious and an identical approach is taken in finding the FT, as is described by Casasent [1977]. The FT is given as

$$\mathcal{F}[\ \phi(x,y)\ ] = \sum_{n=-\infty}^{\infty} i^n \ . \ \mathcal{F}[\ J_n(2k.f(x,y))\ ] * \delta(\omega+n\omega_o). \tag{2.18}$$

There is an infinite number of spectra, each of which contains the FT of a function related to the information function f(x,y).

Schlieren filtering

It is possible to low-pass filter the above FT so that only the n=+1 order is passed. The filtered FT is

$$\mathcal{F}[\ \phi(x,y)\ ]_{LP} = i\ \mathcal{F}[\ J_1(2k.f(x,y))\ ] * \delta(\omega+\omega_o) \tag{2.19}$$

If the magnitude of the phase modulation is small then the Bessel function has a linear dependance (or at least a monotonic increasing dependence) on its argument. The FT then reduces to

$$\mathcal{F}[\ \phi(x,y)\ ]_{LP} = i2k.\mathcal{F}[f(x,y)] * \delta(\omega+\omega_o) \tag{2.20}$$

The first order is the FT of the information function for small phase modulations. This can be retransformed to give an image of f(x,y) from the phase modulation for display purposes. Alternatively it can be spatially filtered for image processing. In fact as all of the Bessel functions except J_0 increase with their argument for its low values then only the zero order need be blocked for image display. This clearly improves image intensity and sharpness. As a corollary, a contrast-reversed image results when only the zero-order spectrum is passed.

Historically, the term Schlieren filtering was used only to refer to the blocking of the negative and zero-order components of the frequency spectrum. It is now common for the term to be used to refer to any of the possible filtering operations that result in a visible image from a phase modulation.

2.1.3. General pixelated phase-modulating SLMs

The work carried out at the US Naval research labs to characterise the optics of the PEMLM is also useful for describing a general pixelated phase-modulating SLM. The approaches of Fisher et al. [1984] and Ling et al. [1985] will be described and the theory of the first approach will be extended. This involves writing the deformation as a Fourier superposition of cosinusiodal deformations. The phase modulation is thus an infinite product of simple phase gratings of the form described earlier. The propagation of light through the system can be described in terms of this but is in general unwieldy. Firstly an approach which gives an elegant description of the transfer characteristics of an SLM in a Schlieren imaging system is examined.

Convolving a phase pixel with an array

Recall that the general approach to treating amplitude SLMs can be summarised symbolically as

$$t(x) = [\, f(x) \,.\, comb(x/a) \,] * pixel(x/L) \tag{2.21}$$

$$T(\omega) = [\, F(\omega) * comb(a\omega) \,] \,.\, envelope(\omega L) \tag{2.22}$$

where $\mathcal{F}(t(x)) = T(\omega)$ and $\mathcal{F}(f(x)) = F(\omega)$. This is a useful representation for an arbitrary real pixel function which is multiplied by a constant determined by the sampled value of the information function f(x). In general it is not possible to use the analogous description of an array of phase modulating pixels of an arbitrary "shape", whose local magnitude is determined by a sampled information function. The representation

$$t(x) = [\, e^{if(x)} \,.\, comb(x/a) \,] * pixel(x/L) \tag{2.23}$$

can only be validly used to describe an array where the phase modulation is uniform across each pixel and then pixel(x/L) = rect(x/L).

However the general representation of an array is

$$t(x) = \exp[\, i[\, f(x) \,.\, \mathrm{comb}(x/a)\,] * \mathrm{pixel}(x/L)\,] \qquad (2.24)$$

where the convolution is within the exponential and so the analogous approach to Fourier transformation is not possible.

Ling et al. [1985] were able to use this approach by considering the SLM pattern to be composed of a collection of *domains* of pixels with the same modulation depth within each domain.

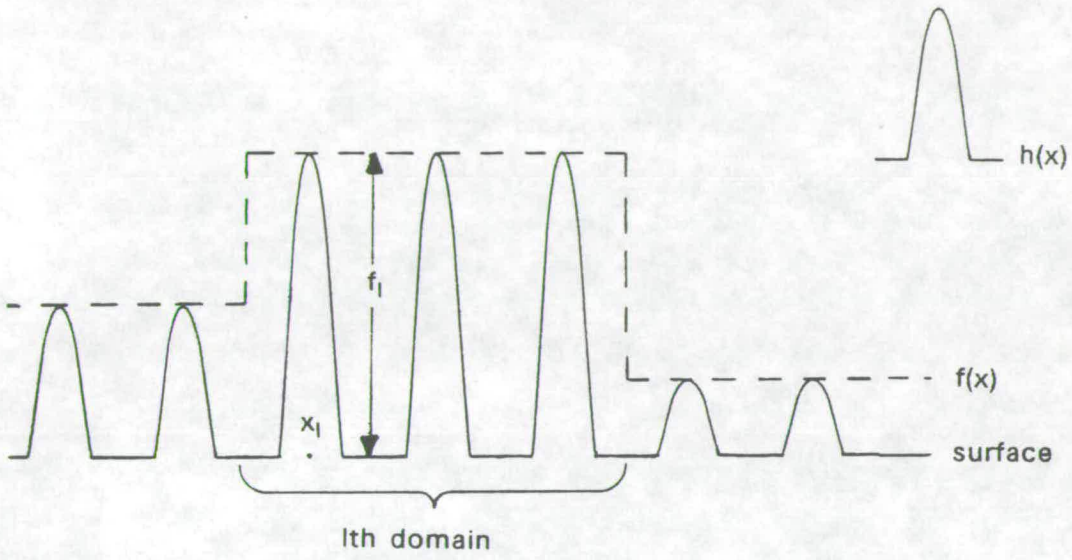

Fig 2.1 Deformed mirror array

Fig. 2.1 is a depiction of a one-dimensional deformed mirror array. The array is partitioned into L domains each of which contain N_l identical pixels. The phase modulation, $\phi(x)$ of the reflected light can be represented as

$$\phi(x) = \sum_{l=1}^{L} \phi_l(x) \text{ where}$$

$$\phi_l(x) = \mathrm{rect}[(x - x_l - N_l p/2)/N_l p] \,.\, \{[\mathrm{rect}(x/p).\exp[i2k.f_l.h(x)]] * [1/p \,.\, \mathrm{comb}(x/p)]\} \qquad (2.25)$$

This should be thought of in the following way: The $\text{rect}(x/p).\exp[i2k.f_l.h(x)]$ term describes a single pixel. It has magnitude of one for $-p/2 < x < p/2$ and magnitude of zero elsewhere. Within the active part of the array, described by $h(x)$, the phase is modulated by an amount $f_l h(x)$. This pixel is repeated on an infinite array. The first rect term selects the membrane elements associated with the lth domain, multiplying all the others by zero.

Neglecting constant phase terms, the amplitude distribution in the Fourier plane due to this lth domain is thus

$$\Phi_l(\omega) = \mathcal{F}(\phi_l(x)) = [\exp[-i2\pi\omega(x_l+N_lp/2)]. N_lp \text{ sinc } (N_lp\omega)] * [\mathcal{F}(\text{rect}(x/P) \exp[i2k.f_l.h(x)]) . \text{comb}(p\omega)] \tag{2.26}$$

The $\text{comb}(p\omega)$ factor gives a replicated spatial frequency spectrum, the nth order of which can be written as

$$\Phi(\omega)_{ln} = S_n(f_l) [\exp[-i2\pi\omega(x_l+N_lp/2)] . N_lp \text{ sinc}(N_lp\omega)] * \delta(\omega-n/p) \tag{2.27}$$

$$\text{where } S_n(f_l) = 1/p \int_{-p/2}^{+p/2} \exp[i2k.f_l h(x) - 2n\pi x/p] \, dx \tag{2.28}$$

is the FT factor of equation (2.26) evaluated at $\omega = n/p$.

If the nth component only is allowed to pass beyond the Fourier plane then the amplitude distribution in the image plane is given by the FT of $\Phi(\omega)_{ln}$

$$\sum_{l=1}^{L} q_l(x) = \sum_{l=1}^{L} S_n(f_l) \text{ rect}[(x-x_l-N_lp/2)/N_lp] \tag{2.29}$$

and the intensity distribution by the squared modulus of this:

$$I(x) = \sum_{l=1}^{L} \text{rect}[(x-x_l-N_lp/2)/N_lp] \; |S_n(f_l)|^2 \tag{2.30}$$

There are no cross terms because the L rect functions do not spatially overlap. The intensity in the lth domain of the image due to passing the nth Fourier spectrum is $|S_n(f_l)|^2$. This is referred to by Ling et al. as the *1-d sensitometry transfer function* and they use it to calculate the transfer characteristic of SLMs with commonly found pixel functions for any diffraction

order.

This approach appears to be quite successful in describing the transfer characteristic of an imaging system using a phase modulating SLM as the input. However this theory gives little consideration to the spatial information contained *within* each order of the Fourier spectrum. The theory was developed in terms of a device not primarily intended for Fourier plane filtering of the information function.

It is possible to describe the SLM in such a way as to show clearly how the Fourier components of the information function are distributed in the Fourier plane. The basis of this theory is the approach of Fisher et al. [1984] which will now be described. This will then be developed to describe the propagation of the components of the information function.

Superposition of phase gratings

The approach of Fisher et al. [1984] is described below. A similar construction is used as before to describe the surface deformation and phase modulation. Namely the array is partitioned into domains of constant peak-deformation and the phase modulation by the whole array is written as

$$\phi(x) = \sum_{l=1}^{L} \phi_l(x) = \sum_{l=1}^{L} \text{rect}[(x-x_l-N_l p/2)/N_l p] \; . \; \exp[\, i2k.f_l . \sum_{m=1}^{Nl} h(x-mp-x_l) \,] \qquad (2.31)$$

The exponential term describes the modulation imposed by the lth domain which has N_l pixels. Because of the rect function, the sum over m can be extended to infinity. The sum is then an infinite periodic function and can be rewritten as a Fourier series.

$$\phi(x) = \sum_{l=1}^{L} \text{rect}[(x-x_l-N_l p/2)/N_l p] \exp[\, iC_{0l}/2 \,] \; . \; \exp[\, i \sum_{m=1}^{\infty} C_{ml} \text{cos} m\omega_o x \,] \qquad (2.32)$$

where $\omega_o = 2\pi/p$ and

$$C_{ml} = 4k.f_l \; H(m\omega_o)/p \qquad (2.33)$$

and $H(m\omega_o)$ is the FT of the pixel function h(x) evaluated at $\omega = m\omega_o$. The

final term of this expression can be rewritten as a product of exponentials:

$$\exp\left[\sum_{m=1}^{\infty} iC_{ml}\cos m\omega_o x\right] = \prod_{m=1}^{\infty} \exp\left[iC_{ml}\cos m\omega_o x\right] \tag{2.34}$$

Each of these terms can be replaced using the Jacobi-Anger identity as in section 2.1.2:

$$\exp\left[iC_{ml}\cos m\omega_o x\right] = \sum_{n=-\infty}^{\infty} i^n J_n(C_{ml}) \exp[imn\omega_o x] \tag{2.35}$$

The result of combining the infinity of such terms representing the contribution from each component of the deformation is in general very complicated.

The amplitude distribution in the Fourier plane is the convolution of the FT of the $\mathrm{rect}[(x-x_l-N_lp/2)/N_lp]$ term with the delta functions $\delta(\omega+n\omega_o)$. All the harmonics of ω_o are present, as for a simple phase grating, but their relative intensity is determined by the cross terms in the infinite product. Fisher et al. make the approximation that for $m>1$, $J_0(C_{ml})=1$ and $J_{n>0}(C_{ml})=0$ resulting in an amplitude distribution in the Fourier plane of

$$\Phi_l(\omega) = \exp[iC_{0l}]\ [\ J_0(C_{1l})\delta(\omega) + J_1(C_{1l})(\delta(\omega+\omega_o) + \delta(\omega-\omega_o))\ ]\ * \mathcal{F}[\mathrm{rect}[(x-x_l-N_lp/2)/N_lp]] \tag{2.36}$$

This can be filtered by Schlieren optics as described before. What Fisher does not say is that by making these approximations in the coefficients, we are reducing the function describing the array to a modulated cosine function as described previously. The tacit implication of this is that for small phase modulations, the array can be validly represented by a superposition of cosinusoidal gratings whose *lowest* spatial period corresponds to the inter-pixel spacing.

Without doing this, there is still no explicit description of the correspondence of the features in each spectrum with the Fourier components of the information function. This is because the frequencies of the deformed array are harmonics of the spatial frequency associated with the inter-pixel spacing . This of course is the highest frequency contained in the band-limited information function. The advantage of writing the information in terms of

low-frequency phase gratings will be illustrated for a particular case in the following section.

Before doing this, it is interesting to consider briefly the effect of neglecting the high order terms. To do so, consider the case of a "square" phase grating with a depth of modulation of A radians. The grating "rulings" alternately advance and retard the phase of transmitted light by A/2 radians. By using the Fourier analysis of a square wave, the grating can be described by the function $e^{i\phi(x)}$ where

$$\phi(x) = 2A/\pi(\cos(x) - \cos(3x)/3 + \cos(5x)/5 - \dots) \tag{2.37}$$

The FT of this is

$$\mathcal{F}(\exp[i\phi(x)])$$

$$= \mathcal{F}(\exp[i2A/\pi \cos(x)]) * \mathcal{F}(\exp[i2A/3\pi \cos(3x)]) * \mathcal{F}(\exp[i2A/5\pi \cos(5x)]) \dots$$

$$= \sum_{n=-\infty}^{\infty} i^n J_n(2A/\pi)\delta(n\omega) * \sum_{n=-\infty}^{\infty} i^n J_n(2A/3\pi)\delta(3n\omega) * \sum_{n=-\infty}^{\infty} i^n J_n(2A/5\pi)\delta(5n\omega) \dots \tag{2.38}$$

A complete consideration of the terms in this multiple convolution is not necessary at the moment. The approach which was introduced above was to discard all except the first series. In this case,

$$\mathcal{F}(\exp[i\phi]) \simeq \sum_{n=-\infty}^{\infty} i^n J_n(2A/\pi)\ \delta(n\omega) \tag{2.39}$$

The intensity in the first order spectrum is greatest at the first maximum of J_1 which occurs where $2A/\pi = 1.84$. This means that $A = 0.92\ \pi$ radians. This is close to the value of $A = \pi$ radians that might be expected when all terms are considered in the multiple convolution.

2.1.4. A new representation of a phase filter

Consider a phase modulating SLM in one dimension. In any real device there is an inactive area between all the pixels whose reflectivity can be assigned a fixed phase value and unit amplitude. In the active part of the

pixel, the phase is variable. This need not be a constant over all of a given pixel but the form of the variation should be the same for each pixel.

If each active pixel were to carry the same phase value then the reflected light would be modulated by a multiplicative factor of $e^{if(x)}$ where f(x) is as illustrated in Fig. 2.2.

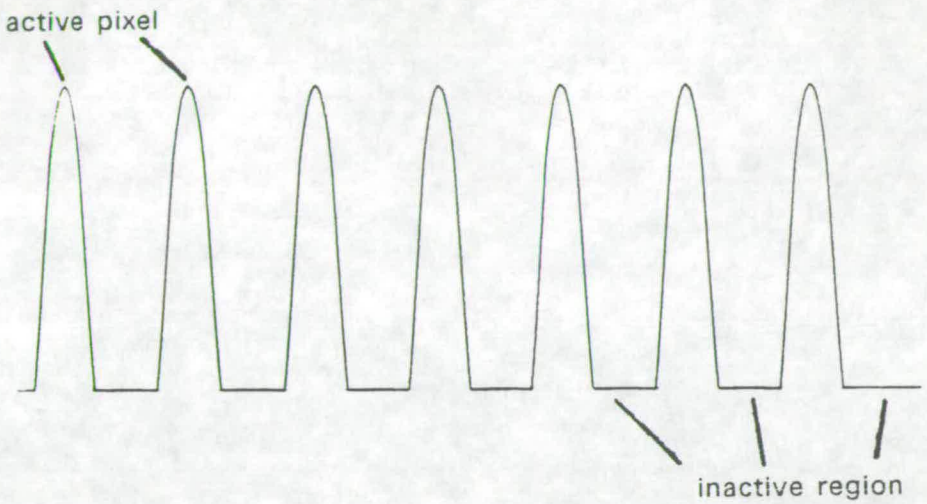

Fig 2.2 Deformed mirror array

Taking the approach of Fisher et el. as described in the last section, f(x) would be decomposed into its spatial frequency harmonics. However at the end of Fisher's argument all but the lowest frequency components are neglected. This discards the information about the "shape" of the pixel but preserves the spatial information in the filtered image.

That is, the information function would be approximated by

$f(x) \simeq A \cos(2\pi\omega_o x)$

and the first order of the Fourier plane would be

$$i\, J_1(A)\, [\, \delta(\omega+\omega_o) + \delta(\omega-\omega_o)\,]. \tag{2.40}$$

The amplitude in the image plane is described by

$$i\, J_1(A)\, .\, \cos(2\pi\omega_o x) \tag{2.41}$$

and the spatial information is retained in the local value of A.

If alternate pixels of the object were switched to a different phase value then there would be additional terms in the Fourier plane due to the half spatial frequency component. This approach does not explicitly show the presence of such terms in the Fourier plane though they presumably be demonstrated by a numerical evaluation of the product of appropriate sinc functions convolved with the delta function array. See the full expression for the FT in equation (2.36).

It is proposed that the information function should be rewritten as a sum of components of frequency less than the sampling frequency. Therefore the presence of these components of the information can be explicitly shown in the Fourier plane.

The case of the half-frequency phase grating is examined below in detail to illustrate this approach.

The simplest way to represent the grating is by the function f(x)

$$f(x) = A/2\, \cos\, (2\pi x\omega_o) + B/2\, \cos\, (2\pi x\omega_o/2) \tag{2.42}$$

which is illustrated in Fig. 2.3. The function can be sampled on a regular array to give the correct value of the phase for active "ON", active "OFF" and inactive regions. The relative value of these phases can be set by choosing the constants A and B.

The phase modulation is represented by

$$e^{if(x)} = \exp[i/2\, (A\cos x\omega_o + B\cos x\omega_o/2)]$$

$$= \exp[iA/2\, \cos(x\omega_o)]\, .\, \exp[iB/2\, \cos(x\omega_o/2)] \tag{2.43}$$

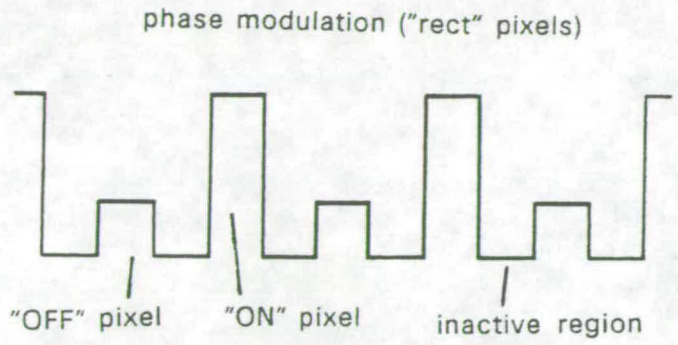

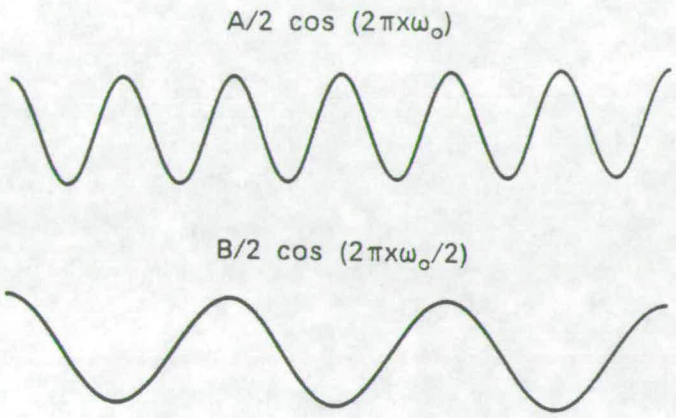

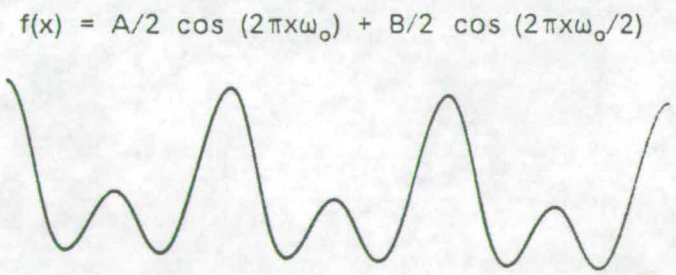

Fig 2.3 "Half-frequency" phase grating

$$\mathcal{F}(e^{if(x)}) = \mathcal{F}(\exp[iA/2\ \cos x\omega_o]) * \mathcal{F}(\exp[iB/2\ \cos x\omega_o/2])$$

$$= \left(\sum_{n=-\infty}^{\infty} i^n J_n(A/2)\,\delta(\omega+n\omega_o)\right) * \left(\sum_{m=-\infty}^{\infty} i^m J_m(B/2)\,\delta(\omega+m\omega_o/2)\right)$$

$$= \sum_{s=-\infty}^{\infty} c_{s/2}\ \delta(\omega-s\omega_o/2) \qquad (2.44)$$

where

$$c_{s/2} = \sum_{n=-\infty}^{\infty} J_n(A/2)J_{s-2n}(B/2)\ i^n\ i^{s-2n} \qquad (2.45)$$

Thus any spectrum of the FT now can be seen to contain a $\omega_o/2$ component in addition to the ω_o component. This means that each spectrum contains the spatial frequency components of the information function f(x). The relative amplitude of these components is determined by the constants $c_{s/2}$. It is clear that this method can be easily extended to more complicated patterns to describe their correspondance to the Fourier spectra.

For this particular case let us examine the $c_{s/2}$ terms in more detail. It can be shown that

$$c_0 = J_0(A/2)J_0(B/2) + 2\sum_{n=1}^{\infty} (-i)^n\ J_n(A/2)J_{2n}(B/2) \qquad (2.46a)$$

$$c_{\pm 1/2} = i\ J_0(A/2)J_1(B/2) + i\sum_{n=1}^{\infty} i^n\ J_n(A/2)[J_{2n-1}(B/2) + J_{2n+1}(B/2)] \qquad (2.46b)$$

$$c_{\pm 1} = i\ J_1(A/2)J_0(B/2) + i\sum_{n=1}^{\infty} (-i)^n\ J_{2n}(B/2)[J_{n+1}(A/2) + J_{n-1}(A/2)] \qquad (2.46c)$$

$$c_{\pm 3/2} = i^2\ J_1(A/2)J_1(B/2) + \sum_{n=1}^{\infty} (-i)^n\ [J_{n+1}(A/2)J_{2n-1}(B/2) + J_{n-1}(A/2)J_{2n+1}(B/2) \qquad (2.46d)$$

and that for A=0 or B=0 these reduce to the expected terms for a simple grating of the appropriate frequency ω_o or $\omega_o/2$.

In the case of A and B being small then the approximations

$$J_0(A/2) = 1 - (A/4)^2 + O(A^4)$$

$$J_1(A/2) = A/4 - 1/2(A/4)^3 + O(A^5)$$

and $J_n(A/2) = O(A^n)$

hold with similar expressions for B. The coefficients can then be approximated by their leading terms to

$$c_0 = 1 \tag{2.47a}$$

$$c_{\pm 1/2} = iB/4 \tag{2.47b}$$

$$c_{\pm 1} = iA/4 \tag{2.47c}$$

$$c_{\pm 3/2} = -AB/16 \tag{2.47d}$$

Thus passing only the $c_{\pm 1/2}$ and $c_{\pm 1}$ terms of the FT leaves

$$\mathcal{F}(I(x)) = i/4\ [B\delta(\omega+\omega_o/2) + B\delta(\omega-\omega_o/2) + A\delta(\omega+\omega_o) + A\delta(\omega-\omega_o)] \tag{2.48}$$

and gives an image of

$$I(x) = i/2[\ B\cos(2\pi x\omega_o/2) + A\cos(2\pi x\omega_o)\ ] \tag{2.49}$$

$$= if(x) \tag{2.50}$$

where f(x) is the information function.

2.2. Experiments with pixelated objects

In the early parts of this chapter it was explained that a pixelated object has a replicated Fourier spectrum. All of the information about the pattern of pixel states is contained in any single spectrum and an image can be formed by allowing only one of these to propagate to the image plane. This process is called desampling as it removes all information relating to the pixelation of the object. The image is not pixelated. In addition it was noted that for pixelated phase filters, it is necessary to remove the zero-order spectrum to obtain any visible image. For spatial filtering of phase or amplitude objects, it

is often necessary to desample to avoid having to repeat the filtering on each spectrum.

In this section some of these topics will be examined experimentally using 16x16 arrays to simulate the behaviour of the SLMs described in later chapters. This will give us a realistic expectation of the quality of images to be obtained from arrays of this size. Optical systems developed for this work will be used in assessment of the SLMs but can be more precisely aligned using the simulated SLMs.

2.2.1. Amplitude objects – the effect of desampling

Fig. 2.4 (a) shows the object used in this first experiment. It is made on high contrast photographic film and simulates a 16x16 amplitude modulating SLM with a diagonal band of pixels switched off. Fig 2.4 (b) shows the Fourier transform of this object as observed on the 6-f system described in the previous section and illustrated in Fig. 1.3. As expected the spectrum is replicated. Fig. 2.4 (c) shows the Fourier transform of an unpixelated analogue of the same pattern. Comparison of these shows that the individual spectra from the pixelated object are similar to the FT of the unpixelated object except that they are of limited spatial extent due to the band-limiting of the pixelation process.

Some spatial filtering operations can now be performed on these objects to show the effect of desampling in the Fourier plane. Fig. 2.4 (d) shows the image formed from passing a single spectrum. Fig. 2.4 (e) shows the additional effect of removing the central part of this spectrum to enhance the edges. The double edge is an artefact present in any image edge-enhanced by binary high-pass filtering. (See Fig 1.4). The effect of slightly increasing the size of the desampling aperture on the image is very interesting. If it is increased to allow through the high frequency components of the neighbouring orders of the Fourier transform then the result in as shown in Fig 2.4 (f). The sharpness of the edges is improved and the effects of pixelation have again become evident particularly in the diagonal stripe. The line through the centre of the stripe joins the positions of the off pixels. This should be compared to Fig. 2.4 (h) in which the slightly different object shown in Fig. 2.4 (g) has been used. The stripe of off pixels is narrower each one being connected to its neighbour

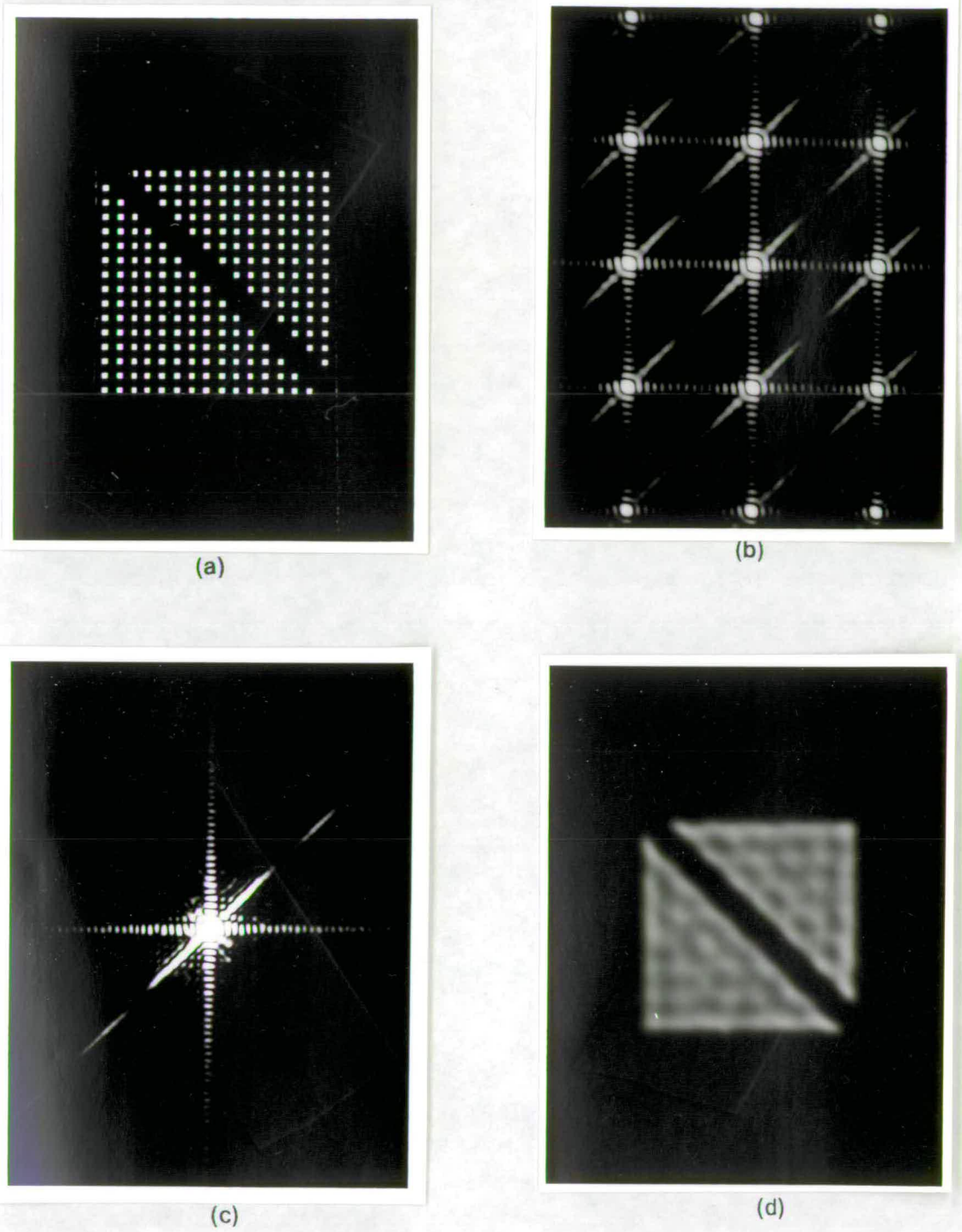

Fig 2.4 Experiments on pixelated amplitude objects

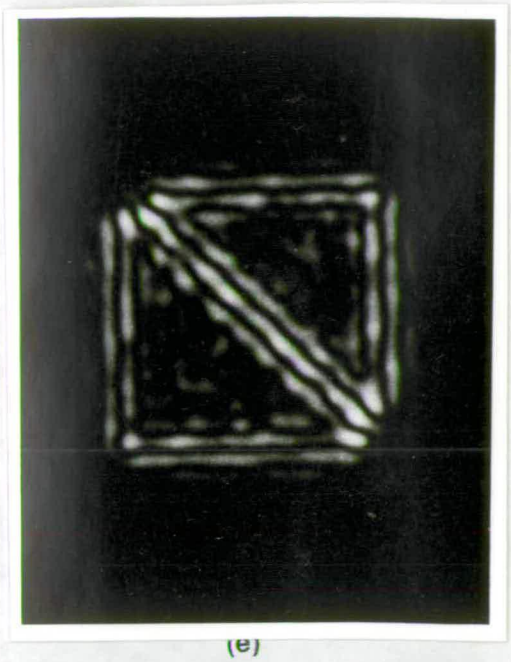

(e)

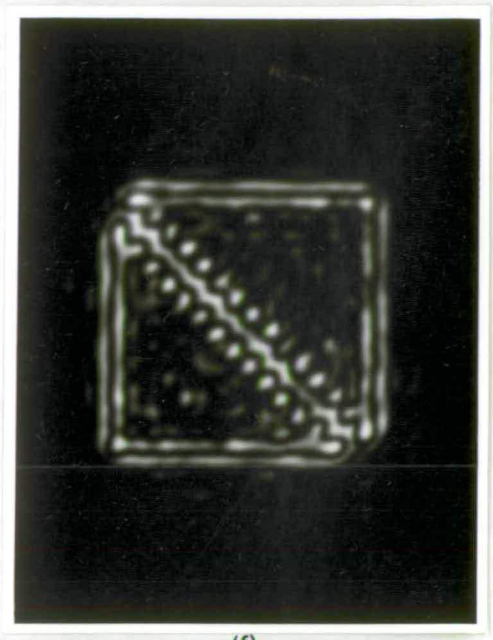

(f)

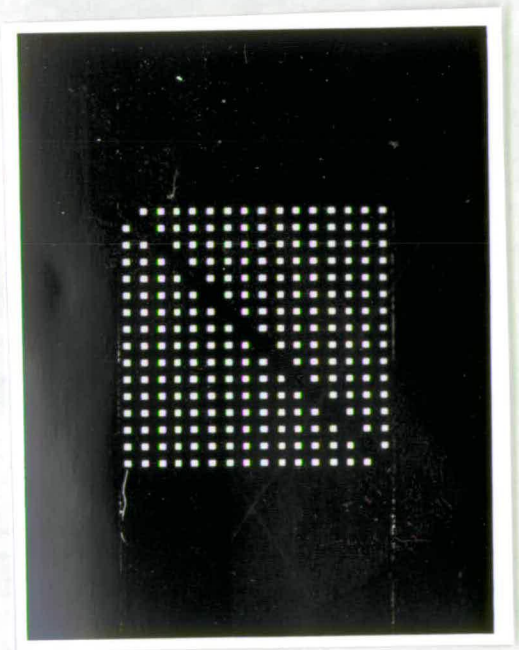

(g)

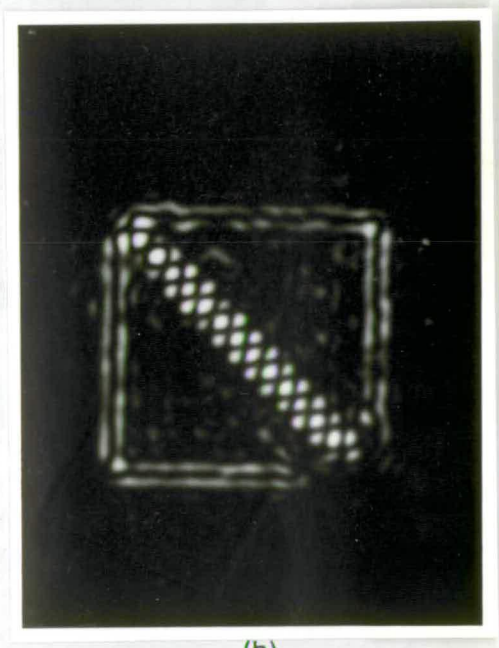

(h)

Fig 2.4 Experiments on pixelated amplitude objects

at a corner only. In the filtered image this shows up as a broken rather than continuous line in the stripe. Effects similar to these are reported in the paper by Anderson [1986]. It should be pointed out in conclusion that identical behaviour should not be expected from mixing the orders of spectra of phase objects as section 2.1 shows that they are not all in phase.

2.2.2. Reflecting phase objects

The SLMs developed as part of this thesis will all be reflecting devices as the silicon backplane used to address them is opaque. For this reason the 6-f optical system as described earlier cannot be used. A similar system which was constructed specifically for the use of reflecting objects is described here. A bare backplane was used as an object in some simple experiments to test the system. This involved conducting Schlieren filtering operations on the test object to find the appropriate filters and to gain experience of this technique.

The optical system used is illustrated in Fig. 2.5. The lens L_c is used to collimate the light from the point source P resulting in a parallel beam of illumination on the object O. The inclusion of a plane mirror here at 45° to the vertical allows the option of an object lying horizontally should this be required. The distance from L_c to O was not fixed as different objects have different thickness. The pellicle beam splitter BS takes the reflected light from O into the side arm of the bench.

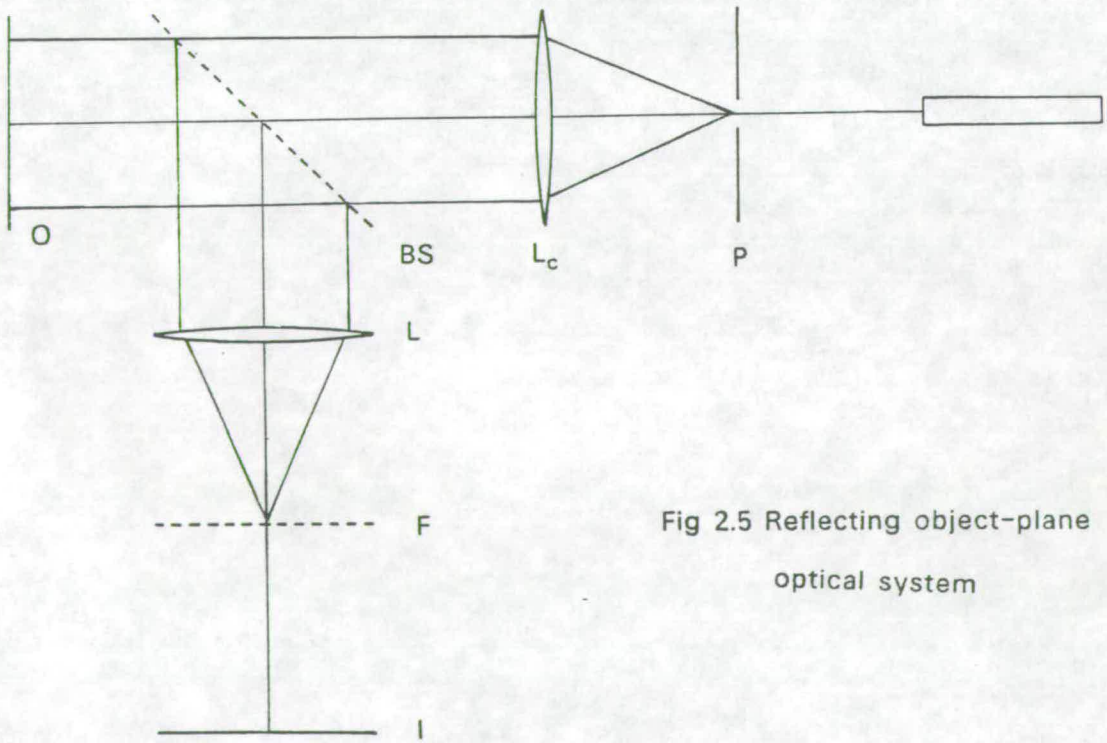

Fig 2.5 Reflecting object-plane optical system

The lens L fulfils the dual purpose of producing a Fourier transform of O at F (the conjugate plane to P) and an image of O at I. It was originally planned that the beam splitter would be placed before L_c dispensing with the need for the second lens altogether. However reflections from the front face of L_c made this approach necessary. An auxiliary lens, not shown in the figure, can be introduced to make I conjugate to F so that with a fixed camera it is possible to photograph either the image or its FT.

Fig. 2.6 (a) is an image of one of the LCIC chips. Fig. 2.6 (b) shows the filtered image obtained when a Schlieren filter is introduced into F. It can be seen that the large flat parts of the object, such as the pixel mirrors, have been filtered out as most of the light reflected from them is diffracted into the zero-order. The circuitry appears lighter as some of the associated light is passed around the stop. In terms of the theory of previous section, the mean phase is close to that of the light reflected from the mirrors. The argument in the Bessel function that determines the intensity observed is very small. The height of the circuitry above the mirrors is reported by Underwood [1987] to be about 0.6μm. Therefore, for the circuitry the phase is up to about 4π different from the mean and so light regions are observed.

This optical system is used to form the images of SLMs shown in chapters three and four.

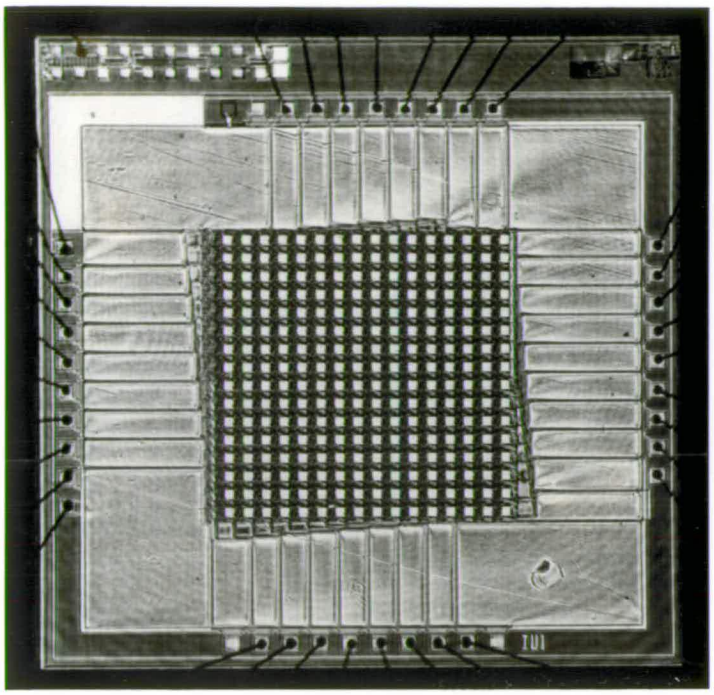

(a) LCIC chip

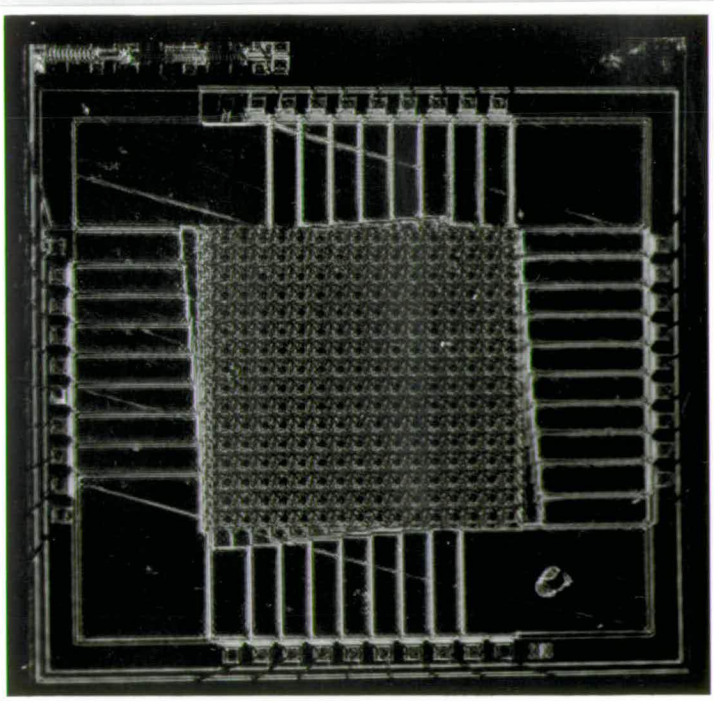

(b) Zero-order removed

Fig 2.6 Example of Schlieren Filtering

Chapter 3

Deformable Mirror SLMs

3.1. Comparison of deformable mirror phase modulation techniques

3.1.1. Survey of deformable mirror SLMs

One method of phase modulating an optical wavefront is to use a deformable mirror structure. This has already been briefly introduced in chapter one when some specific SLMs were considered but is now examined in more detail.

The mirror is locally deformed by electrostatic forces in the direction of propagation of read-out light by an amount depending on the magnitude of the applied electronic or optical stimulus. Light reflected by the different portions of the mirror will be phase modulated in proportion to the size of the deformation. If the surface profile of the mirror is described by s(x,y) then a reflected coherent light distribution, of wavenumber k, is modulated by the multiplication of a factor

$$M(x,y) = e^{i2ks(x,y)} \qquad (3.1)$$

This simple electro-mechanical approach to phase modulation has been realised in a number of ways in SLMs, and will be assessed to select a promising area of study. This selection will be based upon ease of integration of the work with the existing SLM programme of the group. For example, suitability of the LCIC chip to drive an electronically addressed device would

be important. Looking to the future, a further criterion is whether the principles of the device could be further developed towards an optically addressed SLM.

It is possible to distinguish two main groups of deformable mirror structure. In the first group, the mirror is on the free surface of a thick, compressible layer on a rigid substrate. This thickness is typically 5μm; the requirement is that it is large compared to the magnitude of the deformation which is often about an optical wavelength. Stresses created within the body by electrostatic forces cause the free surface to deform in some correspondence to the input. In these devices if the deformable medium is transparent it is also possible to phase modulate by transmission through the medium, dispensing with the need for a mirror surface altogether. In the second group, the mirror is a much thinner film (0.5μm or less) which is supported on a rigid perforated structure. Each segment of the mirror (pixel) is independently displaced at the perforation.

These two types of structure will now be compared. This is done to assess which approach is more suitable both for the construction of an electronically addressed SLM driven by the LCIC chip, and for possible development towards an optically addressed device.

Thick deformable structures

These deformable structures are used in such devices as the Ruticon, the thermoplastic devices and the deformable oil film device.

Of these the Ruticon, described in section 1.3.1, is the only one that could conceivably be addressed both electronically by the LCIC chip and optically.

The others are not considered in any detail here. Both require complicated auxiliary support equipment for temperature regulation or corona discharge preconditioning. Electrically addressed versions of these devices have been, almost without exception, electron-beam addressed. Optically addressed versions are driven by photoconduction or heat-generation.

The γ-Ruticon has already been demonstrated in coherent light applications by Sheridon and Berkovitz [1975] though adequate optical quality

is not generally found. These applications include use as an incoherent-to-coherent converter and as a matched filter in the Fourier plane of a correlator.

It is primarily known as an photoconductor addressed device but an electron beam version has also been examined. This suggests the feasibility of developing a photocathode addressed device like the PEMLM.

A device with electrodes might be impractical due to the high optimal spatial frequency (tens to 1000 lp/mm) of the light modulating medium (an elastomer or synthetic rubber), or due to the high bias voltages usually needed to drive them (20-200V). The optimal spatial frequency is determined by the composition of the mirror and by its thickness. This would need to be characterised and strictly controlled in order to match the mirror to the drive chip.

These facts are arguments against addressing such a deformable mirror with the LCIC chip which has a spatial frequency of 5 pixels per mm and has been operated at voltages of no more than 15V.

Thin deformable mirror structures

The second class of deformable mirror structures has generated a lot of interest recently. These are generally faster and more robust or reliable than the thick mirror structures. Many of these devices are electronically addressed: the microfabrication techniques of the electronics industry are ideal for the high-volume production of complex, small minimum-dimension arrays combining the drive circuitry, electrode and perforated support structure in a single monolithic component. The mirror is often a thin metalised polymer film stretched across the support structure. The resolution of SLMs which use these mirrors is clearly determined purely by the spatial frequency of the support. This approach to SLMs has been developed by a succession of workers from Preston [1969] through to Pape and Hornbeck [1983]. The principle has been extended by Pape [1984] towards an optically addressed device by integrating a photo-sensor into each pixel of the backplane. Petersen [1977] took the degree of integration even further by etching the

deformable mirror from the silicon wafer using anisotropic etching techniques. The review by Brooks[1984] discusses the progress of the development of this class of SLM.

Thin deformable mirrors have been used as the modulating medium in the photoemitter/microchannel plate group of SLMs. (See chapter 1). The photoemitter membrane light modulator (PEMLM) has claims for very high performance including a highly non-linear transfer characteristic.

3.1.2. The production of deformable mirror structures

A series of experiments was conducted to construct deformable mirrors to further assess the viability of their use in SLMs. To make thick mirrors, silicone elastomers were used as the deformable medium. To make the thin mirrors nitrocellulose was used. The production of the aluminium coatings on the mirror surfaces was done with the technical assistance of Eric Davidson and Andrew Garrie.

Thick mirrors

Flat layers of silicone elastomer (synthetic rubber) of the required thickness were made by moulding the compound between glass plates. The compounds used were Dow Corning "3140 RTV" one-part elastomer or "Silastic 3112" two-part elastomer. Dow Corning release spray "Releasil A" and "1200 RTV" primer were also used. There were problems of uneven bonding or release between the glass and the elastomer (depending on whether the glass was to be used as a substrate or as a mould). Attempts at using spin coating techniques to apply the elastomer compounds produced layers of the correct thickness. However the layers did not cure properly due to seperation of the components in the spinning process.

Metalisation of these films was initially attempted by direct evaporation of aluminium but this yielded a dull, electrically insulating surface. This is perhaps due to small-scale roughness of the surface. A second method was devised which involved putting a layer of salt onto one of the glass moulds and metalising this prior to casting the rubber. When the rubber was cured the

salt was washed away leaving a metal layer upon the surface of the rubber film.

These metal layers were electrically conducting and exhibited specular reflection over large areas. It was found that the surfaces tended to break up and become dull over the course of several days. This indicates that the films were not mechanically stable but perhaps tended to relax into the shape of any surface imperfections of the rubber.

Thin mirrors

Thin membranes of nitrocellulose were made by dropping an organic solution of it onto a water surface. The solution was supplied under the brand-name "Zapon" by ICI and is no longer available. Other chemical suppliers do supply nitrocellulose. The solvent quickly evaporates and the film can be lifted from the water using a metal ring. At this stage the films are soft and malleable.

This procedure was standardised as much as possible by dropping the solution in a quantity of about 0.05ml from a syringe onto the water from a height of about 10cm.

After they have dried which typically takes about one hour, the films have consistently been taut, strong and flexible and have areas of several square centimetres. The thickness of the films was variable but strong coloured interference fringes suggest that they are of the order of an optical wavelength thick.

These films were metalised, again by direct evaporation of aluminium. The result was an electrically conducting, reflecting surface on the film which was apparently quite stable compared to the metal on elastomer surfaces.

These films were found to be less strong after the aluminium layer had been added. They very often stretched in the process of evaporation. This is a significant problem for SLMs which require reasonably taut films.

3.1.3. Summary

The information related in the previous two sections strongly favours development of SLMs using thin film deformable mirror structures. The reasoning for this is summarised below.

The "thin" film deformable mirror structures developed by other researchers in the past have generally had better optical quality and longer lifetime than the "thick" mirrors. This is supported by the experimental observations of section 3.1.2.

The anisotropic spatial frequency response of thick mirror structures is undesirable. Although they have a greater first-order diffraction efficiency than pixelated devices this is not a significant consideration for most applications.

Thin mirror structures are highly compatible with the LCIC chip while to use a thick mirror would introduce extra problems without any obvious benefits. This compatibility relates to the driving voltage of the devices, and to considerations of spatial frequency response. The chip voltage of up to 15 volts is suitable for deforming a thin mirror while a thick mirror might require a much greater voltage. Generally the spatial frequency of a thin mirror is determined by the period of the support structure. For a thick mirror however, it depends on parameters of the mirror itself which would have to be matched to the chip.

The performance of existing thin mirror devices is in general better when operating parameters like switching time are considered. The PEMLM is a device with particularly high potential and developments along those lines would be fruitful. The use of a Ruticon type of mirror in such a device would be unnecessarily complicated by outgassing of the rubber film with no obvious compensations.

Present experience and resources in Edinburgh favour a thin film type of device. The LCIC chip lends itself readily as a backplane for a DMD type device. As the chips are made in this faculty, minor processing modifications can be accommodated.

Proposed device

It is proposed to construct a device which is electronically driven by the LCIC chip. The light modulating medium will be a thin metalised film supported on an insulating structure with "wells" above each pixel of the chip to permit local deformations of the mirror. The mirror will be held at a constant electric potential The electrode voltage can take on one of two values which determines the force on the mirror element and the depth of the deformation.

3.2. Determination of physical properties of the films

It has been decided to construct a deformable mirror device using the LCIC chip to address and support a metalised nitrocellulose membrane. The metal used in previous experiments was evaporated aluminium. This is also used in the following work to eliminate a source of variation.

Before it is possible to proceed with constructing the devices some preliminary work must be conducted. This involves determining as far as possible the relevant physical properties of the films such as surface resistivity, tension, mass density , thickness etc.. Pape and Hornbeck [1983] model the deflection of the mirror of their device in terms of some of these parameters. It is also necessary to conduct an assessment of the structure used to support the mirror over the chip and techniques for constructing the device.

In devices the films would be supported over a fraction of their area. For the purpose of these experiments it was sometimes necessary to support the films over their entire area. In these cases the films were mounted on 3"x1" glass slides instead of a metal ring.

Surface resistivity

Four slides carrying a nitrocellulose film were coated to about 95% reflection with aluminium. As a control sample, three additional slides without the nitrocellulose film were coated in the same way.

The surface resistivity of all of these slides was measured by the following technique. A block of copper was clamped to one short edge of the slide. The resistance of the block was found to be less than 0.05Ω. A second copper block was clamped at various distances along the slide parallel to the first. The resistance between the two blocks was measured by a digital multimeter and graphed against the distance between the blocks. The graphs were found to be linear in the region examined. As the resistances measured were significantly greater than the resistance of the blocks, it was assumed that the electric field lines in the aluminium layer were parallel to the long edge of the slide and the surface resistivity was calculated from the slope of the graph.

The values for the aluminium on nitrocellulose were: 1.44, 0.85, 0.89 ,0.73 Ω per square to 5%.

These have mean 0.98 and standard deviation 0.316.

The values for the aluminium alone were: 1.22, 0.91, 0.71 Ω per square to 5%.

These have mean 0.95 and standard deviation 0.26.

These measurements reveal firstly that the surface resistivity of the films can be expected to lie consistently in the 1Ω per square range, and secondly that the nitrocellulose does not seem to affect this property of the aluminium.

If we assume that the volume resistivity of the aluminium thin films is the same as for the bulk material then a measure of the film thickness can be arrived at. Taking the volume resistivity of aluminium to be 2.7μΩ cm and a surface resistivity of 1 Ω per square gives an Al thickness of 27nm.

Mass and thickness

The same samples were used to arrive at figures for the surface mass density of the aluminium and nitrocellulose layers.

The total mass of the four 3"x1" slides carrying aluminised nitrocellulose was measured to ±0.1mg. The films were then cleaned off the glass using acetone then water and when dry were weighed again. The difference in mass

was 4.0mg ±0.1mg. The total surface area of the films was measured to be $76cm^2$ (±10%) giving a mean mass of $52\mu gcm^{-2}$ for the films. Repeating the measurements for the Al on glass slides gave a mass of $8\mu gcm^{-2}$ (±40%). Relating this to the density of Al (about $2.7gcm^{-3}$) gives a film thickness of about 30nm which is in good agreement with the resistivity measurements.

The relative error in the thickness from the resistivity measurements is smaller than that for the mass measurements. It is possibly sensible to take the resistivity as the fundamental measurement for the aluminium and to calculate its mass. This gives a value of $7.3\mu gcm^{-2}$ for Aluminium.

This then implies from the mass measurements that the nitrocellulose has a mass of 45 (±6) μgcm^{-2}.

Taking its density to be $1.25gcm^{-3}$ implies a nitrocellulose thickness of 360nm and a total film thickness of about 390nm.

Tension

The most striking point arising from the making of these deformable mirrors is the great variation in their tension after the metalisation process. It is highly important that the mirrors be taut enough when mounted on their support structure to allow recoverable deformations to be impressed upon them. The tension will govern the performance of any device affecting such things as the peak deformation of a pixel, the switching time. However the variation of the of the tension is too great to allow any plate any reasonable assessment of this parameter. Thus it is important to be able to regulate the tension of the films on the support before making devices.

3.2.1. The structure of the chip

The drive chip is discussed in detail in appendix 2. It consists of a 16x16 array of electrodes which can be set at one of two voltage values. The physical structure of the chip is of particular importance here as it must be assessed and possibly modified to provide a support for the mirror around each electrode. The pixels are $200x200\mu m^2$ with an active area of $100x100\mu m^2$.

The remainder of the pixel consists of circuitry which because of the micro-fabrication techniques is raised above the level of the electrode. Thus the circuitry itself can form the support.

According to Underwood [1987] the typical height of the circuitry above the electrode is about 0.5-1μm. This gives the ratio of the width to depth of the "well" of each pixel of 100-200. This requires a highly tensioned membrane to prevent sag onto the electrode at the centre. For the two device geometries described by Pape and Hornbeck [1983], allowing for non-square pixels, the corresponding ratios are 46.4 and 38.0.

Therefore it would be advantageous to increase the "well" depth by building up an insulating layer above the circuitry. This would have the added effect of reducing the likelihood of short circuits through the nitrocellulose and of increasing the dynamic range of the device. However, using deeper wells generally reduces the deflection obtained for a given voltage and so the well should not be made too deep.

A layer of photoresist material was spun onto one of the wafers and one of the original mask-set used to remove the resist from the electrodes and bonding pads. This was done by the Edinburgh Microfabrication Facility who produce the chips.

It was found that the photoresist increased the well depth to about 3-4μm bringing the width-to-depth ratio into line with that of other similar devices. However it was considered necessary to increase the depth to this level because of the problems of membrane tension. It is not anticipated that using photoresist in this prototype instead of a more robust material such as silicon oxide will present problems.

It is helpful to understand the way in which the chip is bonded and set into the chip carrier which affects the approach to constructing the SLMs. The silicon "die" is about $7x7mm^2$ in area, the central $3.2x3.2mm^2$ of this being the active pixels. The outer 0.5mm wide strip contains the bonding pads, with the area between being interconnect (1.4mm wide). The chip is recessed into a chip carrier (a ceramic holder) by 1 or 2mm. Thin gold wires are welded between the carrier and the bonding pads. The two points of interest are the recessing of the chip, which complicates the process of adding a mirror, and

the bonding wires which are very vulnerable.

3.2.2. Techniques for mirror construction

A number of ways of producing a reflecting membrane stretched over the supporting structure of the chip have been investigated. One of the fundamental problems to be addressed is whether the membrane should be metalised before or after it is fixed to the chip.

Metalisation of the membrane prior to its attachment to the chip has several good points. As remarked before, the membrane has a tendency to sag after metalisation. It can be tensioned again by lowering a square metal frame, thinly coated in electrocure conductive paint, onto the mirror. The weight of the frame stretches the membrane between its four sides, and when the paint dries, the frame can be lowered into the recess in the chip carrier onto the IC surface.

A second important point arises from recognising that metalising and attaching the membrane is the stage most prone to failure. Making the mirror while it is separate from the rest of the device means that only one component is lost in any failure. it is possible to make many mirrors until a suitable one for a device is prepared.

This method also has a number of disadvantages. As the mirror on the square frame is still largely unsupported it is quite vulnerable to tearing as it is positioned on the chip surface. It is difficult to ensure that the mirror on the frame is evenly tensioned and sometimes it can be seen to be wrinkled. There is not much space between the bonding wires and the active area into which the frame is placed. Therefore there is a danger of a wire being broken or short-circuited to the frame. Great care was taken when this step was carried out and in fact the problem was never encountered.

Another problem was that the mirror may not lie in the same plane as the bottom of the frame. Instead it was often found to be above this level, with the consequence that the mirror did not make contact with the support structure. By applying voltages to the mirror and chip, electrostatic forces can be employed to bring the mirror into contact with the support. However this

often caused the mirror to tear around the edge as it was pulled down.

There is an alternative approach of metalising the membrane after it has been attached to the chip. The chip is prepared by laying the membrane on the carrier as soon as it has been lifted from the water surface. At this stage it is still soft and pliable. The best way to stretch the membrane over the support structure is simply to blow very gently onto it. This gives a much more uniform result than using probes to push it into place, and eliminates the possibility of structural damage. At this stage the membrane can usually be removed if unsatisfactory. After one or more hours the membrane dries to give a tensioned uniform film over the active array.

This approach means that there is never any need to handle an unsupported mirror. The tension of the mirror on the supports is much more uniform and there are no problems of it not meeting the support.

However there are complications of the metalisation process to be overcome before the effect of these advantages can be felt. There remains the problem of the sagging of the mirror.

The main problem concerns the behaviour of the chip-membrane structure in the vacuum chamber for the evaporation of the aluminium. The air trapped in the pixel "wells" is likely to burst the membrane while pumping is carried out. Similarly when the pressure is returned to atmosphere the air pressure causes the membrane to collapse onto the chip.

It was attempted to solve this problem by very slowly raising and lowering the pressure, especially in the lower vacuum region, to allow the air to diffuse in and out of the wells. This pumping stage was tested without evaporating aluminium and seemed to be successful. However it was not possible to rigorously assess the final state of the membrane. However when aluminium was evaporated after pumping by this method the devices made showed no sign of functioning. The failure may be due to the aluminium reaching the chip electronics through small holes made in the membrane. It is more likely that the failure is due to the mirror collapsing because air cannot return behind it.

Ultimately the most desirable way to proceed with this approach is to

design a mask for the support layer. This will be used to introduce channels through the insulating material to allow air to escape from behind the mirror. This is also likely to improve the switching speed of the device by reducing the retarding effect on the mirror of the trapped air.

Thus in the following experiments metalising was done prior to attaching the membrane to the chip. The full procedure of SLM construction is summarised below.

The device cross section is illustrated in Fig. 3.1.

Fig 3.1 The deformable mirror device - cross section

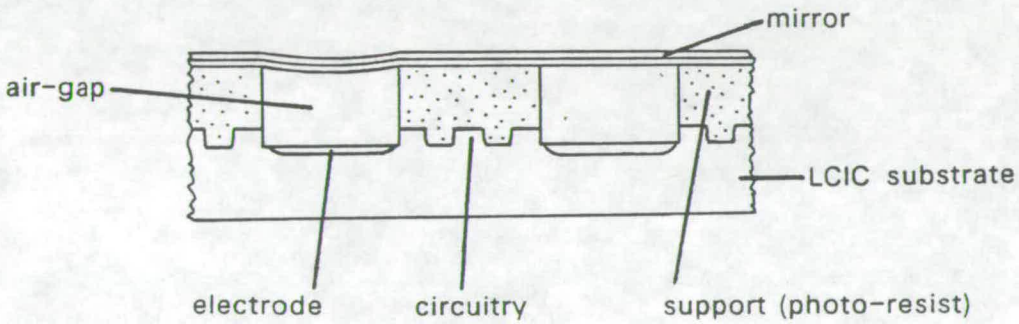

3.2.3. The construction of a deformable mirror SLM

The construction procedure to be described in this section is shown in Fig. 3.2. The first stage is the preparation of the frame assembly which holds the mirror. This consists of three component parts. There is a sheet of perspex with a square hole of side 5mm cut in it. This component is also used in making liquid crystal SLMs (see chapter 4). The frame itself is made from 2mm

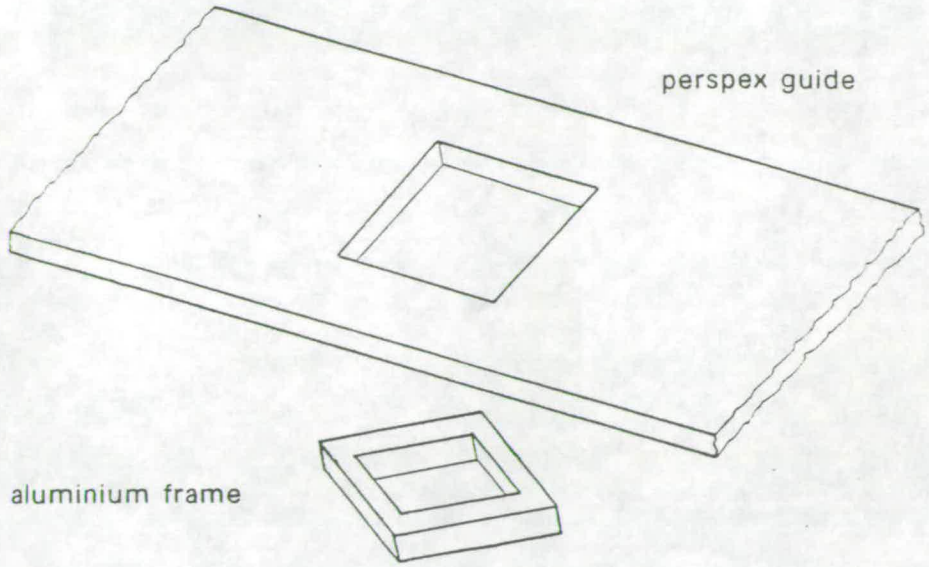

Fig 3.2 The deformable mirror device - construction

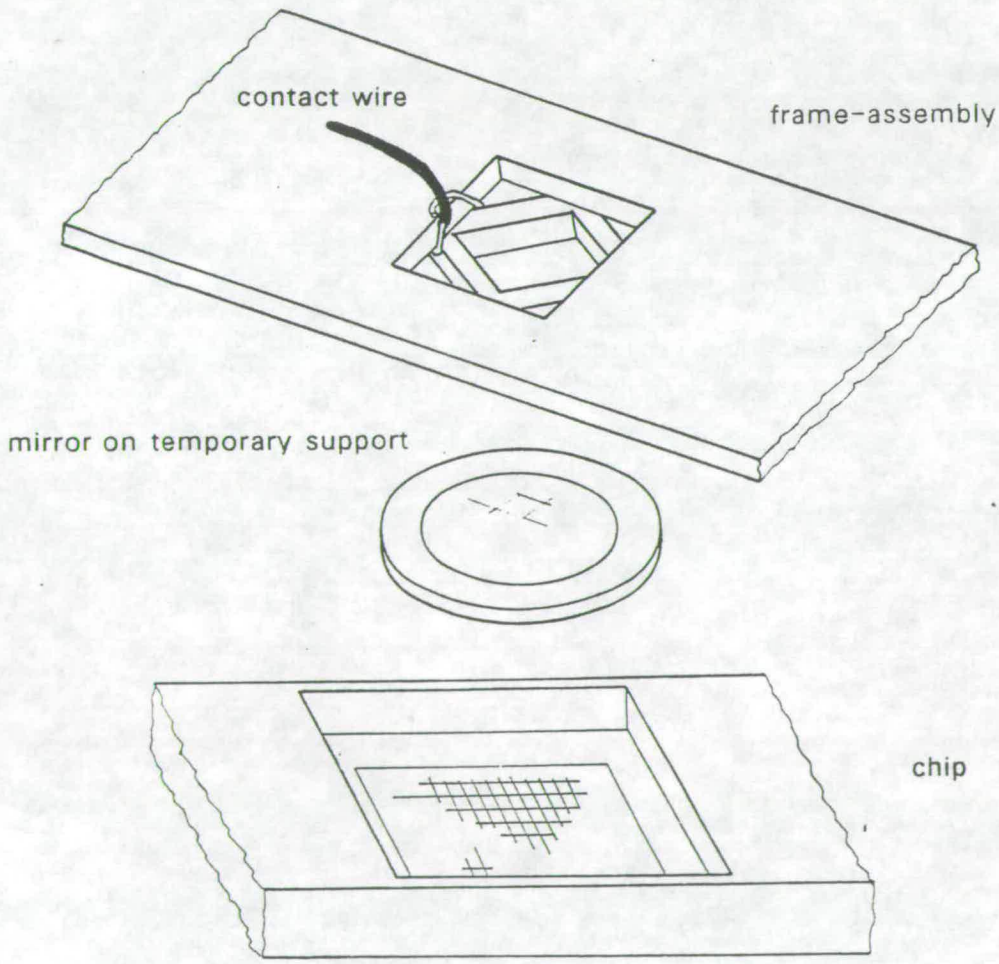

thick aluminium. This is cut to a 5mm square and a 3.5mm square hole is spark-etched in the centre. The lower face is made smooth to carry the mirror. The third component is a fine wire used to establish electrical contact with the mirror.

The aluminium frame is attached with Araldite to the perspex guide over the hole so that the corners of the frame sit across the middle of the edges of the guide as illustrated in the figure. This arrangement gives the frame enough clearance from the guide to fit into the recess in the chip carrier. The space at each edge of the frame is useful for aligning it on the chip and later for aligning the SLM in an optical system. The spaces will be referred to as the "alignment holes".

One end of the wire is looped through the perspex and around the outside of one corner of the frame. (See Fig. 3.2.) It is secured with Araldite and electrical contact is made to the frame with conductive paint.

The membrane is formed on a water surface and lifted off using a metal ring. It is dried and aluminium is evaporated onto its top surface.

The bottom and outer edges of the aluminium frame are thinly coated with conductive paint and the frame assembly is lowered onto the membrane. The membrane is trimmed with a scalpel and rough edges are secured to the frame edge.

Two small balls of "blutack" are placed on the chip carrier about 5-10mm either side of the recess. The frame assembly carrying the mirror is placed upon these. The mirror now sits several millimetres above the chip and can be registered by looking at the interconnect and bonding pads through the alignment holes.

The perspex is now gently pressed down until resistance is felt indicating that the frame and chip are now in contact. When pressure is removed the "blutack" holds the frame assembly in place though it may be desirable to make a more secure join with Araldite.

Finally the free end of the wire is fixed to pin 25 of the chip carrier. This pin is not connected to the chip itself. This allows all connections to the SLM to be made through a standard 40 pin holder.

Fig 3.3 The deformable mirror device - photograph of completed SLM

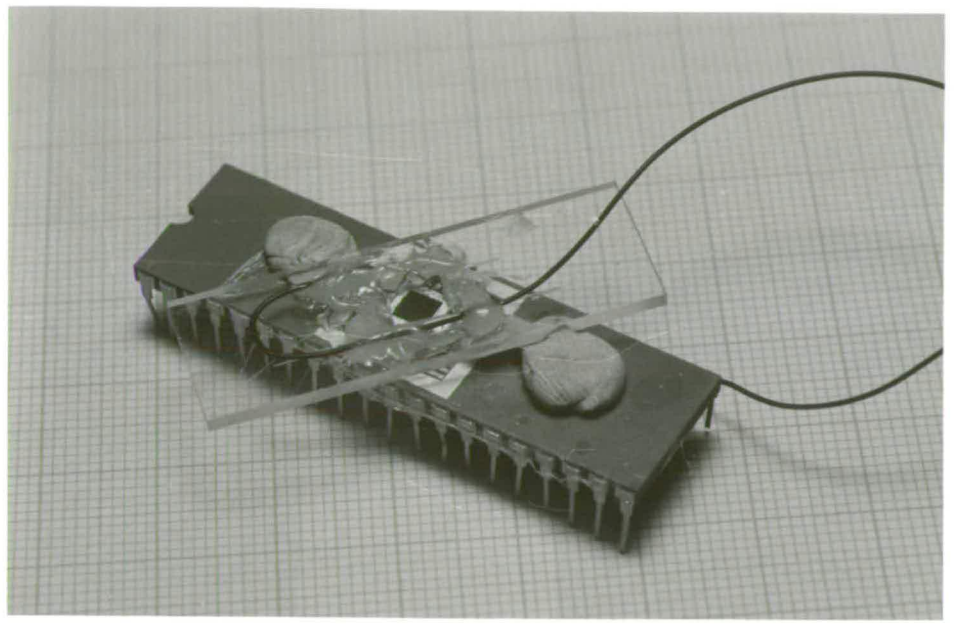

3.3. Assessment of the deformable mirror SLMs

3.3.1. Preliminaries - optical adjustments and electronics

The SLM is mounted in a standard 40 pin ZIF (Zero Insertion Force) socket in the object plane of the coherent optical processing bench described in section 2.2.2. It is illuminated with HeNe laser light of wavelength 632.8nm. The location of the Fourier and image planes are determined by illuminating the interconnect area of the chip through the alignment holes. The structure of this region is very regular compared to the deformable mirror, remembering that the quality of the mirror is far from perfect.

The position of the spatial filter in the Fourier plane is also determined by the diffraction pattern of this structure. The filter used may be either a low-pass filter on the zero or first order, or a high-pass or band-pass filter on

the zero order. (See the section of chapter two on Schlieren filtering.)

The chip was usually driven with V_{DD}=5V and V_{SUB}=−2.5V. (See appendix 2). The column and row data inputs were set at either V_{DD} or ground by mechanical switches. The clock input was not pulsed but held at a steady level of either V_{DD} or ground. The mirror voltage, V_M, was set independently of the chip, at a voltage between +5V and +30V.

3.3.2. Results

The performance of the deformable mirror devices was investigated. The following section illustrates that the basic functions of the device have been demonstrated.

Array switching

Initial experiments were done to examine the deformation of the mirror elements by changing the mirror voltage V_M. The memory elements of the chip were not addressed. Fig. 3.4 (a) and (b) show images of a device with V_M=0V and V_M=22.5V. A band pass filter in the Fourier plane is passing the first and second orders.

Clearly a large number of pixels do not switch however those that do indicate that the basic objective has been acheived. This particular device only operated for a small number of operating cycles. Most pixels became stuck in the deformed position indicating perhaps that the mirror voltage was too high. This poor uniformity and low lifetime has been characteristic of all the devices so far.

Active addressing and memory

Fig. 3.5 (a) and (b) show images of a chip where the working pixels were actively switched by the pixel circuitry. Note that the band of "pixels" in the centre of the array is a tear in the mirror. The reflected light in this area comes from the circuitry and electrodes. The active pixels lie on either side of

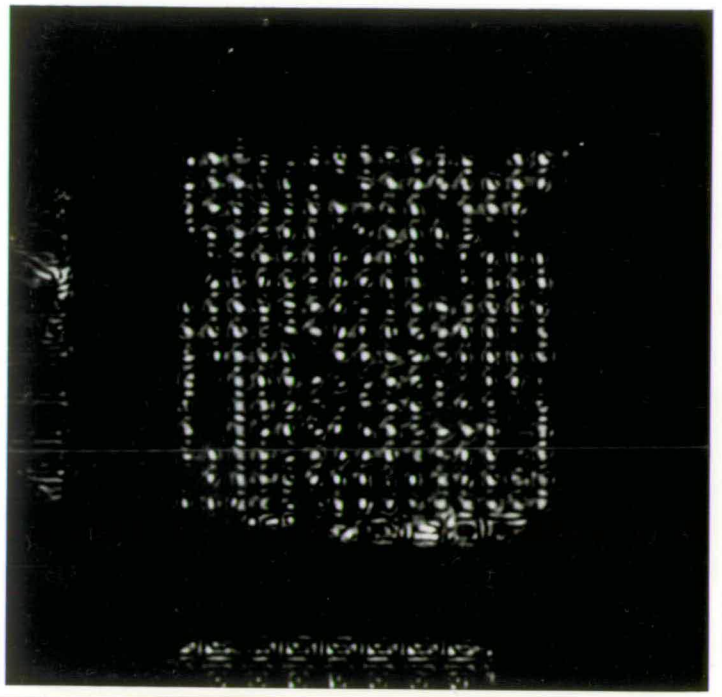

(a) Mirror voltage = 0V : small voltage across air-gap : mirror in relaxed configuration : light diffracted around zero-order stop.

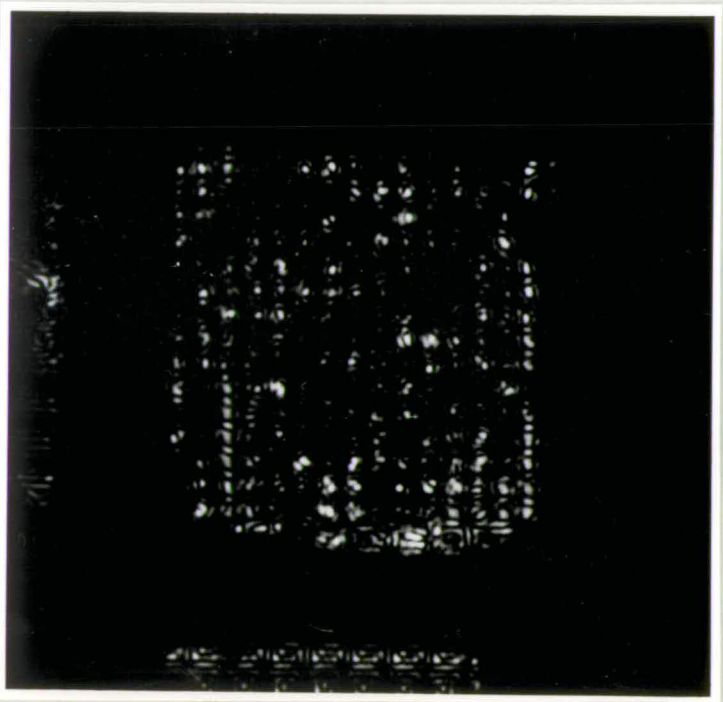

(b) Mirror voltage = 22.5V : larger voltage across air-gap : mirror deformed onto flat electrode : light blocked by stop.

Fig. 3.4 Array switching: These photographs show the result of altering the mirror voltage. The pixels are not being addressed. The SLM is in the object plane and illuminated uniformly. A spatial filter in the Fourier plane removes the zero-order spectrum.

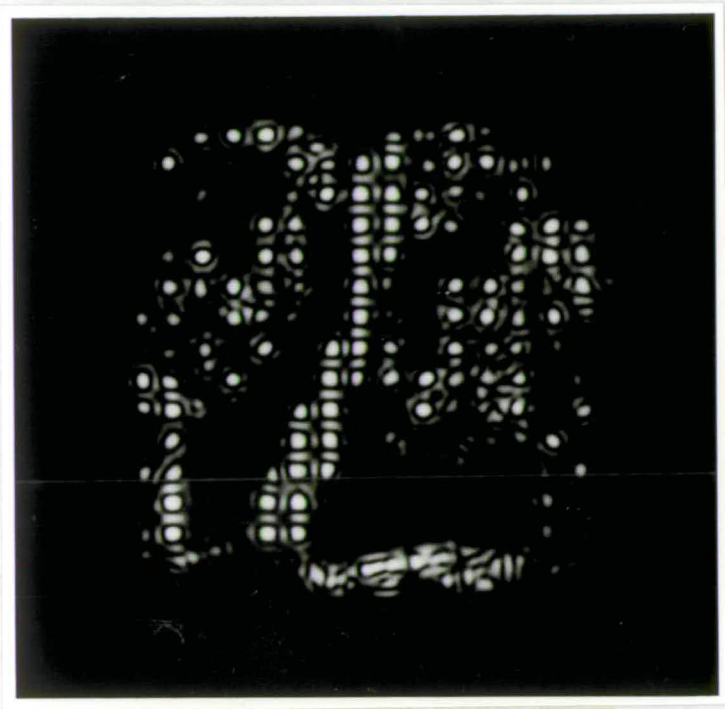

(a) Pixel electrode voltage = 0V

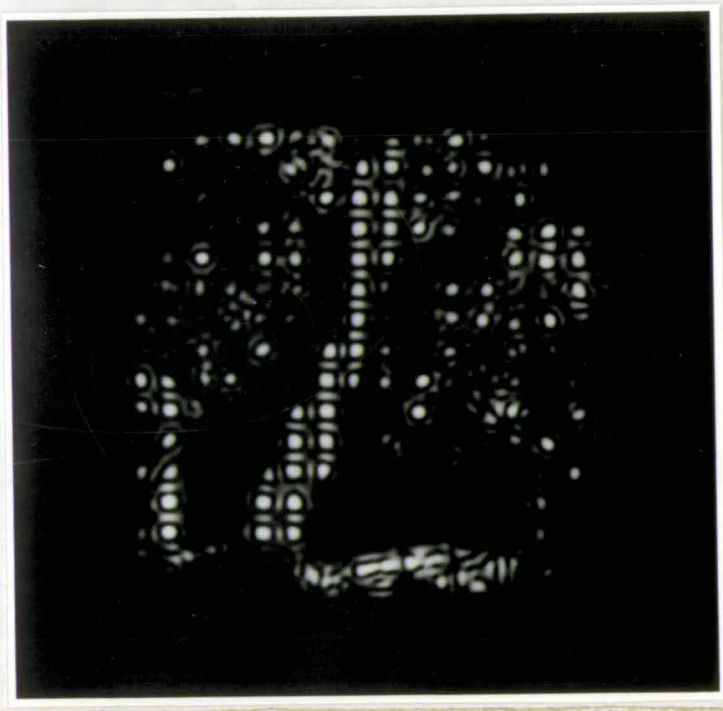

(b) Pixel electrode voltage = 5V

Fig. 3.5 Active addressing: Showing the effect of changing the pixel electrode voltages while the mirror voltage remains fixed. The zero-order spectrum is removed in the Fourier plane.

(See supplementary notes on following page)

Notes on Fig. 3.5 and Fig. 3.6.

As explained in the main text, these figures illustrate the effect of fixing the mirror voltage and changing the voltage on the pixel electrodes. These notes explain what is to be seen in the figures. They should be read with reference to the accompanying sketch which labels the regions of particular interest. Note that many of the effects are more easily seen initially in the desampled images (Fig. 3.6).

Region *A* is the tear in the mirror referred to in the text.

The two regions labelled *B* contain most of the pixels which respond to the change of electrode voltage.

In region *C* is a single pixel which switches from light to dark while the other pixels switch from dark to light. This is more clearly seen in Fig. 3.6. The explanation of this is that the pixel is initially deformed by a different amount than the others. It was explained in sections 2.1.2 and 2.1.3 that the intensity observed in the image plane of optical systems like this is determined to a good approximation by the Bessel function $J_1(\phi)$ where ϕ is the relative phase of the light reflected from a pixel. This is of course proportional to the deformation of the mirror. The oscillatory behaviour of the Bessel function means that the image plane intensity will increase for some initial values of its argument while decreasing for others.

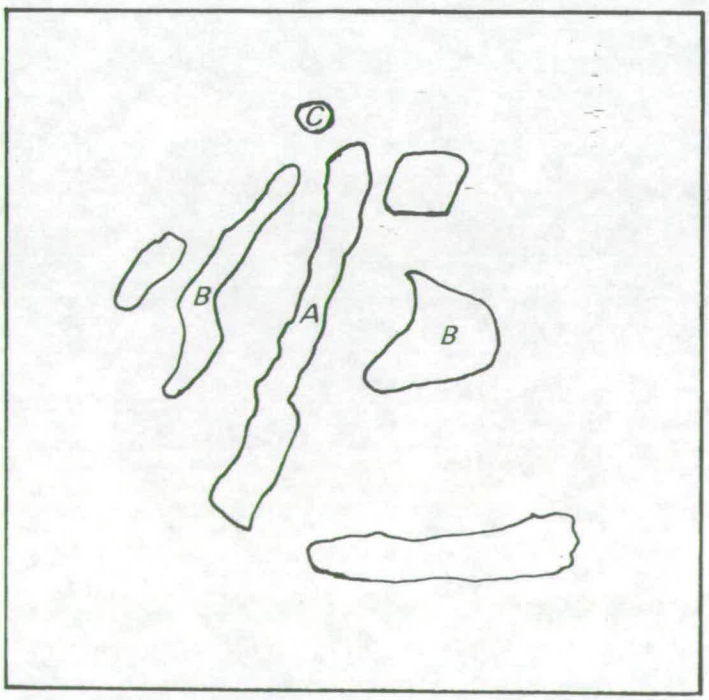

insert

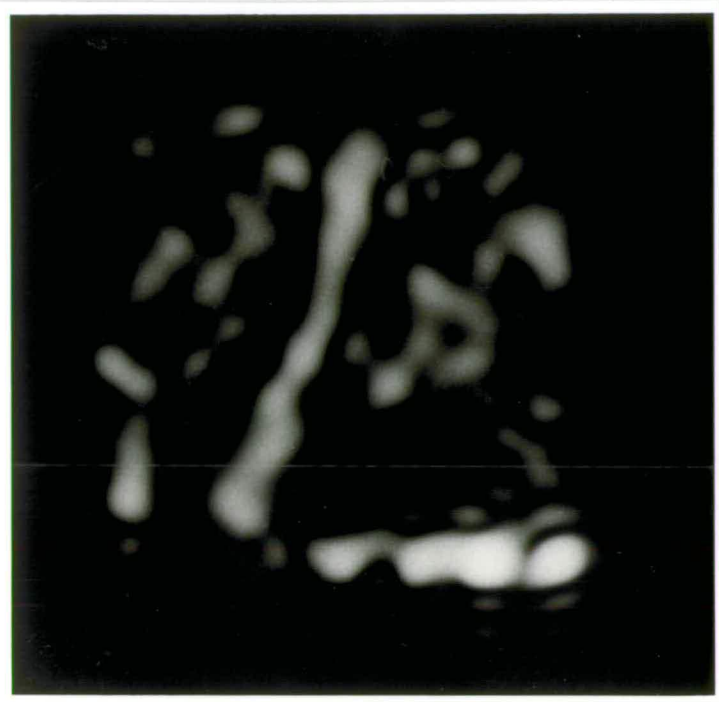

(a) Pixel electrode voltage = 0V

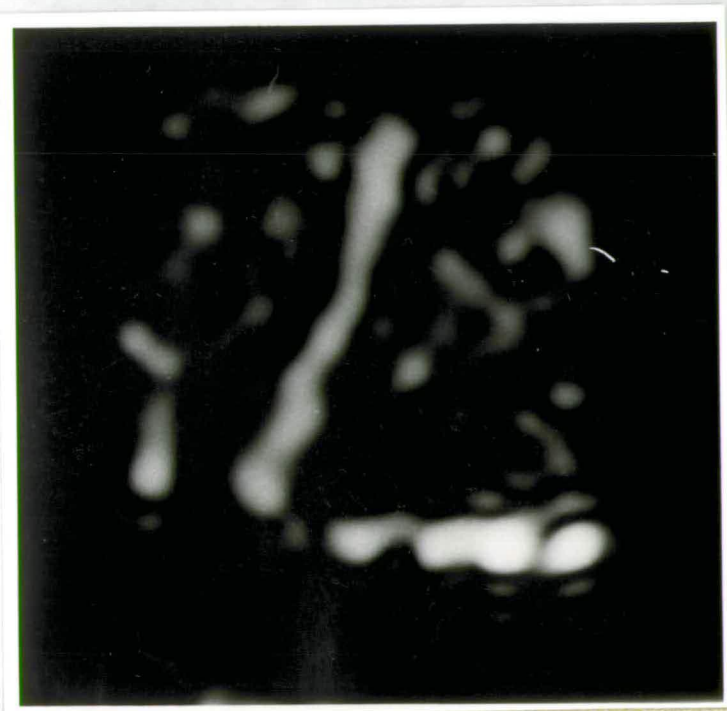

(b) Pixel electrode voltage = 5V

Fig. 3.6 Low-pass filtering: These images are produced from the same objects as for Fig. 3.5. In this case, only a single first-order spectrum of the Fourier transform is being used to construct the image.

(See supplementary notes on preceding page)

this band. The pixel voltages are changed between 0V and 5V and V_M is approximately 20V.

In the first photograph, the data and enable inputs are all at logic value "0". Data can be programmed into the pixels by making the enables all "high" and applying appropriate signals to the data lines. In this case, all the pixels were given a logic "1" value. This is stored by making the enables low again. As is seen from the second photograph, these new data values have been stored in the chip memory.

Low-pass filtering

As explained in section 2.1, to use a pixelated phase object in a coherent processing system requires passing a single spectrum of the Fourier transform and performing filtering operations on it.

Fig. 3.6 (a) and (b) show the effect of passing only a single first-order spectrum of the device. The switching of the same regions is still observable although the pixelation is lost due to the low-pass filtering. If more addressable pixels were available then it would be possible to show spatial filtering of this image.

As the uniformity and depth of phase modulation are not quantified there is nothing to be gained from any detailed analysis of these pictures.

3.3.3. Conclusion

The basic operation of a deformable mirror SLM has been demonstrated. The performance of the devices has been limited due to the poor quality of the mirror structures. It is likely that significant advances will result from improvements in the mirror production techniques.

These improvements may involve changing of the mirror coating techniques or materials. A great variation in mirror quality has been observed due perhaps to differences in evaporating conditions. A study of the effect of the evaporating time and temperature on the final quality of the mirrors may

be useful.

The only mirror coating material examined so far has been aluminium. It is possible that another material would be more appropriate for the mirror. However techniques developed so far have not involved any other material as there were a great number of uncertainties in the techniques themselves.

It will be useful to investigate the possibilities arising from sputter coating instead of evaporation. A major consideration in this technique will be the high substrate temperatures generated. This will clearly have a significant, possibly destructive, effect on the films and is a major reason why sputtering has not been employed so far. The extremely low sputtering rate of aluminium is a second reason for not using this technique. Sputtering could only be usefully employed when other mirror materials are investigated.

The use of the LCIC chip which was designed for another (similar) purpose has not been highly restrictive but advantage could be gained from the inclusion of another mask for a specifically designed support structure. This would include air-channels to aid device construction and enhance its performance as described in section 3.2.3. It may be helpful to add "pillars" of insulating material in the centre of the pixels to reduce the "sag" of the mirror. Clearly this would change the shape of the pixel for light modulation but the principle of operation would remain the same. The main effect of this would only be to change the "envelope" of the Fourier plane spectra. The third improvement of the support structure would be to put a thin insulating layer over the electrodes as well as the circuitry to prevent short circuits from collapsed portions of the mirror (or from contaminant metal if the technique of evaporating after attaching the mirror is continued).

3.4. Post script - The development of an optically addressed deformable mirror SLM

It is intended that the electronically addressed SLM described in this chapter will be further developed towards an optically addressed SLM. This device will be photocathode addressed and work on the principle of the PEMLM described previously. Some preliminary work has already been done on this project and it is appropriate to describe the progress made.

The photoemitter membrane light modulator (PEMLM) and microchannel SLM (MSLM) both operate by amplifying a spatial distribution of photogenerated charge using a microchannel plate (MCP) and depositing the charge onto a light modulating medium. For the PEMLM, the modulator is a thin deformable mirror of the type described previously in this chapter. The Pockels effect in an electro-optic crystal is used in the MSLM.

Until very recently, both of these devices were sensitive to a "write" beam in the ultra-violet or x-ray part of the spectrum and relied upon photo-emission from the input electrode of the MCP itself. It was therefore considered important that the SLMs will be addressed by visible spectrum photocathodes.

A major constituent of all such photocathodes is one or more alkali metals, in particular Caesium (Cs). As these metals are highly reactive it is necessary to make and operate the photocathodes in vacuum.

The book by Sommer [1980] provides a valuable background to the subject of photocathodes and their production. The two simplest photocathode materials are the silver-oxygen-caesium (Ag-O-Cs) and the caesium antimonide (Cs_3Sb) compounds.

The Ag-O-Cs cathode is the only such material with an appreciable response in the red end of the spectrum, extending in fact into the infra-red. It therefore may be convenient to use this particular material if optical systems with several cascaded SLMs are planned. Devices made so far have been designed to modulate light of wavelength of 633nm. The Cs_3Sb cathode has a higher overall sensitivity peaking typically at about 350nm with a cut-off at about 700nm and is simpler in composition. However its widespread use may require using shorter wavelength illumination and redesign of other devices such as the guest-host LC SLM. Any other useful photocathode materials involve more than one alkali metal and more complicated processing.

An ultra-high vacuum chamber was designed as part of the project and constructed in the mechanical workshop of the Physics department. A UHV system was constructed around this for the construction and operation of photocathode addressed SLMs. Part of the chamber is used to evaporate the thin films to make a photocathode. It is then moved using a sample transfer

mechanism, also designed as a part of the project, to a different part of the system where it is joined to the light modulating component of the SLM.

The vacuum chamber can be evacuated to a pressure of about 10^{-9} torr and experiments have been conducted to make Ag-O-Cs photocathodes. The design of the sample transfer mechanism allows the simultaneous processing of four substrates in one pumping operation, thus reducing the time delay from repeated pumping cycles.

In future a number of interesting projects can stem from this system. Initially, a deformable mirror could be addressed by the photocathode. This may dispense with the MCP as a charge amplifier but would use a fine metal grid as the support structure. This approach has been suggested by Somers [1973] and would allow experience to be gained of the non-linear response through investigation of secondary emission processes.

Ultimately a very useful development would be to design a face-plate for a vacuum photo-diode. This may consist of a close-packed array of wires set in a vacuum-tight substrate. This faceplate would allow the interfacing of the photoemissive light sensor possessing useful transfer characteristics to a light modulator outside the chamber. This would greatly simplify device development and would open up new fields such as the possibility of a liquid-crystal device with photoemissive addressing. The details of such a device would require much deeper analysis, but the principle has already been demonstrated for a LC-screen oscilloscope (see Blinov [1983] page 308).

Chapter 4

Phase Modulation by a Liquid Crystal SLM

4.1. An introduction to liquid crystal technology.

Of the many light modulating mechanisms used in SLMs a great number use a liquid crystal (LC) as the modulation medium. This is perhaps because of the widespread use that LCs have seen in display technologies. For this very reason however, very little attention has been paid to the possibility of using a LC SLM as a pure phase modulating device.

The work already carried out in the Applied Optics group by Underwood [1987] on guest-host liquid crystal SLMs forms a useful basis for development of such a device.

There are many useful introductory texts to liquid crystals and their device applications. Elementary concepts are introduced by Bradshaw [1983] and Clark et al. [1980]. Goodman [1973] provides a deeper overview sufficient for

preliminary work to be based upon. De Gennes [1975] gives a very detailed account of the statics and dynamics of the LC states. Blinov [1983] concentrates on the details of the light modulating effects found in LCs.

This section of the thesis is a brief discussion of liquid crystal phenomena and terminology, with a leaning towards the envisaged application of a phase modulating SLM.

4.1.1. Elementary liquid crystal phenomena.

Liquid crystal mesophases

Liquid crystal is the name given to a class of materials which has a state possessing both the flow properties of liquids and the translational or orientational ordering of crystalline solids.

Many of these liquid crystal phases or *mesophases* are found for a particular LC material or *mesogen* only within a particular temperature range. These are referred to as *thermotropic* mesophases. *Lyotropic* mesophases are formed when the concentration of an isotropic solution of a mesogen is increased beyond a certain point. There are also *amphilic* compounds which can exhibit both thermotropic and lyotropic behaviour. Most device applications however use thermotropic LCs and it is to these that our interest will be confined.

The liquid crystal molecules all have the same characteristic rod shape: typically more than one aromatic ring group linked by hydrocarbon or other groupings. Particular chemical groups substituted onto to the chain cause their interesting physical properties which include optical anisotropies. In describing the behaviour of these molecules in a physical system it is useful to introduce the concept of the *director*. The director $\underline{D}$ is a unit vector whose direction represents the local preferred direction of the macroscopic properties of the LC. In many cases this coincides with the local time averaged orientation of the long molecular axis of the LC.

Within thermotropic LCs there are three main subclassifications which are

illustrated in Fig. 4.1.

Fig. 4.1 (a) shows the *nematic* mesophase in which molecular interactions favour a configuration with the director in the same orientation throughout the LC. In the absence of any external forces all the molecules of a nematic liquid crystal are expected to lie mutually parallel.

In the *cholesteric* mesophase of Fig. 4.1 (b), the molecules have a chiral structure which means that neighbouring molecules prefer a non-parallel alignment. This causes a helical twist of the director along a particular direction through the LC. The pitch of the helix, that distance over which the director twists through a complete turn, is typically in the optical wavelength range. Note that there is no translational ordering in this phase. The distinct helices in the figure have been drawn for convenience but have no physical significance.

Other thermotropic mesophases are all described as *smectic*. These mesophases all possess some translational ordering in addition to directional ordering and their subclassifications are labelled from A through to K. It is not proposed to distinguish these here, but simply to note their common properties. The molecules form layers of a thickness of 2-3 nm comparable to the molecular length. Particular mesophases may or may not have translational ordering within the layer. In the particular example of the smectic-A (S_A) mesophase shown in Fig.4.1(c), the molecules all lie perpendicular to the layer but are not ordered within it.

As nematics are uniaxial birefringent materials it is likely that these can be used as the phase modulating medium in the SLM. All of the liquid crystal research applied to SLMs in the Applied Optics group has so far been concerned with nematics. Therefore the remainder of this chapter will concentrate on nematic liquid crystals, building upon the existing experience to produce a device with phase modulating potential.

It should be observed that future developments may involve the use of smectic LCs. These have the advantage of faster switching than nematics, and of bistablity. However their complex electronic drive requirements make them unsuitable for use with the LCIC chip.

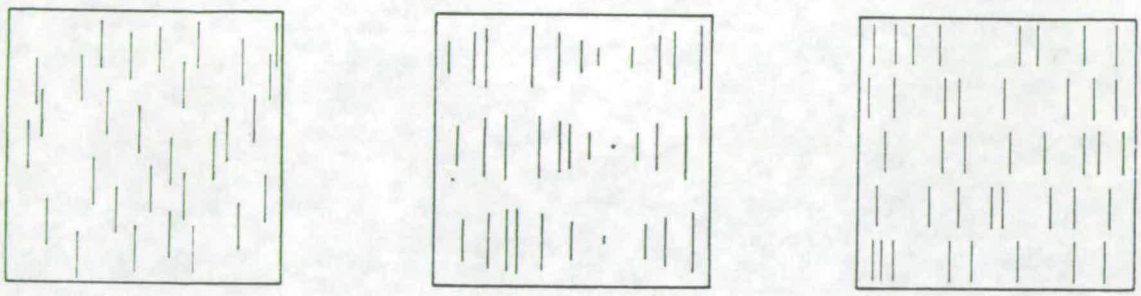

(a) Nematic (b) Cholesteric (c) Smectic-A

Fig 4.1 Liquid crystal mesophases

Fig 4.2 A liquid crystal cell

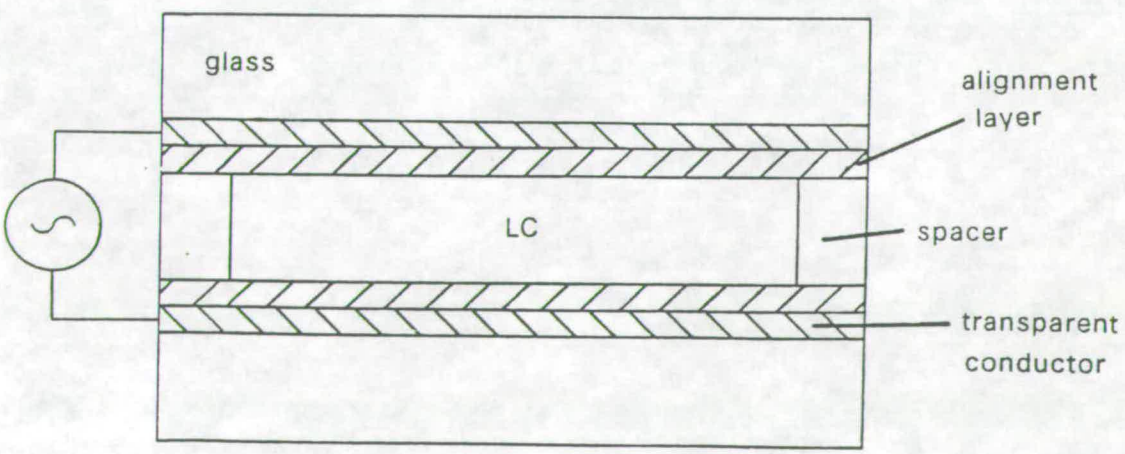

4.1.2. Properties of the nematic mesophase.

We have noted that in nematic liquid crystals the molecules tend to lie parallel to one another in the absence of external forces. To understand the useful properties of these materials, we must also consider their anisotropic nature.

Dielectric anisotropy

A uniaxial medium, of which a nematic liquid crystal is an example, has properties which vary with direction and can be defined by measurements made parallel and perpendicular to a single preferred direction (the director in the case of the LC). Of particular importance in LC studies is the dielectric permittivity having values $\varepsilon_{parallel}$ and $\varepsilon_{perpendicular}$. The dielectric anisotropy, $\Delta\varepsilon$, is defined as

$$\Delta\varepsilon = \varepsilon_{parallel} - \varepsilon_{perpendicular} \qquad (4.1)$$

and describes how the liquid crystal interacts with an external electric field.

When an electric field is applied to a LC, the electric dipoles of the molecules will tend to align to maximise the relative permittivity in the direction of the field.

For LCs of *positive dielectric anisotropy* ($\Delta\varepsilon > 0$), the director will align parallel to the field.

For LCs of *negative dielectric anisotropy* ($\Delta\varepsilon < 0$), the director will align perpendicular to the field.

This makes it is possible to induce a realignment of a liquid crystal by application of an electric field. The following consideration of the structure of a typical liquid crystal cell clarifies how the molecular interactions and electric field realignment of dipoles combine to produce this useful effect.

Liquid crystal cells

A typical LC cell is illustrated in Fig. 4.2. It consists of a thin layer of LC held between two rigid boundaries, such as glass plates. The inner surfaces of the plates are coated with transparent conductive layers to which the electrical signals are applied. The surfaces also have an alignment layer which determines the static configurations of the LC molecules. The plates are separated by a spacer which determines the thickness of the LC layer (perhaps 5–50μm).

Homogeneous and homeotropic alignment

The alignment of the LC molecules in the cell determined by the treatment applied to the surfaces of the rigid boundaries is usually approximated by one of two configurations:

homogeneous alignment where the director everywhere lies parallel to the cell walls.

homeotropic alignment where the director everywhere lies perpendicular to the cell walls.

A summary of the great many materials and mechanisms used to obtain these alignments is presented by Castellano [1983].

Consider now the effect of applying an electric field to the LC between the two electrodes. Note that it is usual to apply an alternating field as a dc voltage will eventually lead to electrolytic decomposition of the liquid crystal.

The reorientation can be induced for either a homogeneously aligned LC with a negative $\Delta\varepsilon$ or a homeotropically aligned LC with a positive $\Delta\varepsilon$. In both cases the field will tend to realign the molecules against the restoring influence of the intermolecular forces to a new configuration of minimum free energy. If the field is removed, the intermolecular forces cause the crystal to relax back to its original configuration. Thus it is possible to change the orientation of the LC molecules by large angles of up to 90° by application of a suitable voltage.

It is appropriate at this point to make several general comments regarding cell voltage and thickness and the amount of reorientation or change in *tilt angle* of the molecules. The phenomena described are also discussed in many texts such as on pages 107–110 of the book by Blinov [1983]. Firstly it should be observed that there is a voltage threshold usually no more than 1V, below which no change in tilt angle occurs. Secondly the tilt at a certain fractional distance through the cell depends on the voltage applied and not on the thickness.

4.1.3. Electro-optic effects in liquid crystals.

Having established in the last section that it is possible to reorientate a LC by application of an electric field, the ways in which transmitted light can be modulated by the LC will now be examined. In general this involves anisotropy of optical properties of the LC such as its refractive index or absorption. In this section some of the more commonly encountered nematic effects are assessed as phase modulating effects. A more complete account of LC electrooptic effects is given by Blinov [1983].

Field-induced birefringence (FIB)

The first effect relies purely on the *birefringence* or anisotropic refractive index of the LC. The director orientation for voltages above and below threshold is illustrated in Fig. 4.3. With no applied voltage the LC is in the homogeneous state with all the molecules lying mutually parallel. Application of a voltage, for a LC with positive dielectric anisotropy, causes the director to rotate towards the cell normal. There is an analogous effect for homeotropically aligned, negative $\Delta\varepsilon$ LCs.

Fig 4.3 The field induced birefringence effect (FIB)

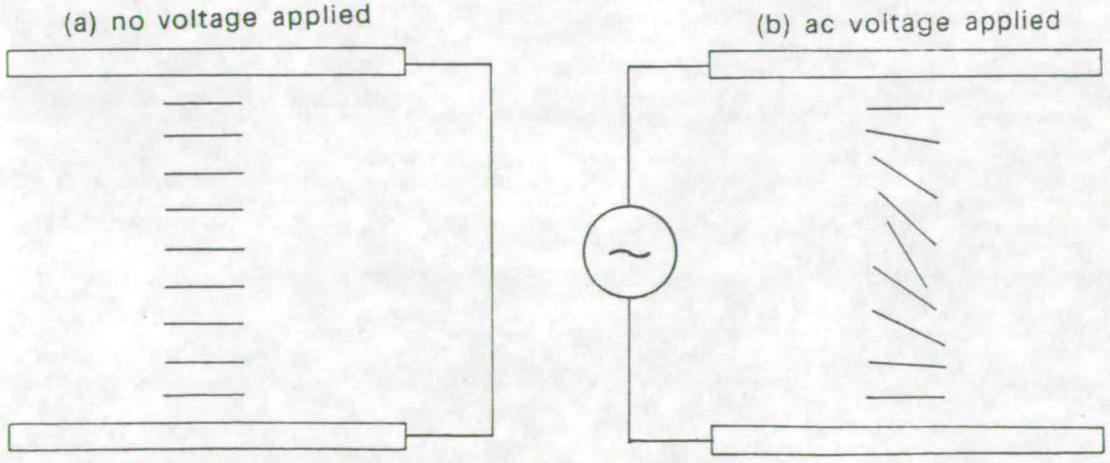

Light modulation is acheived through a difference between the components of the refractive index of the LC parallel and perpendicular to the director, averaged along the propagation direction through the LC. This difference, the birefringence Δn, is typically 0.2 to 0.3.

If normally incident light is linearly polarised at 0° to the director then it experiences a phase modulation depending on the value of the birefringence and the cell thickness. As the absorption of light is usually isotropic within the LC this mechanism will produce a pure phase modulation.

Alternatively, if the light is polarised at a non-zero angle θ to the director then the ordinary and extraordinary components experience a relative phase difference on passing through the cell and the light transmitted though an analyser is intensity modulated. The angle θ is 45° for best contrast.

This is one way of obtaining a pure phase modulation using liquid crystals. It has the added advantage that it can be reconfigured to give intensity modulation. There are many other LC effects in nematics which can give intensity modulations which are better than can be expected from this effect. These will now be examined to decide whether they are suitable for pure phase modulation also. The main criterion remains the capacity for a pure phase modulation. If this cannot be acheived in the other effects then they will not be suitable for this project.

Twisted Nematic (TN) effect

By twisting the cell boundaries of a homogeneously aligned nematic LC layer it is possible to induce a helical twist to the director through the layer. Such a twisted structure exhibits a phenomenon similar to optical activity - it rotates the plane of polarisation of incident light by the twist angle. Whether this rotation occurs in a particular case depends on Mauguin's condition:

$$\lambda << \Delta n \, P_o \qquad (4.2)$$

being satisfied. Δn is the birefringence and P_o is the pitch of the helix (see Blinov [1983] p.126). In the conventional twisted nematic effect the LC

alignment is arranged to give a twist of 90° and is placed between parallel polarisers. The incident light linearly polarised parallel to the director is rotated through 90° as described above and no light is transmitted by the analyser.

When a voltage is applied to the cell, the LC in the central part is realigned into an isotropic orientation. Twisted regions remain at the cell boundaries but their pitch is now too low to satisfy Mauguin's condition and the optical activity is lost. The light emergent from the cell is polarised in its original direction and is therefore transmitted by the analyser.

The TN effect does not depend intimately on the cell thickness as does the FIB effect. Therefore more uniformly transmitting cells are to be expected.

However this effect is not suitable for this project for the following two reasons. The TN effect is incompatible with the opaque silicon backplane because it does not operate in a reflecting mode. This is because the polarisation rotation is reversed during the second pass through the LC and high transmission is observed for all voltages. Intensity modulation can only be acheived in reflection by using the LC birefringence in precisely the same way as for the untwisted case described earlier. Thus the reason for considering the effect at all, improved intensity modulation, is invalidated.

Secondly it is not certain that a pure phase modulation can be produced with the twisted nematic structure. In the low voltage condition incident light polarised parallel to the director will experience the extraordinary component of the refractive index of the LC. For a high voltage, when the director has been realigned, it is the ordinary component of the refractive index that is observed. A continuum of intermediate refractive indices is expected for the intermediate voltages as in the FIB effect.

However it is possible that a significant intensity modulation would be introduced into such a system. In particular, in the higher voltage regime where the optical rotation has disappeared, the thin twisted LC layer at the reflecting boundary may introduce elliptical polarisation states. Compare this with the Hybrid Field Effect described below.

To summarise, this effect is rejected because the intensity modulation in a

reflecting device can be no better than for a simple FIB cell. The phase modulation can certainly not be improved over the FIB effect and may indeed be less good.

The Hybrid Field Effect (HFE)

This effect uses a modified twisted nematic structure where the twist angle is 45° to enable intensity modulation in reflection. It is used with an input polariser parallel to the front-surface director and a crossed analyser. The effect was developed for the Hughes LC light valve, described in chapter one, by Grinberg et al. [1975]. It relies on the twisted nematic effect to produce its "off" state and birefringence to give its "on" state. For zero voltage, transmitted light is optically rotated on its first crossing of the cell and is restored to its original polarisation after its second pass. The analyser blocks all of this light. At higher voltages, the central part of the cell becomes isotropic. All of this is very similar to the simple TN effect. The difference is the birefringent LC layer aligned by the reflecting cell boundary at 45° to the incident polarisation direction. As there is no polarisation rotation, the light arrives at the reflecting boundary polarised at 45° to the director of the LC. This is the angle which maximises the effect of the birefringence. Depending on the thickness and birefringence of this layer, both of which are voltage dependent, the light will emerge in general in an elliptical polarisation state. Thus the transmission will go through cycles of high and low transmission.

The HFE has found use in place of the TN effect for reflecting devices and it has a faster switching speed relative to TN. Its "off" state transmission is more uniform and lower than for a FIB cell as it does not depend closely on the thickness uniformity. This gives a much better contrast. The uniformity of the "on" state transmission still depends strongly on the uniformity of cell parameters such as the LC thickness.

Despite its better intensity modulation, this effect also must be excluded from the project as a phase modulator. It is inherent to the HFE that it cannot produce a pure phase modulation. At voltages for which the polarisation rotation does not occur, the polarisation direction of incident light must be at a large angle to the director of one of the birefringent layers. Thus in general

elliptically polarised light will always emerge.

The Guest-Host Effect

This is the effect used by Underwood [1987] in the prototype amplitude modulating SLM developed in the Applied Optics group. It is an intensity modulating effect and is included here for completeness.

A guest-host LC is a nematic LC (the host) to which has been added a dichroic dye (the guest). The dye molecules lie at a particular angle to the director of the host LC and have an anisotropic light absorption coefficient. Thus voltage dependent transmission curves of the GH mixture are observed.

4.1.4. Conclusion– the selection of a LC effect for a phase modulating SLM.

The major requirement for the effect chosen is that it should exhibit a high dynamic range of phase modulation, but with little associated modulation of the amplitude of transmitted light.

Based on this premise, the FIB effect seems to be the best of those discussed previously. Any amplitude modulation observed as a part of the effect would be due to absorption anisotropies of the LC. According to Wu et al. [1984] these are negligible.

The TN effect was excluded because it does not give us any advantage over the FIB effect when used in a reflecting cell. The HFE effect was excluded on the grounds that the twisted LC is likely to introduce elliptical polarisation and cause a strong intensity modulation. Indeed this is precisely the mechanism upon which the effect relies.

It should be possible to reconfigure a FIB device as an amplitude modulator between polaroids at 45°. Apart from increasing the applicability of the device this may be a useful for its initial assessment without the complication of Schlieren imagery.

In the second part of this chapter, the FIB effect will be evaluated in more detail by experiments on liquid crystal test cells.

4.2. Liquid crystal test cells.

It was proposed in the previous section to construct a LC SLM using the field-induced birefringence effect. The main aim of this is to produce a pure phase modulating device, but it is anticipated that intensity modulation will be acheived in the same device.

Before fabricating the device it is necessary to conduct some preliminary investigations on the theory and practice of the FIB effect in test cells. This will allow us to assess and optimise the performance of the device

4.2.1. A model for intensity and phase modulation by a FIB cell.

Let us recall the light modulating mechanism in a parallel nematic cell. There is a preferred direction in the cell defined by the director of the LC. When there is no applied voltage the LC molecules lie parallel to the cell walls and light polarised parallel and perpendicular to the director sees the extraordinary and ordinary components of the refractive index n_e and n_o respectively. As the rms voltage across the cell increases the molecules are realigned towards the homeotropic configuration and the refractive index seen by the light polarised parallel to the director at the front face approaches n_o. Thus the cell behaves as a birefringent plate with a fixed ordinary component of refractive index and a voltage-dependent extraordinary component, continuously variable between n_o and n_e.

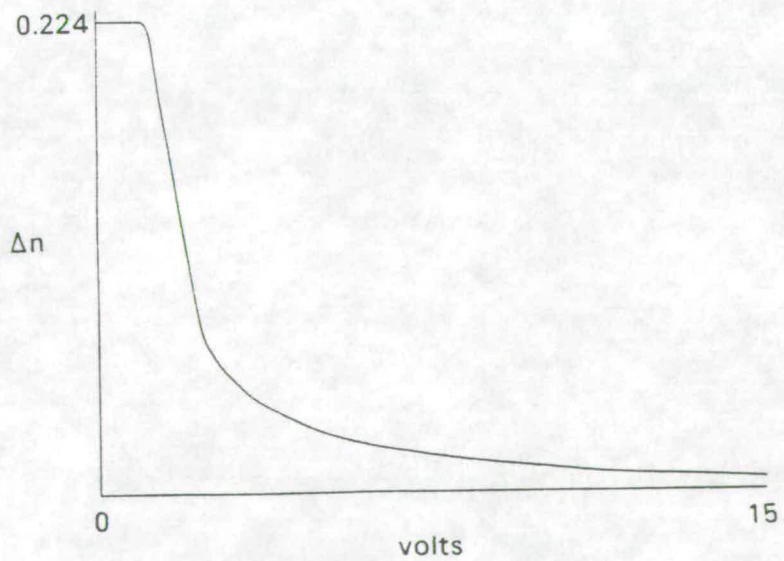

Fig 4.4 Birefringence of BDH E7

Fig. 4.4 shows the form of the birefringence against voltage curve. This has been drawn with data extracted from the paper by Wu et al. [1984]. This applies to BDH E7 liquid crystal for light of wavelength 633nm which will be used in the following experiments.

This birefringence retards the relative phase of the extraordinary component of light by an amount $\delta(V)$ where

$$\delta(V)= kd\Delta n(V) \tag{4.3}$$

where d is the thickness of the LC through which the light propagates and k is the wavenumber of the light.

Intensity modulation

The light intensity I transmitted through a birefringent plate between crossed polarisers at 45° to its optical axis is

$$I=I_o\sin^2(\delta/2) \tag{4.4}$$

The analogous result for uncrossed (i.e. parallel) polaroids at 45° is

$$I=I_o\cos^2(\delta/2) \tag{4.5}$$

These results are derived in appendix 1.

Combining the data presented in Fig 4.4 with these three equations permits calculation of the voltage dependence of the transmission of a cell between polaroids.

Fig 4.5. (a) shows the behaviour calculated for a 12μm thick cell between crossed polaroids. At the high voltage part of the graph where isotropic behaviour of the LC is observed the transmission is low as expected. As the voltage is reduced the LC relaxes towards the parallel orientation and the birefringence increases. The right-hand maximum on the transmission curve corresponds to a value of $\delta=\pi$. As the voltage is decreased further towards

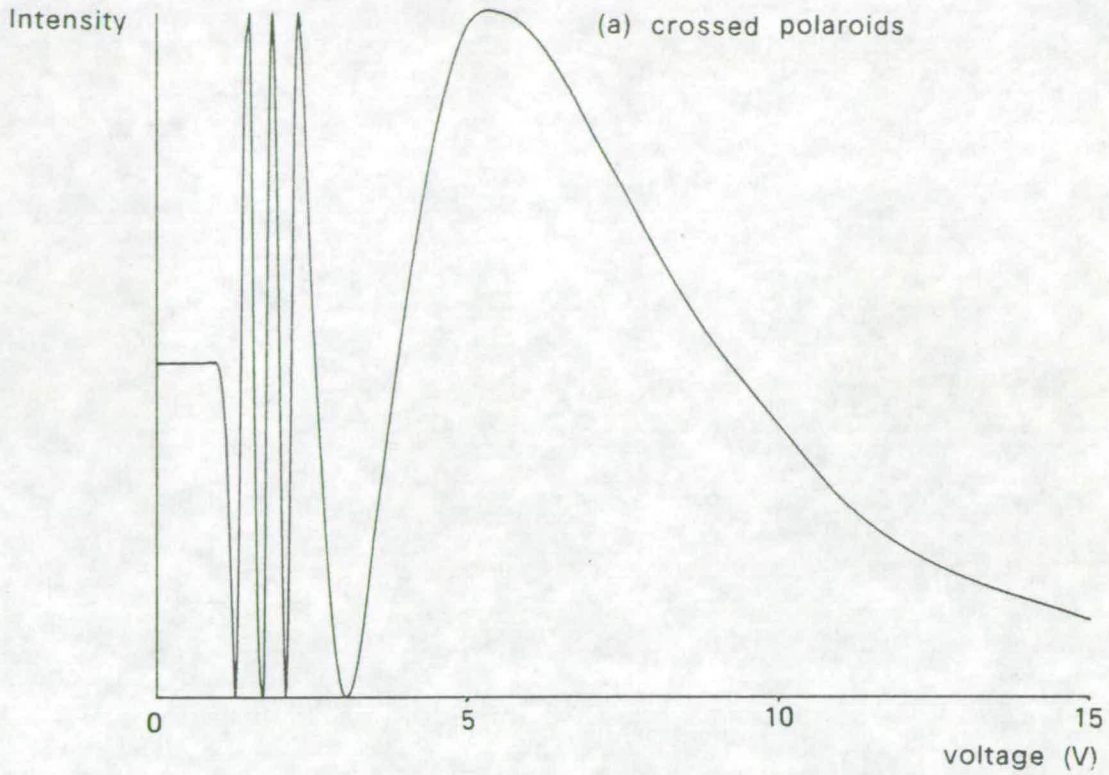

Fig 4.5 Calculated transmission curves (FIB)

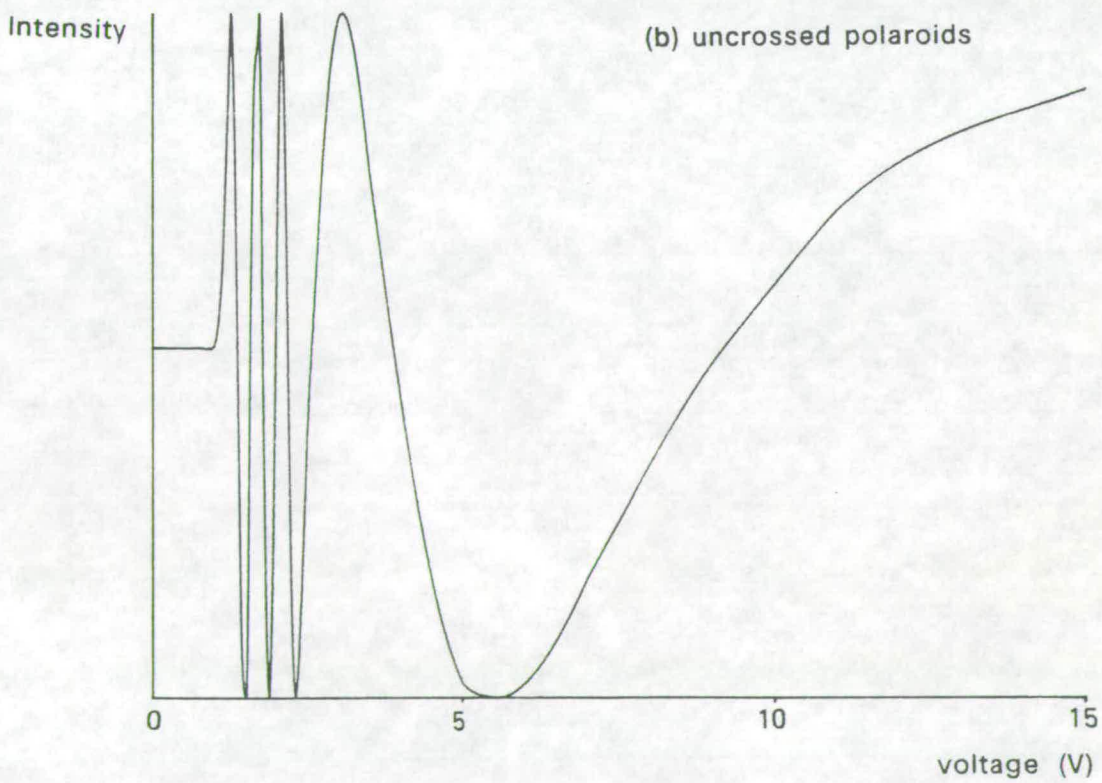

zero the transmission changes between maximum and minimum values, each extremum corresponding to a further increase of π radians to the phase difference δ. The intensity value at zero volts will depend on the thickness and maximum birefringence of the liquid crystal. Fig. 4.5 (b) shows the complementary transmission curve for parallel polaroids.

Phase modulation

When the light incident on the cell is polarised parallel to the extraordinary axis, transmitted light is phase modulated by an amount depending on the voltage. This phase modulation is precisely the same as the relative phase difference introduced between the e- and o- components for intensity modulation. The phase δ of the transmitted light (relative to the value for $\Delta n = 0$) is therefore

$$\delta(V) = kd\Delta n(V) \qquad (4.6)$$

and of course has the same form as the birefringence curve Fig. 4.4.

Sources of deviation from ideal behaviour

According to Wu et al. [1984] the effect of LC pre-tilt and absorption anisotropy are likely to be insignificant.

It was commented in section 4.1.3 that a twist of the LC through the cell may have the effect of introducing an unwanted intensity modulation where pure phase modulation is required. This would occur through a mechanism similar to the HF effect where the twisted birefringent layer introduces elliptical polarisation. However, for small twists the ellipticity should not great and the deviation will be tolerable.

Non-uniformities of cell thickness will drastically affect the cell transmission uniformity as the phase difference is proportional to this thickness. Similarly any non-uniformities in the cell voltage will be significant especially in the regime just above threshold where δn changes rapidly with

voltage.

4.2.2. The construction of test cells.

The structure of the test cells used in the experiments is illustrated schematically in Fig. 4.2 earlier in the chapter.

3mm thick float glass was supplied by the Technical Glass Co., with a transparent conducting coating of indium tin oxide (ITO) on one surface of nominal resistance 200Ω per square. An aluminium layer is evaporated along one edge of each plate to provide a good electrical contact. The LC is aligned in the homogeneous configuration by an obliquely evaporated layer of magnesium fluoride (MgF_2) having an approximate thickness of 150–200nm. The evaporation of the thin-film layers for the test-cells and for the SLMs themselves was done with the technical assistance of Eric Davidson and Andrew Garrie.

Polyester strips of nominal thickness 12μm were placed along the long edges of the cells to act as spacers. The plates were clamped together above the spacers by two "bulldog clips".

The liquid crystal used in the test cells was the nematic E7 supplied by BDH Ltd. It was introduced into the cell either before the top plate was put into place, or afterwards using capilliary action to draw the LC into the cell.

At all times during cell construction care must be taken to avoid any contamination. Dust or grease can disrupt the LC alignment, affect cell thickness or cause short circuits between the electrodes. Construction of the cells was carried out in a laminar flow cabinet and gloves were worn whenever cleaned components were handled.

4.2.3. The liquid crystal testing apparatus.

The experimental apparatus used to examine the LC test cells is illustrated in Fig. 4.6. This is similar to that reported by Vass et al. [1986] for investigation of twisted nematic cells and Underwood [1987] for guest-host cells.

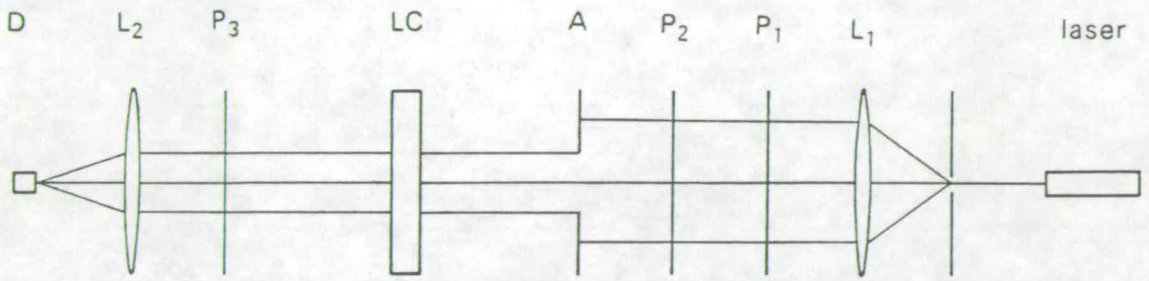

Fig 4.6 LC test-cell apparatus - optical system

Fig 4.7 LC test-cell drive circuit

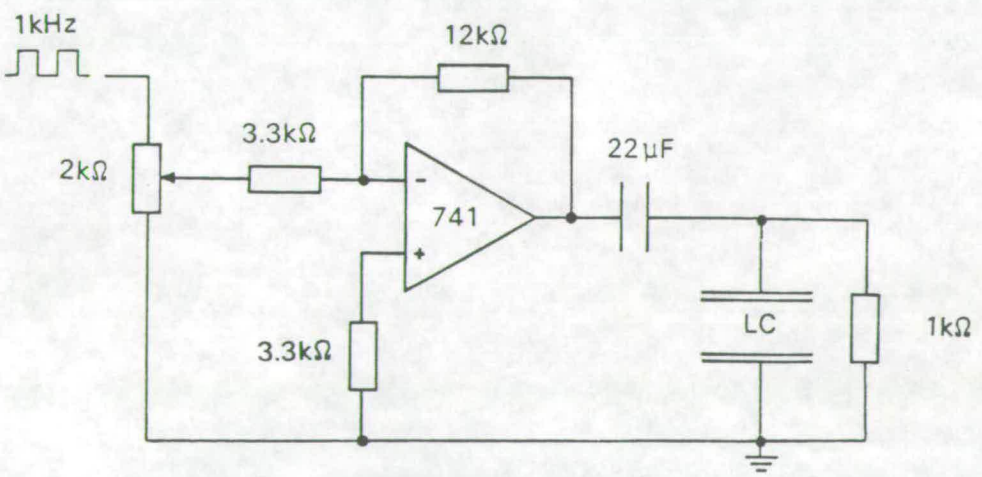

Light from the 10mW HeNe laser is collimated by lens L_1. The intensity, polarisation direction and width of the light beam incident on the LC cell (LC), is controlled by the polarisers, P_1 and P_2, and iris diaphragm A. Any light transmitted by the analyser P_3 is focussed by lens L_2 onto the photodetector D.

The extinction (ratio of maximum to minimum transmission) of the polariser/analyser pair (i.e. P_2 and P_3) was measured to be greater than $4x10^3$.

The circuit used to drive the LC cell is shown in Fig. 4.7. Adjustment of the position of the wiper of the 2kΩ potentiometer applies a fraction of the 1kHz square wave voltage to one electrode of the LC cell through a fixed gain amplifier and a dc blocking capacitor. The other electrode of the cell is held at earth potential.

The experiment is automated by using a BBC microcomputer to drive a stepper motor which sets the potentiometer to one of 480 positions.

The output of the photodetector, which is a RS photodiode with integral amplifier, was measured by the analogue port of the BBC.

The computer is used to set the cell voltage and measure the corresponding light transmission over a range of voltages. The settling time between each measurement is usually set to a value between 0.25s and 1s

4.2.4. Measurements on parallel nematic test cells.

Transmission against voltage

The apparatus described above was used to measure the transmission of the test cells with incident light polarised at 45° for crossed and uncrossed polaroids. The polaroids were initially crossed by minimising the output of the photodetector. The liquid crystal cell was introduced to the system and its orientation adjusted, for zero cell voltage, to maximise light transmission. This gives the required arrangement.

A set of typical transmission curves measured by the microcomputer is

shown in Fig. 4.8 (a) and (b) for crossed and uncrossed polaroids respectively. The general trend shown by the curves is the expected pattern of mutually complementary maxima and minima similar to Fig. 4.5.

It was often observed in practice that the extreme values of the curves are not all the same, the discrepancy being greater at lower voltage values. This is consistent with wedging of the cell producing a greater spread of phase differences and thus transmissions at these voltages where the birefringence values are larger.

In some instances, such as illustrated here, the transmission values for a voltage of about 3.5 volts corresponding to $\delta=2\pi$ are not explicable by this argument. These were found for particular regions of all of the cells. It is significant to note that the same effect was observed by Vass et al.[1986] for twisted E7 cells of the same thickness at the same voltages. It may be hypothesised that this is due to regions of the cell being twisted because of imperfect LC alignment. This effect can also be observed in the experimental data presented by Blinov [1983] p.122 showing transmission against voltage for a 55µm 2.v cyanophenyl ester LC. Although this is not commented upon, the minimum of least good extinction corresponds to a 2π phase retardation. It is not intended to investigate this in detail but to note the possibility of anomalous behaviour of SLMs in this particular voltage regime.

Ellipticity

In using the FIB effect to produce a pure phase modulation it is important that incident plane polarised light emerges in the same state. Otherwise elliptically polarised light will produce an intensity modulation if there is any polarisation analysing component in the system. Without any analyser this is still undesirable as it means that the two orthogonal polarisation components have been phase modulated by different amounts. For this reason, it is important to know to what degree it can be expected that the transmitted light remains plane polarised in the original direction.

This was investigated experimentally by arranging that the incident light to test cells was polarised parallel to the director at the front face. The light

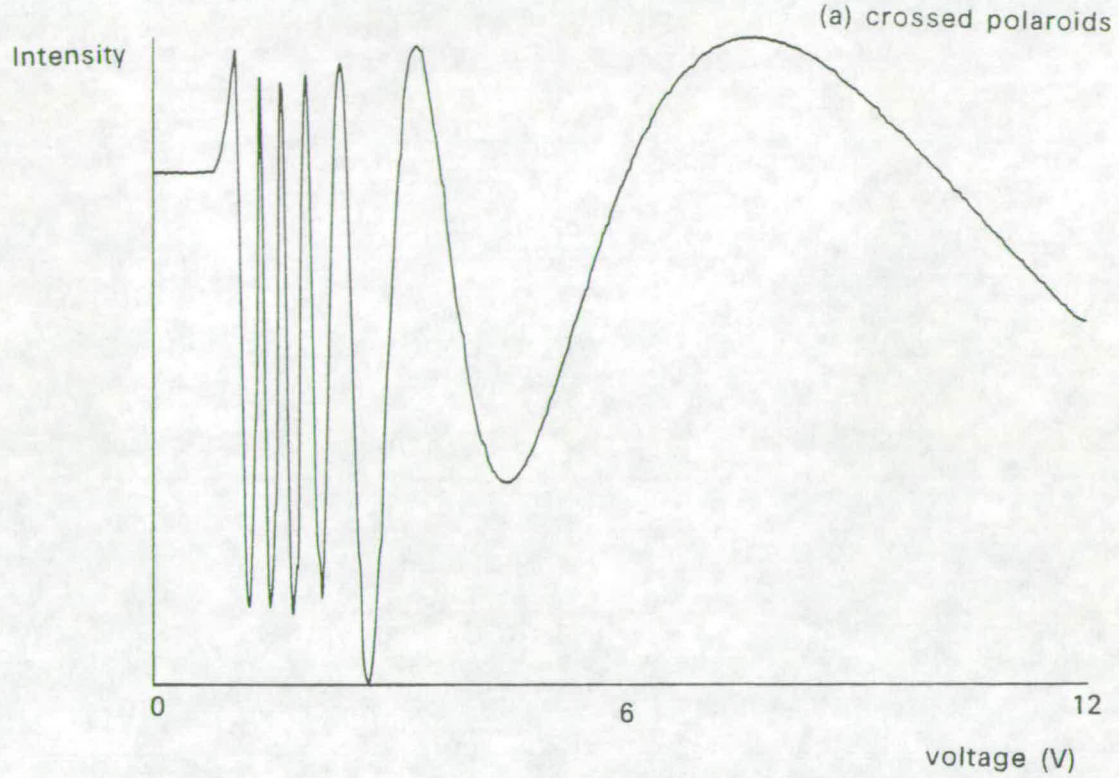

Fig 4.8 Measured transmission curves

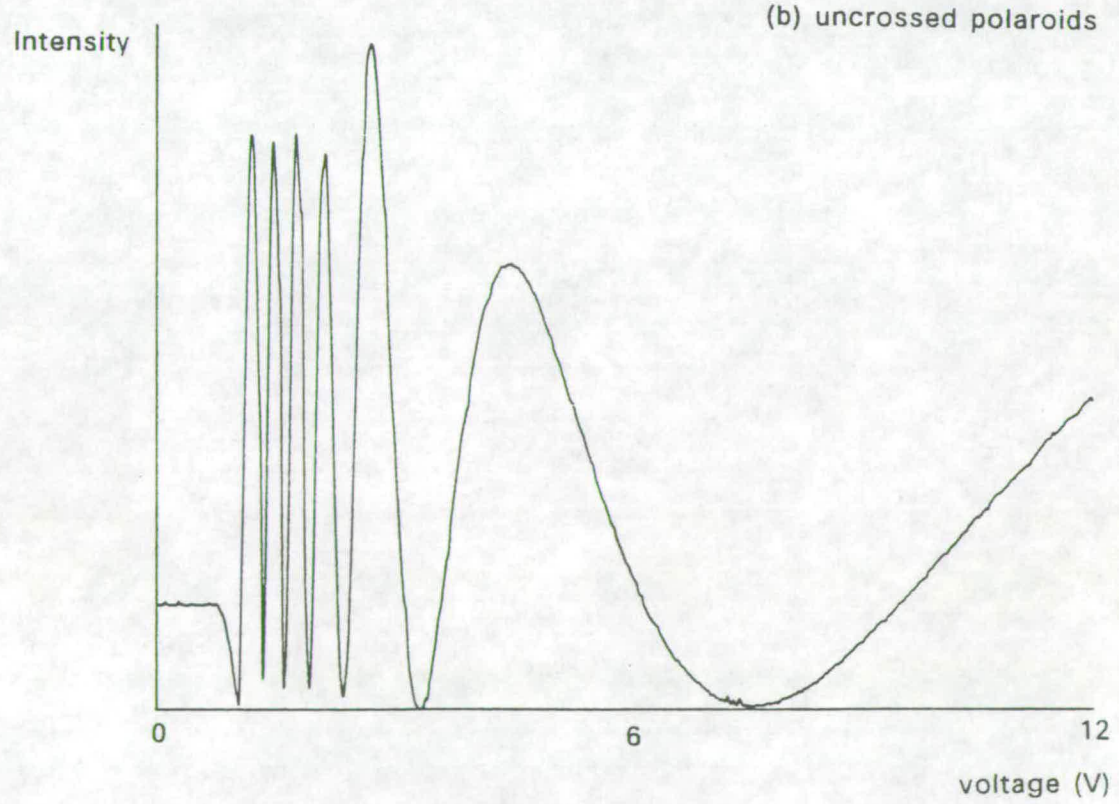

transmitted by a crossed analyser was measured by the photodiode over a range of voltage values. The orientation of the components was arranged by first crossing the polarisers and then adjusting the LC cell for a minimum of transmission when no voltage is applied.

It was found that the light transmitted by the crossed analyser was never more than about four percent of the incident light. This gives an indication of the amount of intensity modulation to be expected from SLMs when used as phase modulators.

Scattering effects

Fig. 4.9 illustrates the scattering phenomenon observed when the voltage is raised over a wide range (0V to 10V over two seconds).

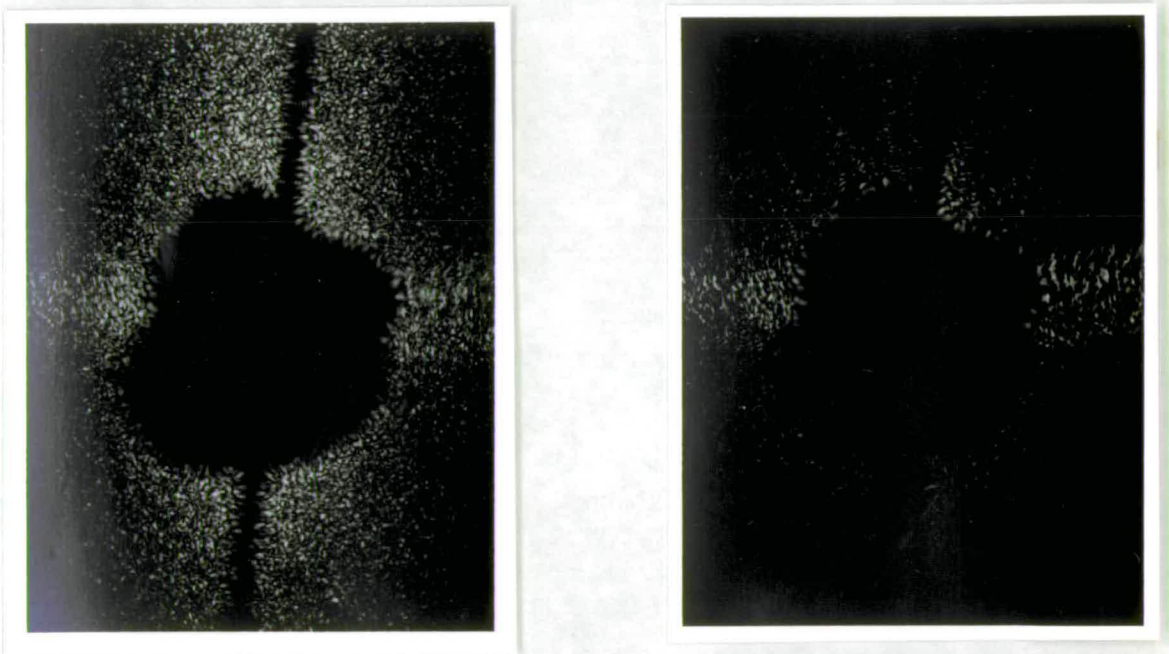

(a) (b)

Fig 4.9

Fig. 4.9 (b) is a photograph of the ambient transmitted light for 0 volts with the bright centre portion removed. This is done to exclude the possibility of this light scattering within the film. Fig. 4.9 (a) shows the large amount of light

scattered around the stop during switching. It was observed that only light polarised in the extraordinary direction is scattered. Blinov [1983] comments of page 122 of his book that back-flow of the LC is responsible for scattering and depolarisation of light when the cell voltage is rapidly increased. This scattering would seem to be occuring in this case and raises the question of whether dynamic depolarisation effects would be an alternative cause of the anomalous transmission values described earlier.

Further investigation confirmed that the light transmission at the $\delta=2\pi$ region was not due to any dynamic effect in the liquid crystal. Static transmission measurements in this range yielded the same peak value as in the earlier scanning measurements.

Preliminary switching investigation

A prototype SLM will have a binary mode of operation. For intensity modulation the two values of transmission should have as high a ratio as possible. For phase modulation the two states should correspond to relative phase differences of $(2n+1)\pi$ radians. Both of these conditions are realised by switching between a local maximum and a local minimum of curves in Fig. 4.8.

It is important to know the switching time between the states of interest to allow evaluation of the potential framing rate of a device. The apparatus of experiment 1 was altered to permit evaluation of these parameters.

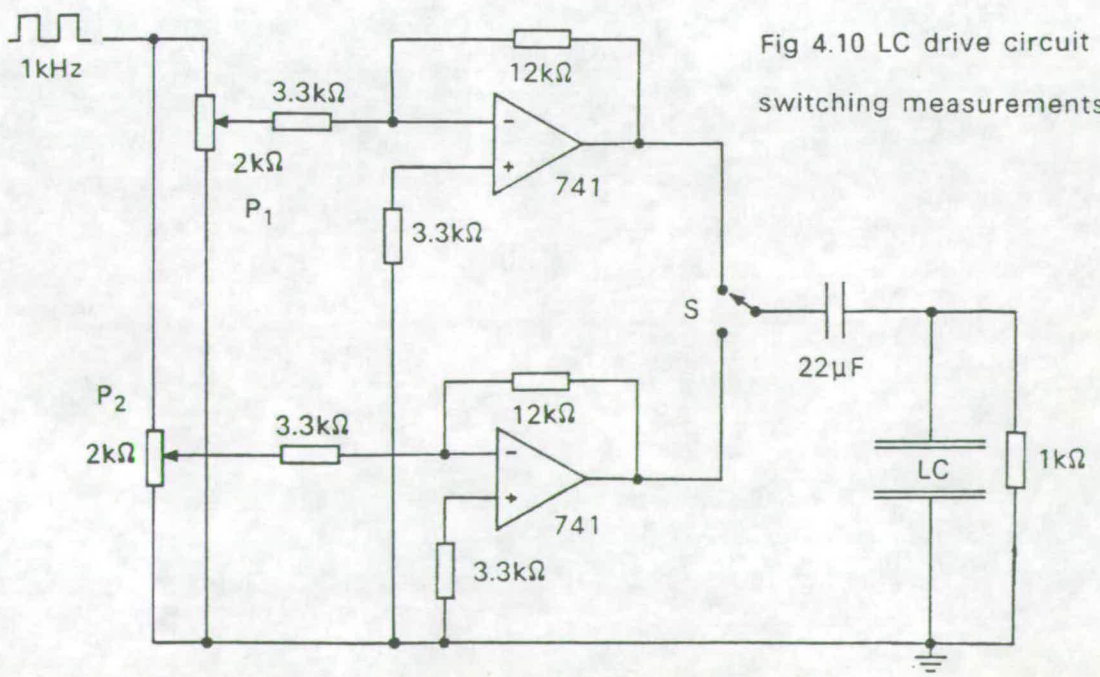

Fig 4.10 LC drive circuit - switching measurements

The amended drive circuit is illustrated in Fig. 4.10. It consists of two of the circuits used in expt. 1 in parallel. The output of one of these is selected by the mechanical switch S to drive the LC cell. The magnitude of the driving voltage for either position of the switch is selected by manually setting the potentiometers P_1 and P_2. The voltage across the cell is monitored by one trace of a dual-trace storage oscilloscope. The output of the photodiode is displayed on the second trace of the scope. The optical arrangement of the apparatus is exactly as in previous experiments as shown in Fig. 4.7.

As a preliminary experiment the voltage levels were set to be 0V and 10V amplitude. The polaroids were crossed at 45° to the LC director. Fig. 4.11 (a) and (b) are photographs of the oscilloscope traces observed when the voltage is raised and lowered respectively between the two values. Note that the time base settings of the oscilloscope differ by a factor of ten. From these it can be seen that the cell responds perhaps thirty times more slowly to the decreasing voltage signal. Therefore it is on this part of the switching process that attention must be concentrated to optimise the device speed.

The cell used in the following experiment is the same one used earlier for the static transmission measurements to allow the best possible comparison. The upper voltage applied to the cell was increased to 12V, the largest that could be obtained from the existing electronics.

Fig 4.12(a) is a photograph of the oscilloscope trace after the voltage is switched from 12V to 0V. The upper trace represents the cell voltage: the 12V signal is observed at the extreme left-hand edge just before switching. The lower trace shows how the light transmission of the cell evolves with time after the voltage is switched. The time base of the scope was chosen to accomodate all of the main features of the trace in the screen. The width of the screen represents a time of about 1s.

It is instructive to compare this trace to the measured transmission curve Fig. 4.8(a). This has been redrawn as Fig. 4.12(b) with a reflection in a vertical axis to allow easier comparison with the trace.

The features of the trace and curve can be matched up point by point giving information about the speed at which the liquid crystal has relaxed through the orientations observed in experiment 1. (If the time base were

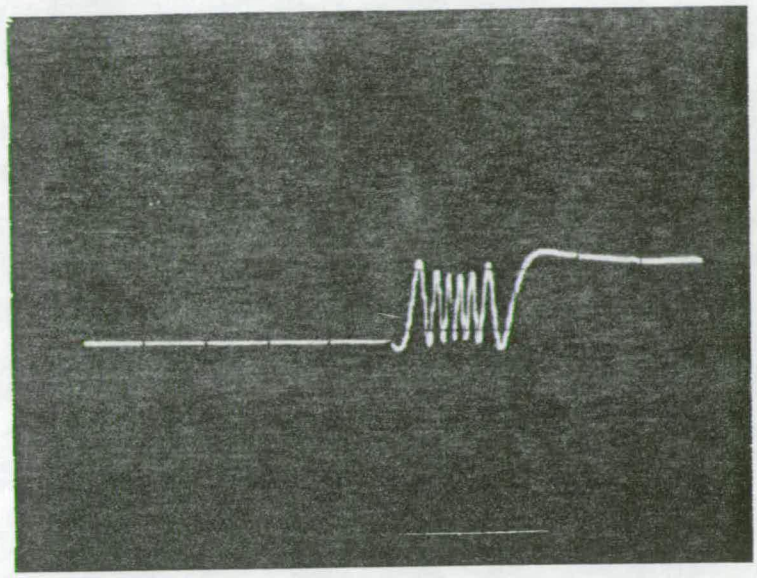

(a) 0V–10V (time base – 20 ms/div)

Fig 4.11 Oscilloscope traces – LC switching

(b) 10V–0V (time base – 200 ms/div)

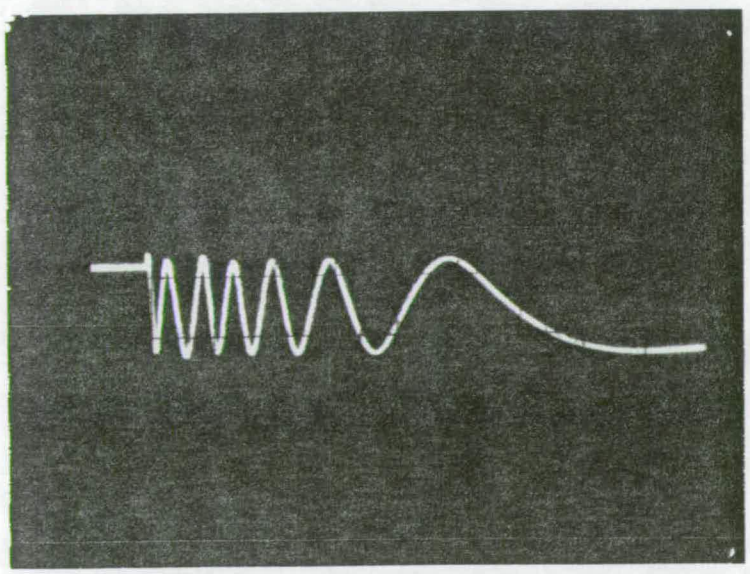

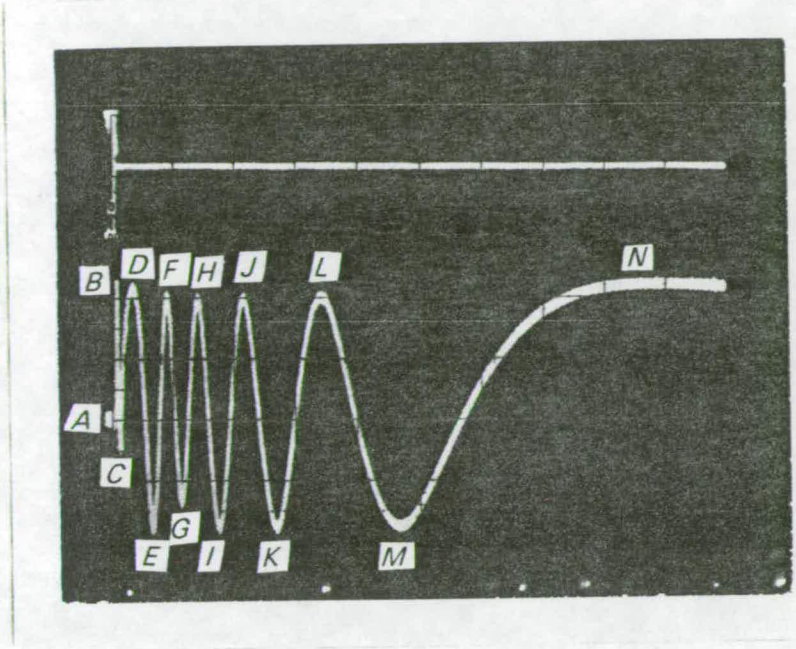

(a) Oscilloscope trace – 12V–0V

Fig 4.12

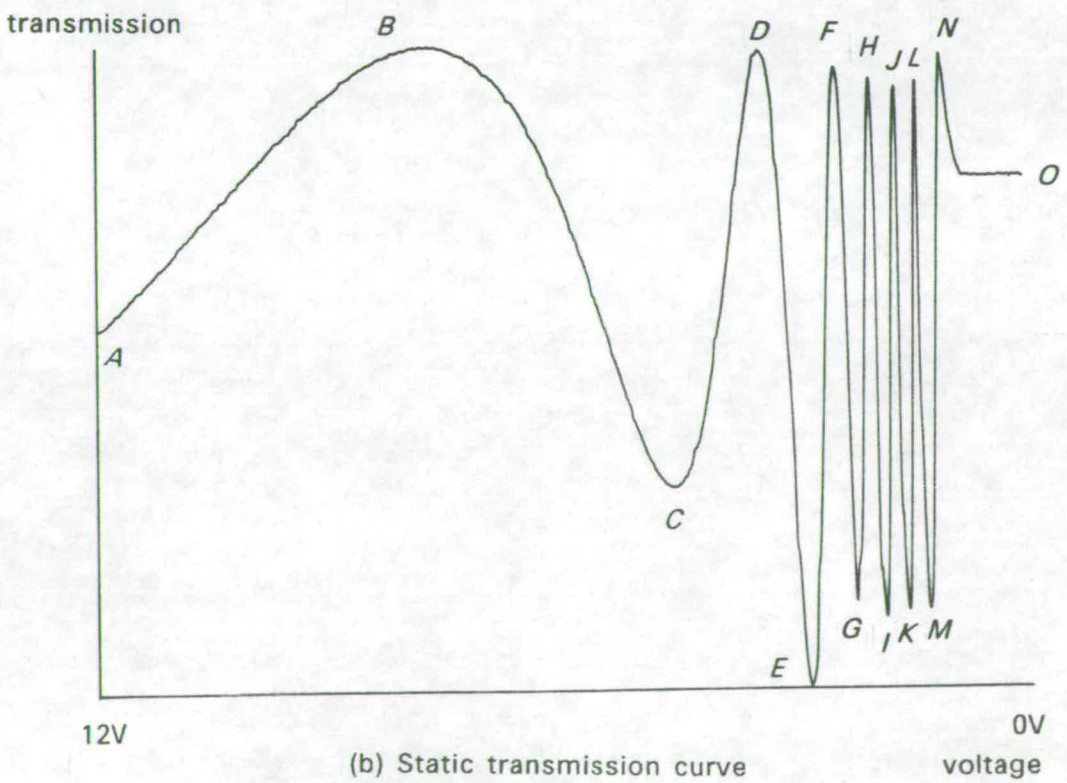

(b) Static transmission curve

slowed down it would be seen that the trace beyond the final maximum labelled *N* would tend to a value corresponding to *O* on the transmission curve.)

The extent to which Fig. 4.12(a) has been compressed relative to Fig. 4.12(b) gives an indication of the switching speed of the LC for different amounts of deformation of the LC structure.

Thus a device which has the fastest switching time would be operated between points *A* and *B*, or points *B* and *C*. Note that points *A* and *C* as observed in expt 1, do not have a good extinction of light. However high contrast has been acheived by using parallel polaroids and making the point *B* into a minimum with a low transmission. Note that the higher the maximum driving voltage, which determines the intensity at *A*, the better the contrast would be.

Switching times and contrast ratios

The storage oscilloscope was used to measure the light transmission of the cell after the voltage was switched in either direction between values corresponding to neighbouring extrema of transmission. This was done in the high voltage regime of the cell where it is expected to operate most quickly.

Fig. 4.13 shows the traces obtained when switching between points *A* and *B* of the transmission curve with uncrossed polaroids. The time base of the scope was set to 2ms per division and the cell was driven at 1kHz.

Note that there is a period of time during switching in which the cell electrode is 'floating'. Over this period of about 1–2ms, the cell voltage decays to about half of its original value before being taken to its final value when contact is reestablished.

Switching time is measured between the beginning of this period of time and the moment when light transmisssion has changed to within 10% of its final value.

The switch–on time was measured from Fig. 4.13 (a) to be 3ms ± 1ms.

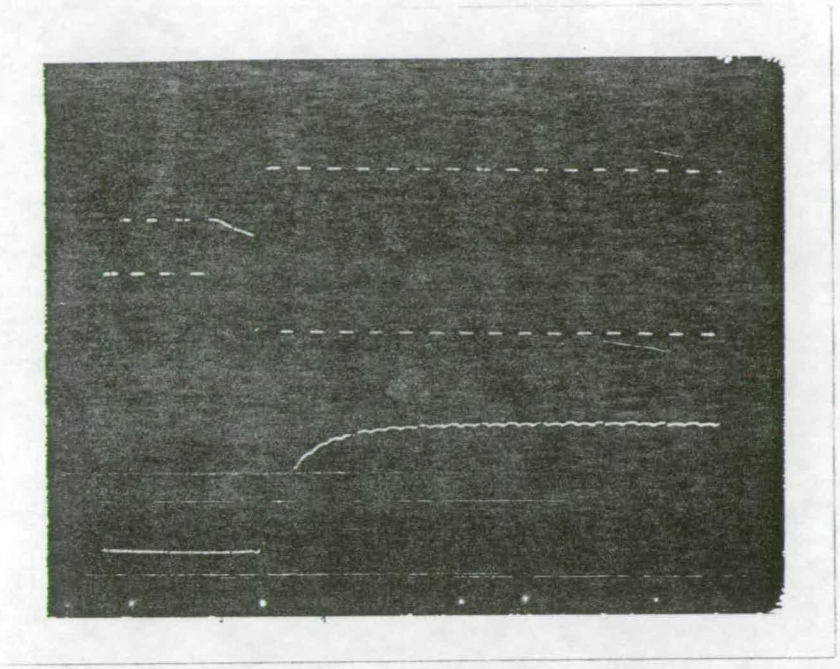

(a) Switch ON (2ms/div)

Fig 4.13 Oscilloscope traces

(b) Switch OFF (2ms/div)

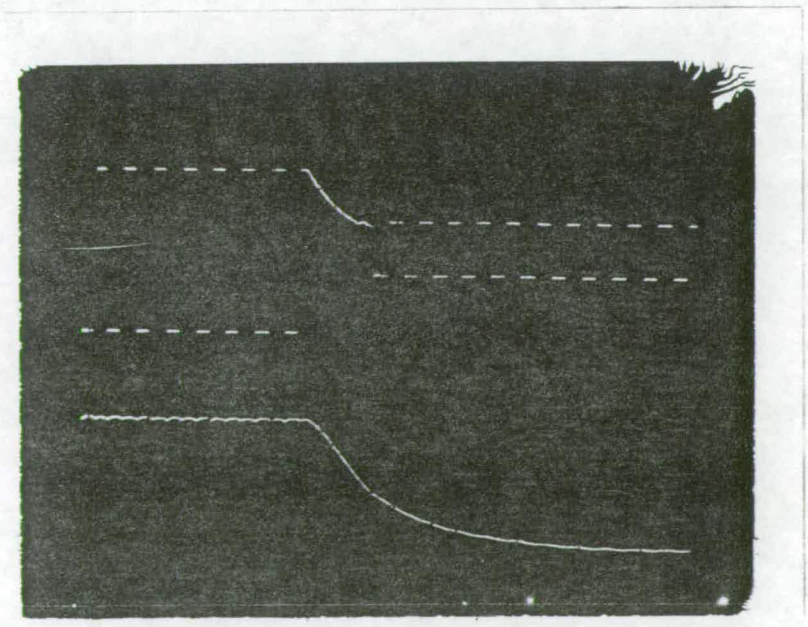

The switch-off time was measured from Fig. 4.13(b) to be 5ms ± 1ms.

Repeating the experiment with a time base setting of 5ms per division suggests that, after 10ms and 20ms from switching on and off respectively, the transmission is immeasurably close to its final value.

Note that although the *optical* switch-off begins immediately the switch is opened, the switch-on does not begin until contact has been made after the "dead time". Thus it may be desirable to use a faster electronic switch to change the voltage, giving a more realistic measure of the intrinsic switching time of the liquid crystal. Although this would greatly improve the accuracy of the measurements of switching times, such detail is considered unneccesary at the moment.

Precise measurements of the switching times between other pairs of points were not made. However the qualitative result that using the cell in its high voltage regime gives faster switching times was verified.

The extrema at the low voltage end (beyond *B*) are very sharp. As a consequence it was difficult to adjust the voltage in this range to give these values of transmission. This makes the measurements in this regime difficult and is also a very strong argument against operating a device at these voltages at all.

It was previously remarked that operating the cell between uncrossed polaroids, would make the point *B* into a good minimum leading to higher contrasts than for crossed polaroids.

This was done and typical on/off contrast measurements were made between points *A* and *B* using a digital voltmeter to measure the photodetector output.

The highest value of ratio of "on" intensity to "off" intensity was observed to be 100±2.

It should be noted that by increasing the maximum cell voltage (which in these experiments was limited to be about 12V), and which determines the transmission at point *A*, would readily increase the contrast by a factor of up to 2.

4.2.5. Consequences of test cell measurements for SLMs.

A binary SLM using the Field-Induced Birefringence effect in a parallel nematic LC would be best operated in the regime where the cell voltage is high and the liquid crystal is nearly isotropic. This is done for for three reasons. The molecules are subjected to greater torques by the intermolecular and electrostatic forces which cause the cell to switch quickly. The birefringence changes with the voltage more slowly. This makes it easier to set the drive voltages to give extreme transmission values. The birefringence is lowest in this region which minimises the effect of non-uniformities of pixel voltage and LC thickness.

For intensity modulation, the light incident to the SLM should be linearly polarised at 45° to the LC director. An analyser can, in theory, be placed either parallel or perpendicular to this. However, as the device operates in reflection, crossed polarisers are preferred to block out any light reflected from the SLM cover glass. Despite this observation, it was remarked earlier that the transmission corresponding to a phase difference of 2π was sometimes not sufficiently low for high contrast. Therefore it may still prove necessary in some cases to operate the devices with parallel polaroids using the $\delta=\pi$ point as a minimum.

Values of contrast of 100 have been observed in the test cells and can be expected from the SLMs. For some applications such as binary amplitude spatial filtering a higher value of contrast may be desirable. However this contrast should be adequate for many applications, especially those where a thresholding operation is performed on the optical output such as in optical computing.

For phase modulation the device would be operated between the same voltage levels. This has the same advantages of speed and uniformity as for intensity modulation. In addition, this makes it possible to set the voltages accurately while the polarisers are configured for intensity modulation. To operate as a phase modulator requires only the rotation of the input polariser to be parallel to the director and the removal of the analyser. From the measurements made on test cells, it is expected that only small amounts of the emergent light will be orthogonally polarised. Thus it is not expected that

any significant intensity modulation will be observed.

The final section of this chapter describes the construction of such devices, how the necessary pixel voltages are generated and the initial evaluation of their performance.

4.3. The field-induced birefringence SLM.

4.3.1. Structure and fabrication of the SLM.

The procedure for assembly of the SLM is similar to that used by Underwood [1987] for guest-host devices. The main improvement has been the use of MgF_2 instead of brushed Poly Vinyl Alcohol as the alignment layer. Its assembly is described below and illustrated in Fig. 4.14.

The drive chip

The drive chip is described in some detail in appendix 2. The surface of the chip is prepared by the oblique evaporation of MgF_2. This serves both as an alignment layer and as an insulator to prevent electrolysis of the LC.

The spacer

The spacer used to define the thickness of the LC layer is cut from a sheet of nominally 12 µm thick polyester. The spacer is cut by hand using a scalpel into a U shape of external dimension of 5mm and internal dimension of 3mm, to fit within the interconnect region of the chip.

The perspex guide

This component is a 2mm thick piece of perspex with a 5mm square hole cut into it to accomodate the cover glass. It positions and holds the cover glass in place on the IC.

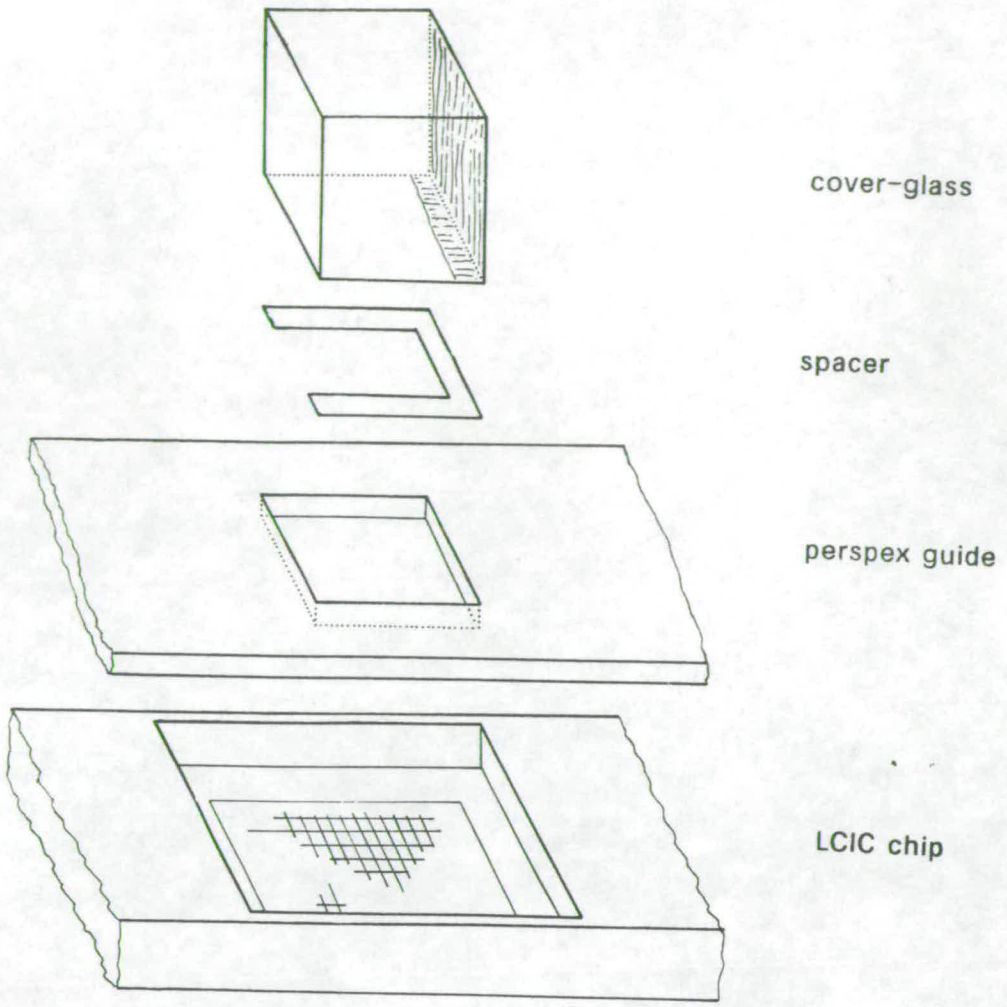

Fig 4.14 The FIB SLM - construction and photograph of completed device

The cover glass

The cover glass has an area of $5x5mm^2$ to cover the IC and is about 6mm thick. The glass was cut from a sheet supplied by Optical and Electronic Coatings Ltd.. The sheet was supplied polished optically flat on both sides, with ITO of resistance 300 Ω per square coated on one side and an anti-reflection layer on the other. After the glass is cleaned, a thin strip of aluminium is evaporated along one edge of the ITO surface and up the adjacent side face of the glass, to which electrical contact can be made. Finally a MgF_2 alignment layer is evaporated onto the ITO surface as for the drive chip.

Assembly

The device is assembled in clean conditions in a laminar flow cabinet. Firstly the spacer is placed over the interconnect area of the chip. If it is misaligned then it can be carefully moved with a probe made from a thin piece of insulated wire bent double. However this should be avoided as there is a risk of damage to the IC surface or to the bonding wires.

Secondly, the perspex guide is placed above the centre of the IC and glued to the chip holder. A thin piece of wire of approximate length 10cm and bared at both ends is glued to the top of the guide. This will make contact to the ITO counter-electrode.

After the contact between the ITO and aluminium is checked the aluminium is primed with a thin layer of Electrocure metallic paint to which the contact wire will be attached.

When the glue and paint have dried, a drop of the LC is placed on the active area of the chip with a syringe.

The glass is lowered gently through the perspex guide onto the spacer. Any surplus LC is squeezed out of the open edge of the spacer. The glass is lightly clamped in place and Araldite adhesive is applied around its edges to fix it to the perspex. One end of the wire is contacted to the glass with more

conductive paint. The other end of the wire is attached to pin 25 of the chip holder. This pin is not connected to the chip. This allows all electrical inputs to the SLM to be made via a 40 pin IC holder.

Finally Araldite is applied to the wire/glass bond to strengthen it. The device is left overnight to ensure that all bonds and contacts are secure.

4.3.2. Electronic drive of the SLM.

Appendix 2 describes the electronics of the drive chip of the SLM. The voltage appearing on the pixel electrodes is a square wave changing between levels of 0V and the positive rail voltage V_{DD}. This voltage is nominally 5V but can take values between 3.5V and 15V. For pixels having different logic values (0 or 1) the square wave has opposite phase. A square wave train changing beween those same values of 0V and V_{DD} is applied to the counter-electrode. Thus for logic "0" pixels, the pixel and counter-electrode voltages change in phase and there is no potential difference across the LC. For logic "1" pixels, the voltages change in anti-phase and so a square wave of amplitude $\pm V_{DD}$ is generated across the LC.

In general it is desirable that both voltage values across the LC be variable - not just the logic "1" value. This makes it possible to arrange for the SLM to be driven between two positive voltage values as recommended in section 4.2.5.

Therefore the circuit illustrated in Fig. 4.15 was devised to drive the counter electrode and supply the chip clock input to produce these conditions. The two resistors R ensure that the mean voltage at node N, which is applied to the counter-electrode, is $V_{DD}/2$. A square wave train of amplitude V_C is fed into node N through the capacitor C. With suitably chosen values of R and C, the counter-electrode voltage is a square wave changing between values of $(V_{DD}+V_C)/2$ and $(V_{DD}-V_C)/2$. The clock signal is a square wave of the same frequency between V_{DD} and zero generated from an open-collector inverter chip.

As a result the liquid crystal voltage has a value of $\pm(V_{DD}+V_C)/2$ and $\pm(V_{DD}-V_C)/2$ for logic "1" and "0" respectively. These are both pure ac so there

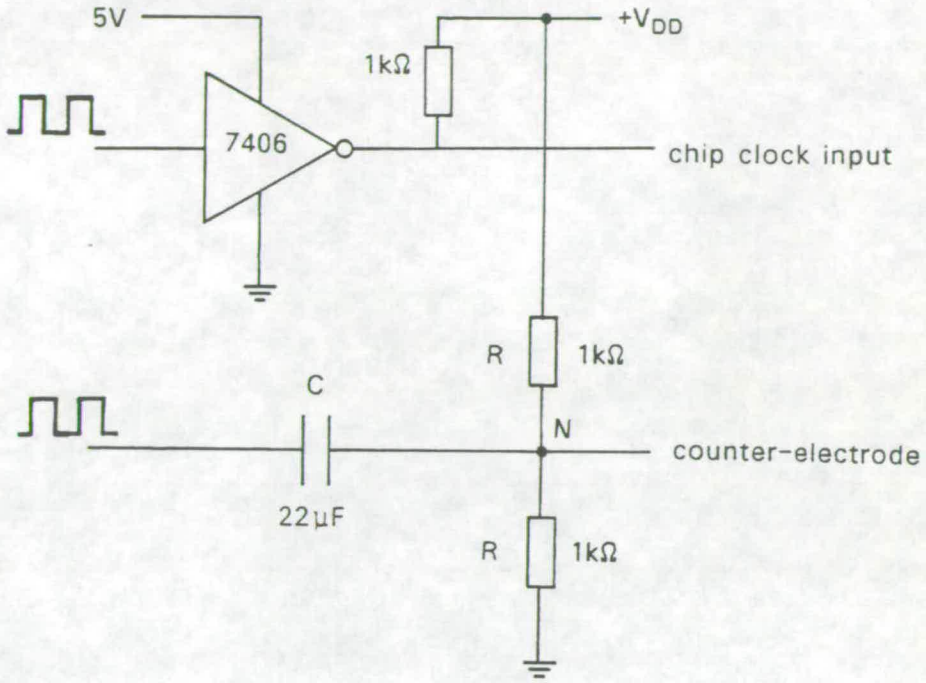

Fig 4.15 Clock generating circuit

Fig 4.16 Clock signals

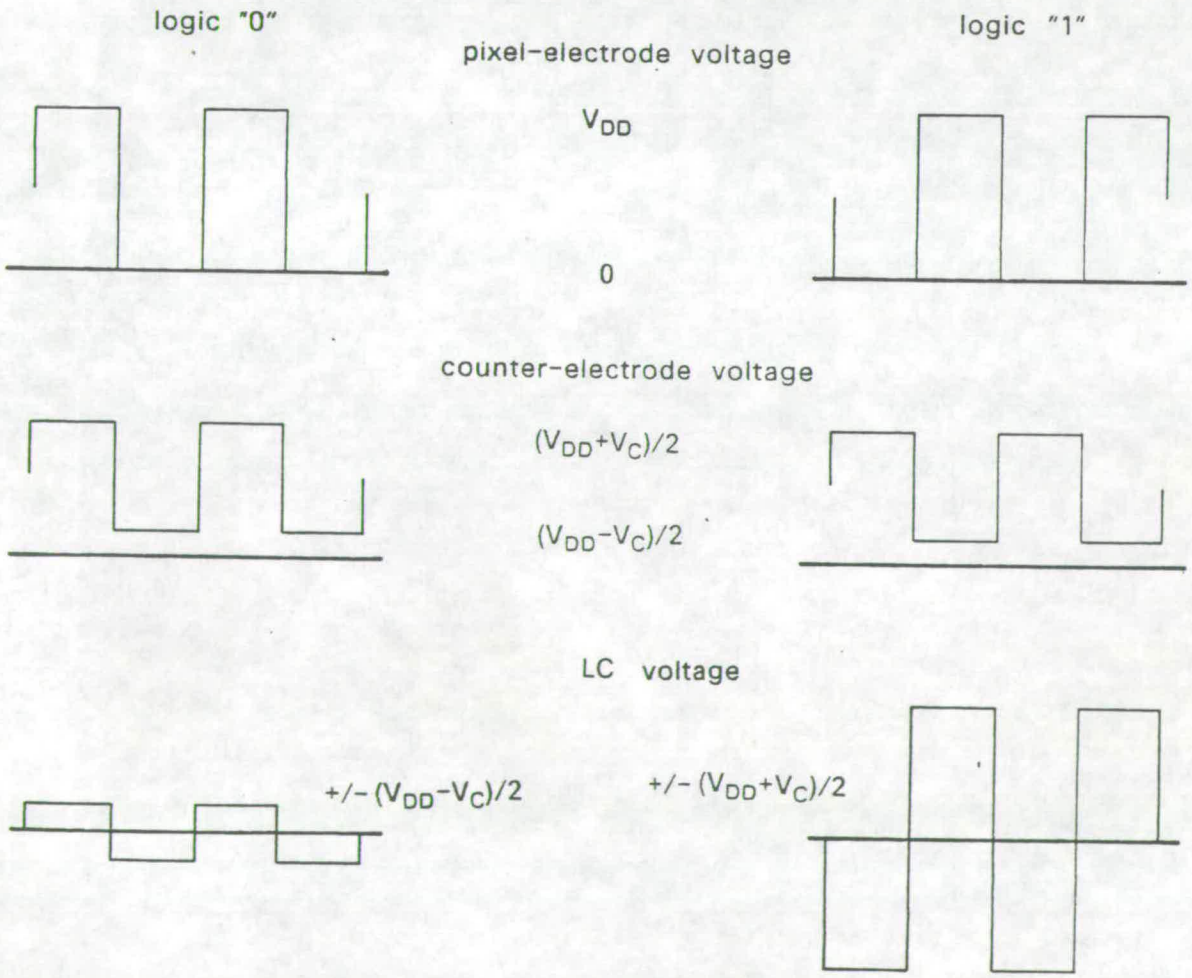

is no electrolysis of the LC and can be set to any two values by appropriate choice of V_{DD} and V_C.

These voltage signals are illustrated in Fig. 4.16.

The data and enable inputs of the chip are set to zero or V_{DD} as desired by an array of 32 switches.

4.3.3. Initial evaluation of the SLMs.

An initial batch of two SLMs was prepared according to the method of section 4.3.1 and were put into the object plane of the optical system described in section 2.2.2. The polariser and analyser required for operation of the SLMs were inserted into the system. The devices were illuminated by parallel coherent light from a HeNe laser and some photographs were taken of the images.

Device no.1

Fig. 4.17 (a) shows the image of this device with a pattern of alternate light and dark lines programmed into the chip. Fig. 4.17 (b) shows the effect of changing the phase of the counter-electrode voltage signal. This should have the effect of reversing the contrast of the pattern. This is observed to occur over some regions of the device. There are many areas of the device in which the programmed pattern is not apparent and in which no contrast reversal is observed. This suggests that the fault is due to the liquid crystal layer rather than the wrong voltage being on the pixel electrodes. This device was not used for any further experiments.

Device no.2

Fig. 4.18 shows the device, without any applied voltages, viewed through the crossed polaroids. As the birefringence has the same value across the device, the fringes are due to a variation in thickness of the liquid crystal layer.

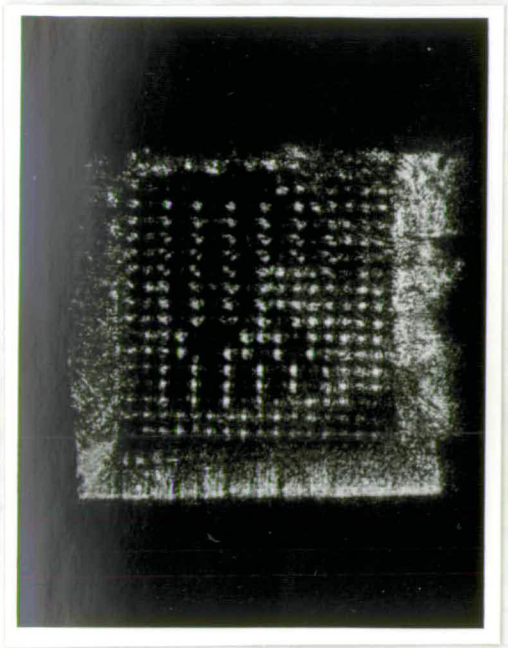

(a) grating pattern

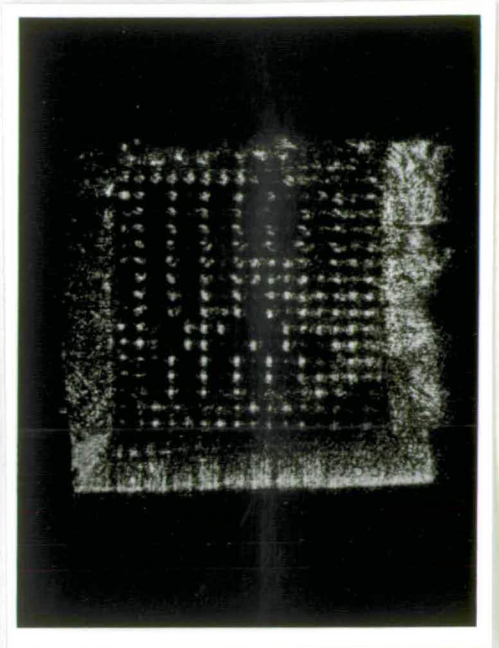

(b) reversed counter-electrode phase

Fig 4.17 Contrast reversal in device no.1

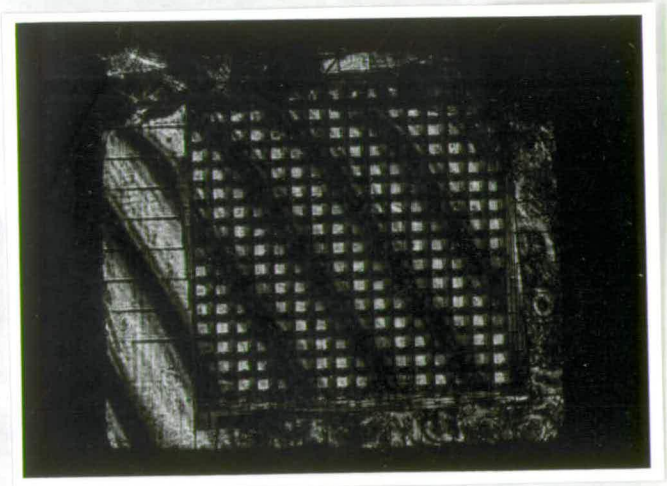

Fig 4.18 The wedging in device no.2

The phase difference introduced between the extraordinary and ordinary polarisation components of light will differ by 2π between neighbouring light or dark fringes. Taking the birefringence of E7 to be 0.224 after the measurements of Wu et al. [1983] gives a change of cell thickness of approximately 1.5μm between neighbouring fringes or a change of about 7.5μm between the two opposite corners of the active area of the device.

This wedging is likely to severely restrict operation of the device in the regime of higher birefringence. The wedging is useful however to set the polaroids. They can be crossed accurately at 45° by maximising the contrast of the fringes.

It was not found possible to operate the device in the manner described in the previous section by adjusting the supply and counter-electrode voltages. Several pieces of evidence suggest that the connection to the counter electrode was in fact broken, and that its voltage was determined capacitatively by the pixel electrodes.

The first piece of evidence is that changing the phase of the wave train to the counter-electrode, as described for the other device, has no effect. This ought to reverse the contrast of any pattern on the device.

Fig. 4.19 (a),(b) and (c) forms further evidence. In all these photographs, the same five-row segment has been programmed with a chequer-board pattern. In Fig. 4.19 (a), all of the remaining pixels have a logic "0" value. If it is assumed that the counter electrode voltage is the mean of all the pixel voltages then it is in phase with the logic "0" pixels and the chequerboard pattern is seen. In Fig. 4.19 (b), half of the remaining pixels have been reprogrammed to logic "1". Now the mean pixel voltage and counter-electrode voltage are $V_{DD}/2$ and the voltage across the LC is the same for each pixel. The chequerboard is not seen. In Fig. 4.19 (c) all of the remaining pixels are at logic "1" and the counter-electrode is following the logic "1" pixels. The pattern is again seen but with the expected contrast reversal relative to Fig. 4.19 (a).

Thus is it expected that despite the floating counter-electrode, that reasonable contrast patterns can be obtained with this device provided that most of the pixels are in the same state. This is shown to be the case in Fig.

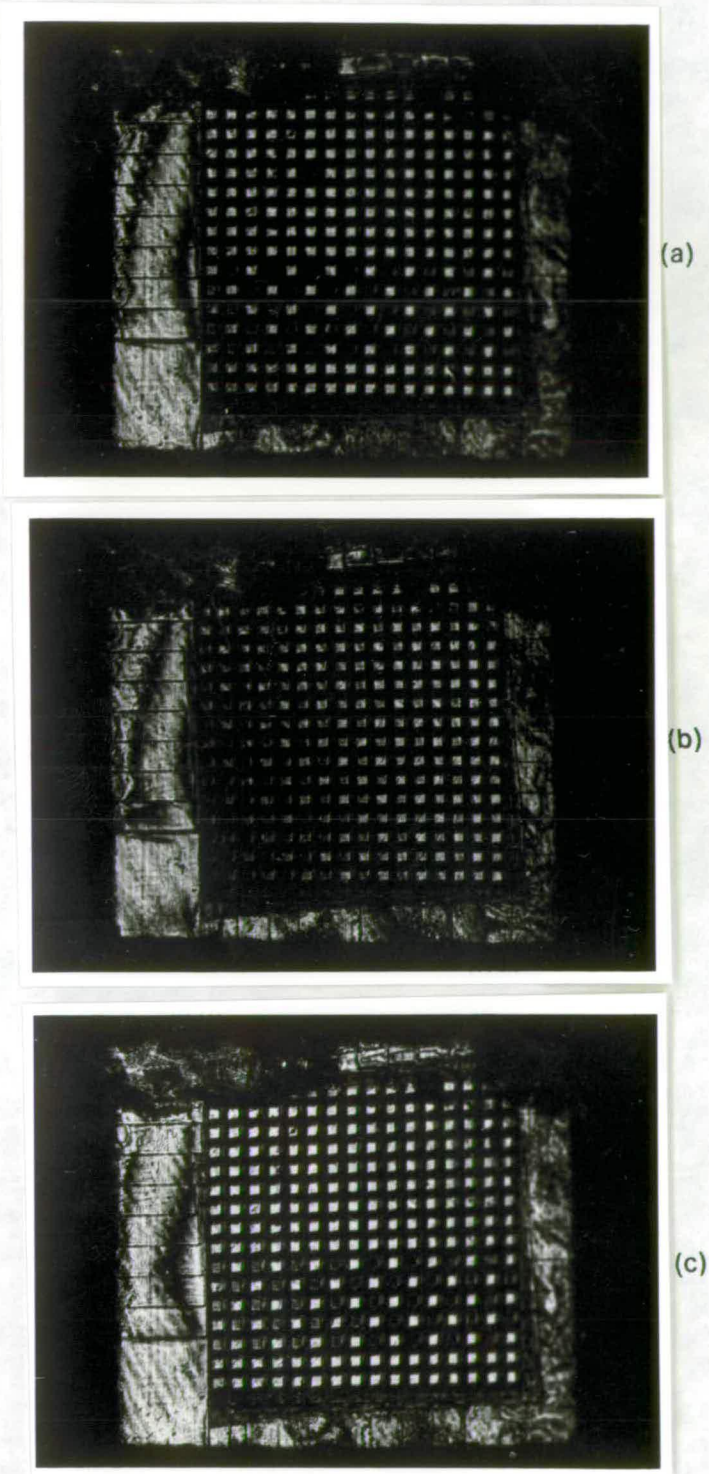

Fig 4.19 Testing the counter-electrode connection of device no.2

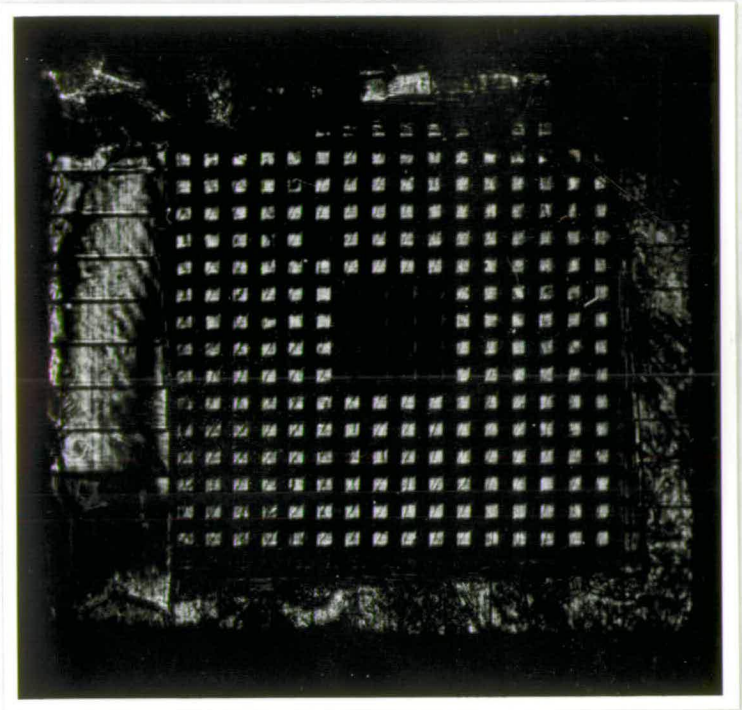

(a)

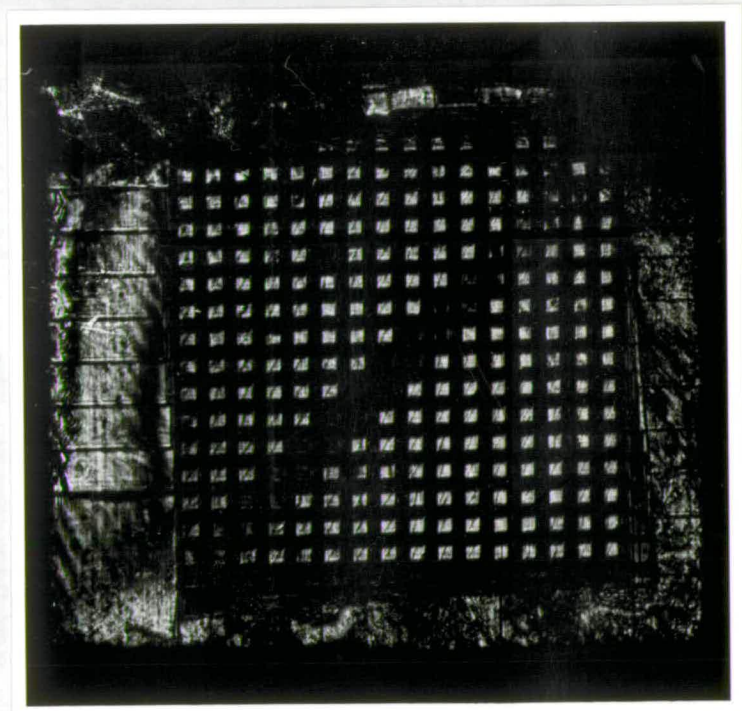

(b)

Fig 4.20 Sample patterns on device no.2

4.20 (a), (b) and (c) for a number of sample patterns.

It was decided therefore to proceed to illustrate some of the applications of the SLM using this device. In chapter five, it is used both as an intensity modulator and as a phase modulator to illustrate its value in a coherent optical processing system.

To complete this chapter, it is appropriate to briefly describe the improvements to SLM production acheived since that work was carried out. One further batch of SLMs has been constructed. These have been much more uniform and behave as expected when addressed. The improvement in uniformity is due to a modification of the method used to make the spacer. Two strips of the polyester are cut using scissors and are manipulated into place on the interconnect. Using scissors makes a much cleaner cut than the scalpel. Strip spacers are an improvement over the previously used "U" shape which can have a "tail" of spacer at its internal corner badly affecting the thickness uniformity. Due to time constraints, these devices were not used to improve upon the results which will now be presented in chapter five.

Fig 4.20 (c)

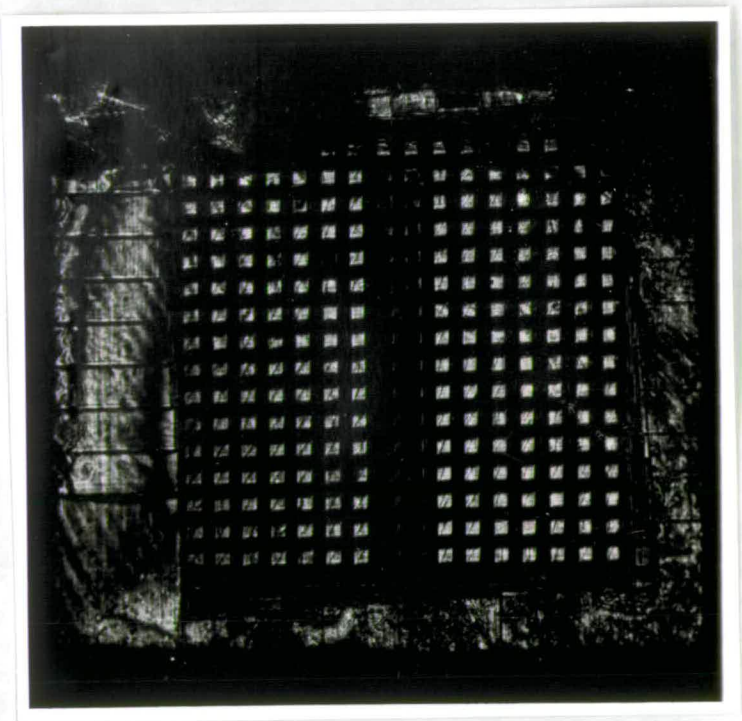

Chapter 5

Application of the FIB SLM in Coherent Processing Systems

The FIB SLM was described in the previous chapter and briefly demonstrated as an amplitude modulator. In this chapter, the device will be used in some image enhancement experiments both as an amplitude and phase modulating filter. This will show that there are many useful and interesting projects to be conducted in the future using these devices. In some cases the results are affected by the low resolution of the 16x16 pixel modulator but the promise of this light modulation effect is clearly illustrated.

5.1. Binary amplitude spatial filtering

In section 1.2.1, the subject of coherent processing was introduced by showing the results of a simple binary amplitude filtering operation. A triangular object was edge-enhanced by removing its lower spatial frequency components in the Fourier plane. The filter used was a small circular stop produced on high contrast photographic film. In this experiment an SLM is used in place of the transparency in the Fourier plane.

The optical system used to carry out this experiment is the variable magnification Fourier processor described by Willson [1987] and illustrated in Fig. 5.1.

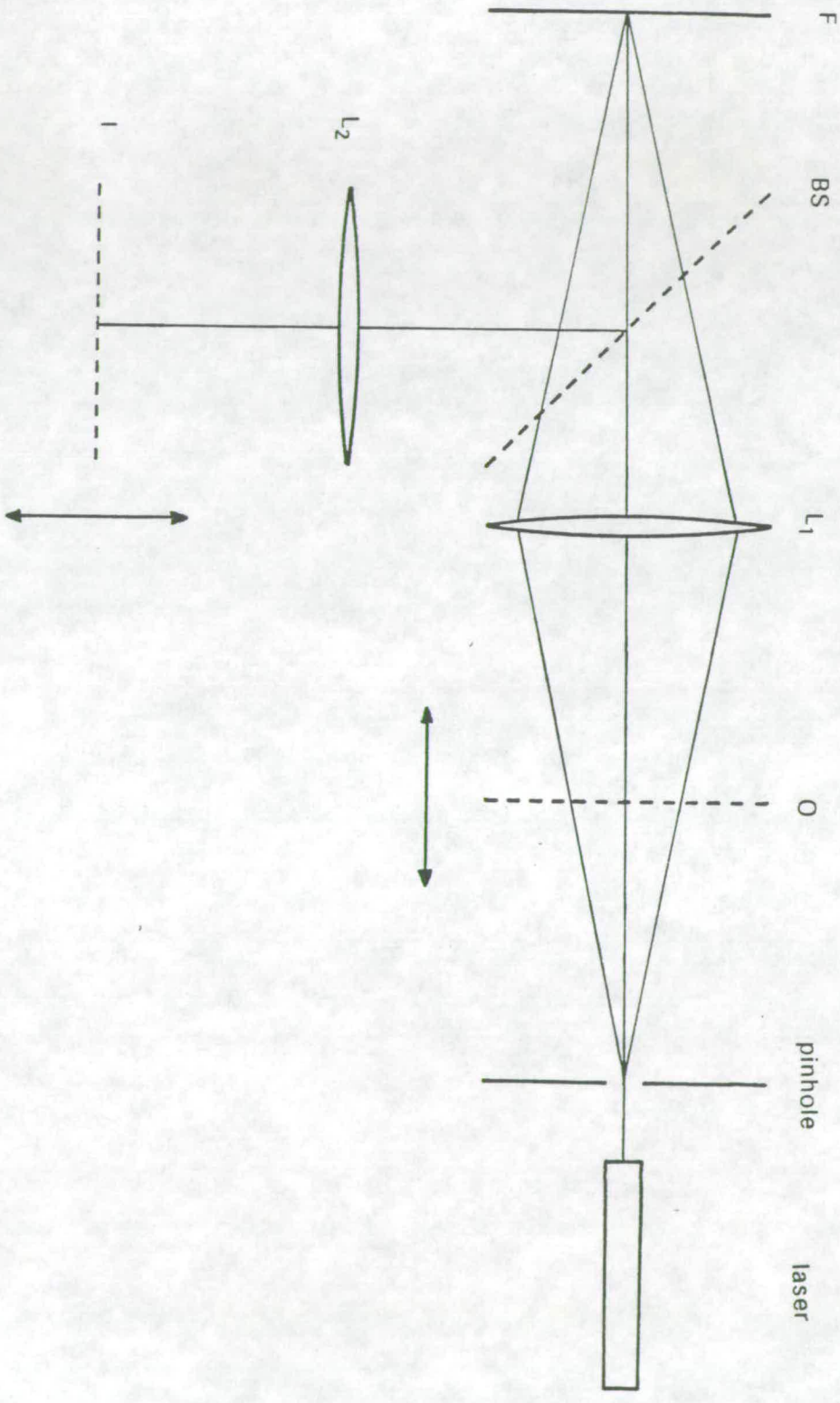

Fig 5.1 Variable magnification Fourier processor

Fig. 5.2 The effects of varying the sampling rate of a pixelated Fourier plane filter for a triangular aperture in the object plane. These are photographs of the images obtained by changing the scale of the FT of the object relative to the pixel spacing. This has the effect of changing the size of the images relative to the replication spacing.

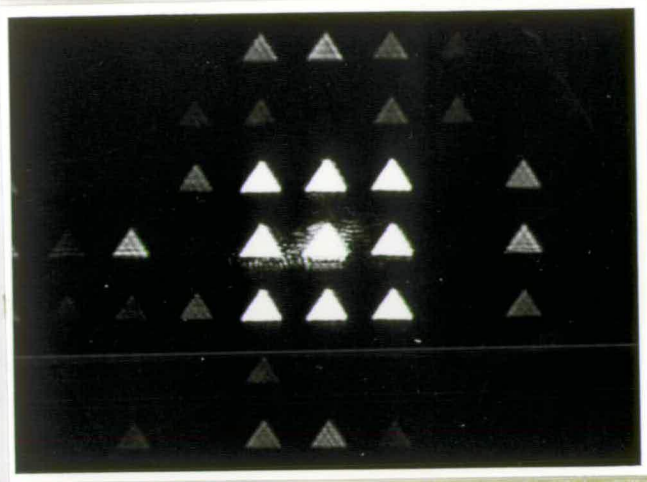

(a) oversampling - pixels closely spaced relative to the scale of the FT - replication spacing large relative to the size of the triangular images.

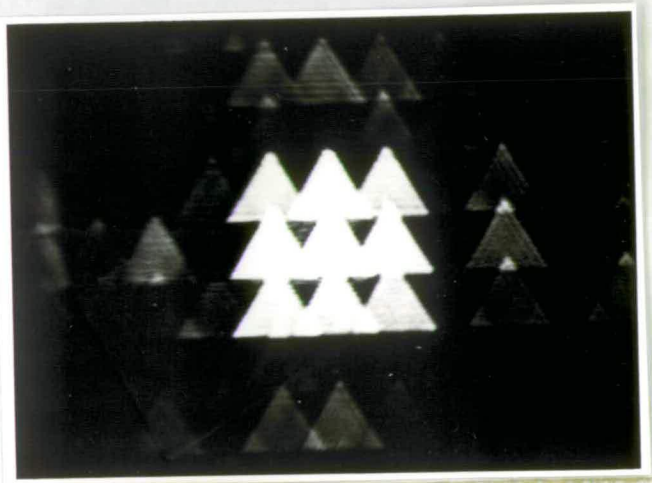

(b) undersampling - samples widely spaced relative to the scale of the FT - replication spacing small relative to the size of the triangles which therefore overlap.

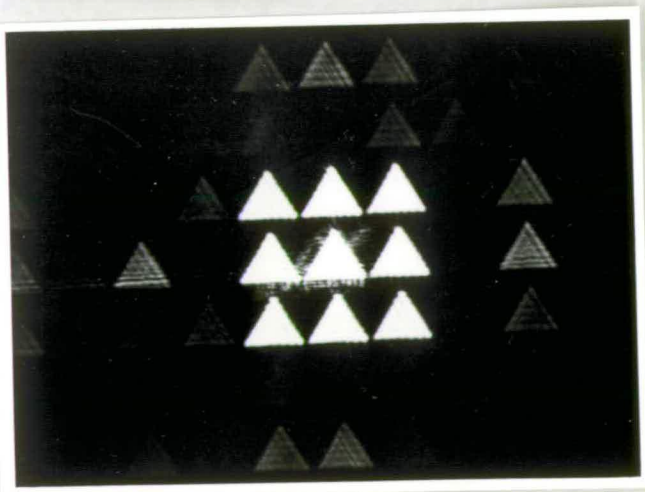

(c) optimum sampling rate - replications are made as large as possible without overlapping.

(a) All pixels of the SLM are switched "ON"

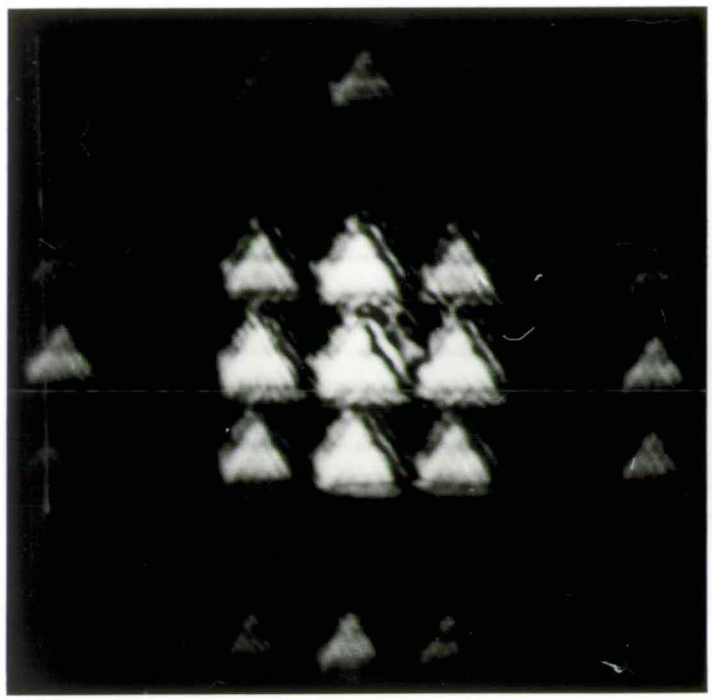

(b) Pixels in the centre of the SLM are switched "OFF"

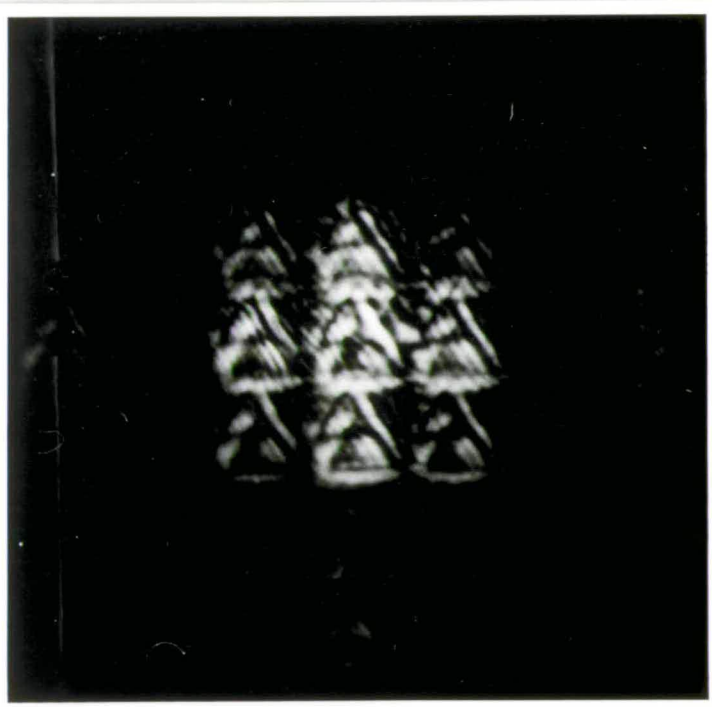

Fig. 5.3 Edge-enhancement by binary amplitude spatial filtering: These photographs show the images resulting from using a binary amplitude SLM in the Fourier plane to high-pass filter a triangular object.

Changing the position of the object O alters the scale or magnification of its Fourier transform in the FT plane F. The image plane is therefore not fixed but must be found for a given magnification of the FT. This system is necessary when using pixelated filters in the Fourier plane to avoid the effects of over- or under-sampling as shown in Fig. 5.2 (a) and (b). The optimum case of Fig. 5.2 (c) is where the replicated images do not overlap but are as large as possible. The pixelated filter here is a "bare" SLM backplane. Note the ringing due to the strong low-pass filtering effect of the filter. This is to be expected in any application of the 16x16 array. Note also the asymmetric "envelope" that modulates the replicated spectra. This is due to the circuitry in each pixel which is of varying height above the mirror. This means that the "pixel" function, as defined in chapter two, is complex. The envelope function, being the FT of the pixel function is therefore non-symmetric.

When the backplane is replaced by an amplitude modulating SLM with all pixels switched on, the image is now that shown in Fig. 5.3 (a). A central group of pixels is switched off to carry out the edge-enhancement process and the filtered image is shown in Fig. 5.3 (b).

The image does consist of an array of edge-only triangles. However the edges are not as clear as those of the photographic experiment shown in Fig 1.4. In addition to the effect of low-pass filtering on the images, the imperfections in the images could be due in part to the SLM having a lower contrast than the photographic filter.

5.2. Phase gratings

The use of the FIB SLM as a phase modulator can be demonstrated effectively by using it to record a phase grating. It has been found best to programme the modulator while it is still in its amplitude modulating mode and then to change the relative orientation of the SLM and input polariser by 45°. Having maximised the contrast in the amplitude mode the two pixel states will have a phase difference of $(2n+1)\pi$ radians. Clearly no grating pattern will be observed in the image plane, but according to the theory of section 2.1.4, intermediate orders would be introduced into the Fourier plane spectrum. Fig. 5.4 (a) and (b) show the FT plane for a grating of vertical columns and for a chequerboard grating respectively.

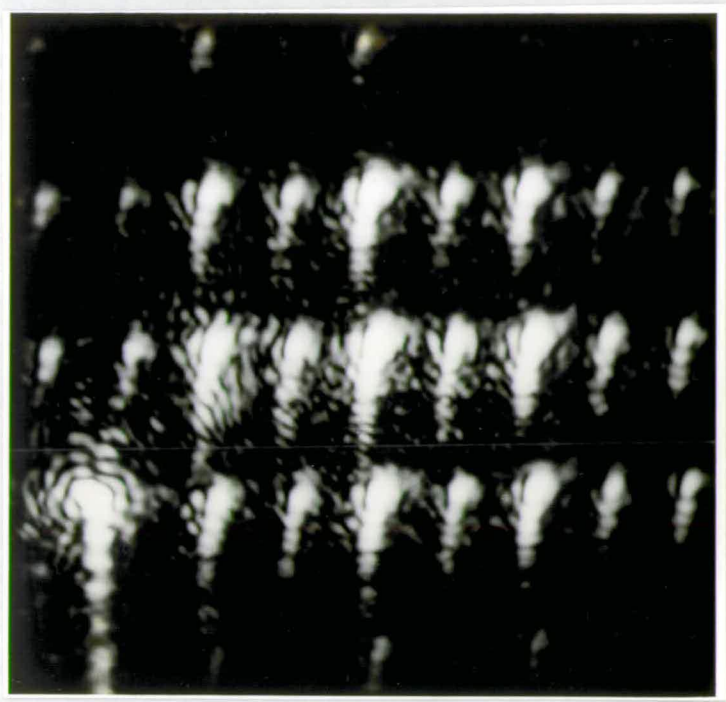

(a) vertical grating

Fourier transform.

Object.

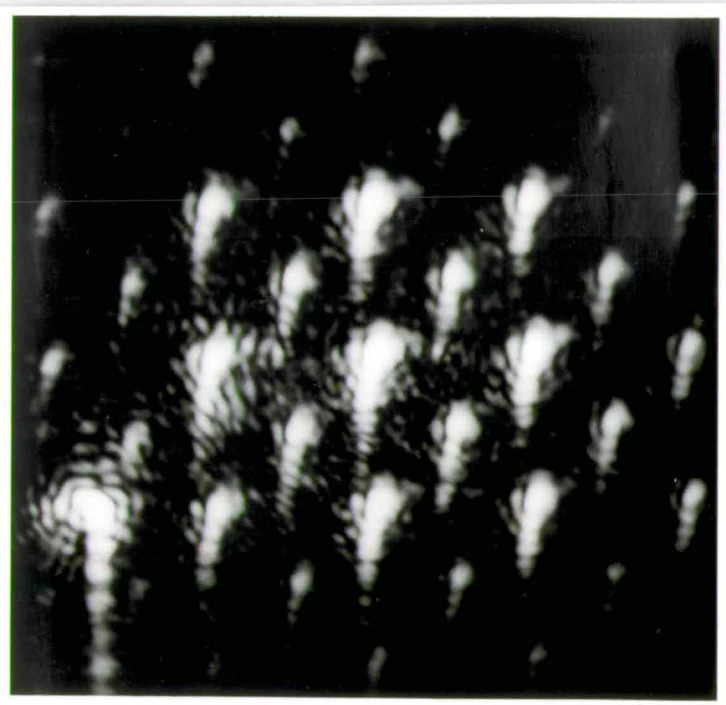

(b) chequerboard

Fourier transform.

Object.

Fig. 5.4 Fourier transforms of phase gratings: Periodic "grating" patterns of phase 0 or π radians were recorded on a phase-modulating SLM. The device was illuminated uniformly in the object plane. The figures are photographs of what was observed in the Fourier transform plane. The sketches show segments of the pattern in the object plane. NOTE: Dark and light squares are used in the sketch to represent phases of 0 and π radians. They do not represent opaque and transmitting pixels.

There is evidence that the the modulator does not carry a pure phase grating but that there is in addition a small amplitude modulation. This can be seen by viewing the image with a TV camera and monitor and adjusting the contrast and intensity controls of the monitor to enhance the grating. This modulation is of a much lower contrast than that seen when using the device in the amplitude mode. Such an amplitude grating alone would be insufficient to cause the strong intermediate orders observed in the Fourier plane. At present it is only possible to speculate on the cause of this amplitude modulation. It may be due to the incident light not being at precisely 0° to the LC director and polarisation analysis being conducted by an obliquely inclined optical component such as a beam splitter. Alternatively there may be a small twist in the LC cell causing some weak modulation of amplitude by a Hybrid Field Effect mechanism.

Further analysis of the Fourier spectrum of these phase gratings would give useful data for the validation and extension of the theories of chapter two. To do this properly would require some knowledge of the phase of the light reflected from the inactive parts of the array.

There are considerable practical consequences of furthering this work in the area of interconnection in hybrid optical and electronic computing. This subject was mentioned briefly in section 1.2.2 under the heading of Optical logic. It is possible to envisage a system in which simple grating patterns can be formed on an SLM and the diffracted light is routed to one of a number of locations using holographic elements. The absence of absorption losses is a strong argument for the use of phase modulators.

5.3. Schlieren filtering

When a general pattern is recorded on an SLM as a phase modulation then, according to chapter two, it can be converted to an analogous intensity pattern by Schlieren filtering. For a pixelated object this most usefully involves passing only one of the first order spectra of the Fourier transform. Fig. 5.5 (a) shows the image of an SLM with all pixels at the same phase when a square aperture passes one of the (0,1) orders of the FT. The side length of the aperture is slightly less than the inter-spectral spacing to ensure that the output is formed from components of only one spectrum.

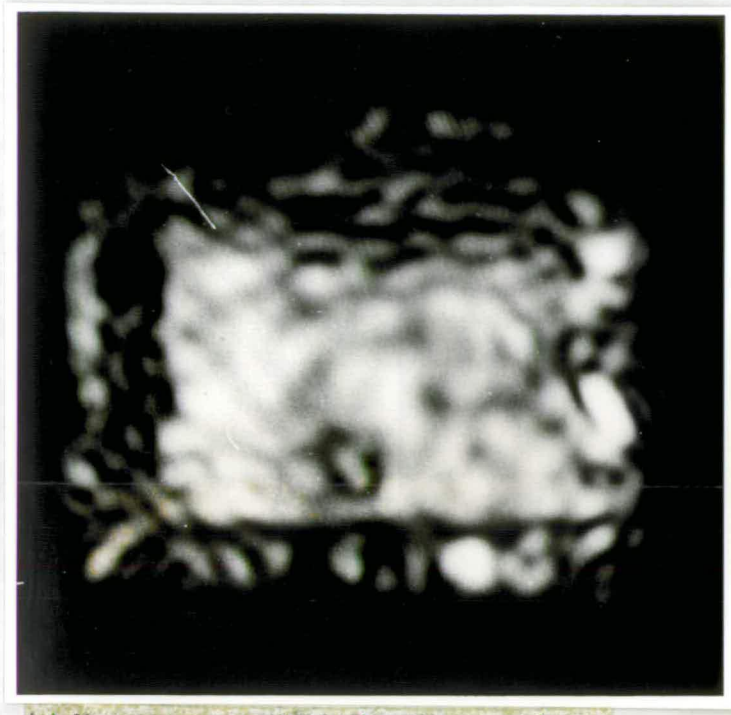

(a) No pattern – all pixels at same phase.

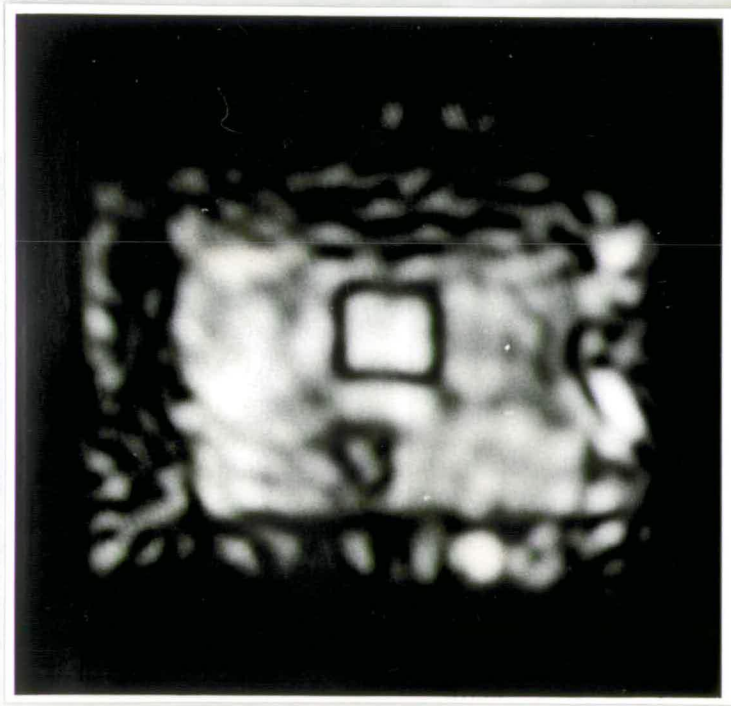

(b) 4x4 square

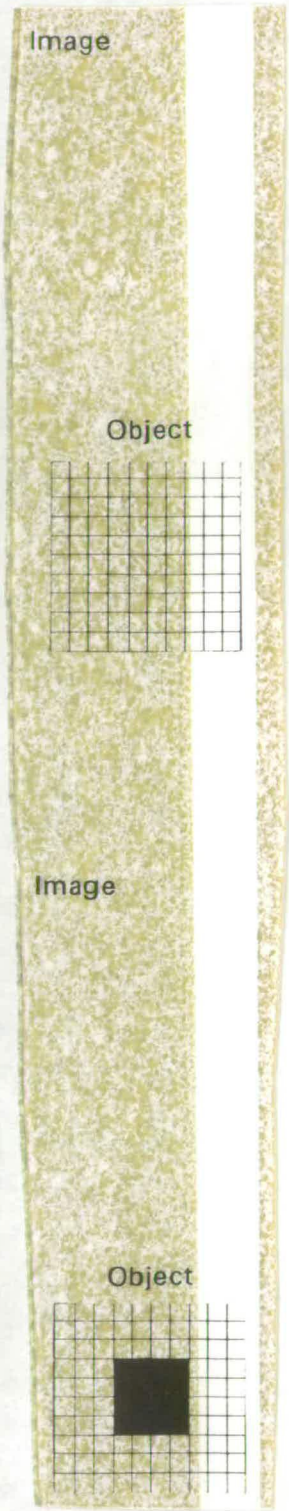

Fig. 5.5 Schlieren filtering: A phase modulating SLM in the object plane is illuminated uniformly. Phase patterns recorded on the device are rendered visible in the image plane by a Fourier plane filter passing a single first-order spectrum. The photographs show the images observed for the input pattern sketched beside it. NOTE: Dark and light squares are used in the sketch to represent phases of 0 and π radians. They do not represent opaque and transmitting pixels.

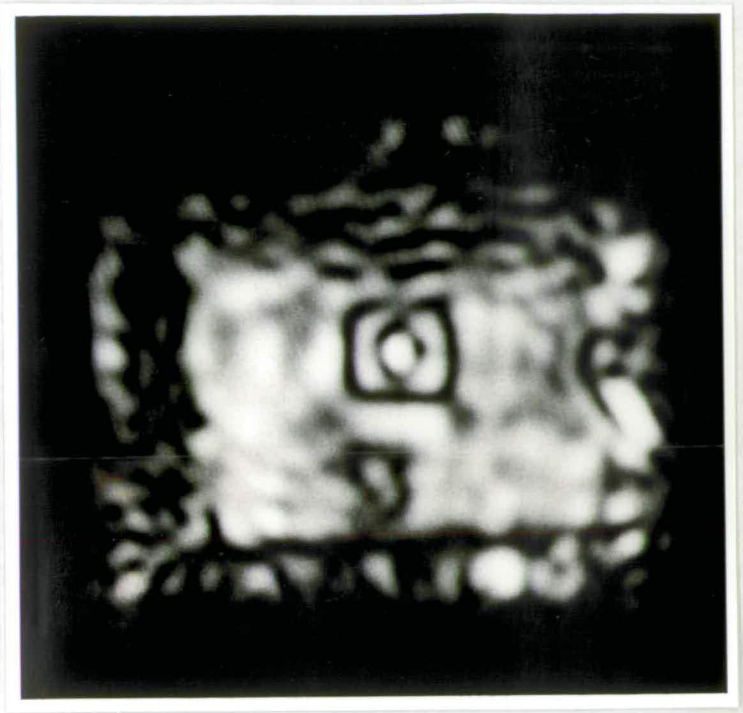

(c) Square box

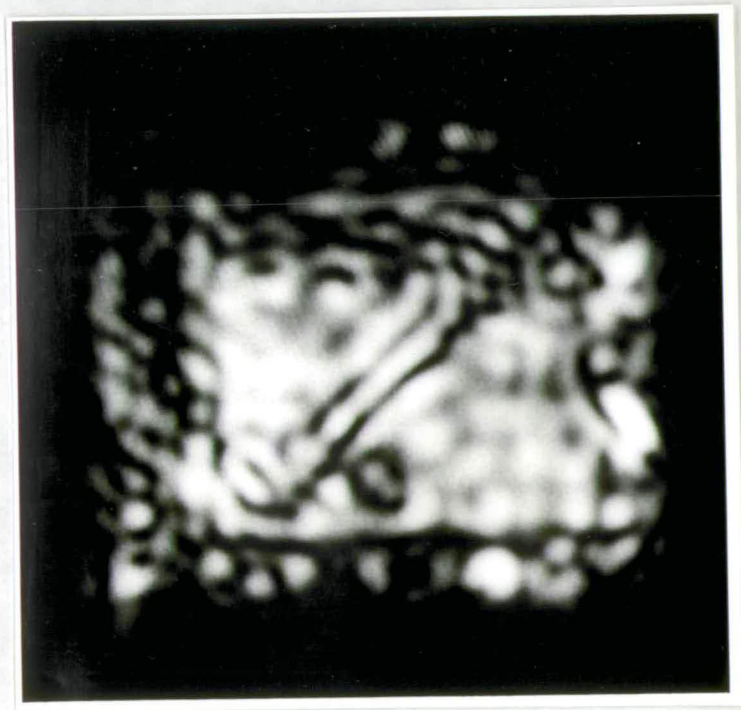

(d) Diagonal stripe

Fig. 5.5 (b), (c), and (d) show the result of changing the phase of some of the pixels by π radians according to a pattern. The patterns are respectively a 4x4 square of pixels in the centre, a square box of length 4 pixels and a diagonal stripe of pixels. An "edge-suppressed" form of the patterns is clearly seen in the image plane.

The results are interesting in two respects: that the pixels of different phases have similar intensities and that the domain boundaries between two phases are marked by a dark line.

Interpretation

The methods discussed in chapter two can be applied to explain these results. To a first approximation, the intensity observed in the image plane is proportional to $J_1(\phi)$ where ϕ is the phase of the light in the object plane relative to the mean phase. We know that the values of ϕ for the OFF and ON pixels, Φ_{OFF} and Φ_{ON}, differ by π radians. However, their values relative to the mean cannot be specified without knowledge of the phase of the light reflected from the inactive parts of the array.

The results can be explained by assuming that the mean phase is such that $J_1(\Phi_{OFF}) \simeq -J_1(\Phi_{ON})$. This means that the intensity observed for both values of phase for the active pixels is about the same. However their amplitudes are of opposite sign. This is the cause of the dark lines.

Assume that the modulus of the light from neighbouring domains is the same but that they are out of phase. If the domains were "blurred" into one another, destructive interference in the areas of overlap would result in the dark lines. In this case the "blurring" is interpreted as the effect of the diffraction of light by the aperture in the Fourier plane. It is simple to see that a square aperture whose width is the inter-spectral spacing has a FT of a sinc function whose "width" is the pixel spacing. The result of convolving the object with this sinc is to "blur" the image as required.

Similar edge suppression of pixelated phase objects is described by Anderson [1986] who refers to it as "dark-edge enhancement". The blurring is acheived by defocussing or by using a Fourier plane aperture as above. In the

latter case, the width and contrast of the edges can be varied within certain limits by altering the size of the aperture.

5.4. Binary phase spatial filtering

This experiment is similar to the binary amplitude spatial filtering described in section 5.1. In this case an image is filtered by changing the phase of portions of its FT by π instead of removing them with an amplitude modulator. This method is much less widely used or understood than amplitude modulating, and to consider it fully is beyond the scope of this work. However, the experiment shows that there are interesting effects in this approach to be exploited.

The same triangular object was used as in section 5.1 and it was filtered by using the SLM to change the central portion of the FT by π radians. Fig. 5.6 (a) and (b) show the original and filtered images. The effect of the filtering operation is an edge enhancement operation giving dark edges on a light ground. In this case it was found that the image was affected only by the switching of two neighbouring pixels. The asymmetry of this filter pattern is presumably the cause of the anisotropy in the image. The discreteness of the filter array makes it impossible to define the ideal pattern. Using a device with greater resolution would allow this anisotropy to be reduced.

The suppression of edges by reversing the sign of the low order Fourier components has been illustrated numerically. Fig. 5.7 (a) shows an approximation to a square wave made by the synthesis of ten sine waves using a Fortran program. Fig. 5.7 (b) shows the result of changing the sign of the lowest harmonic in this series. Fig. 5.7 (c) and (d) are the squares of these graphs corresponding to observed intensities. The same enhancement of the edges by a dark and light line (the minimum and local maximum at the edge) can be seen as for the experiment.

5.5. A binary phase correlator

Horner and Bartelt [1985] and Flannery et al. [1986] describe the use of binary phase filters in the Fourier plane of an optical correlator system. This is

(a) Replicated unfiltered images.

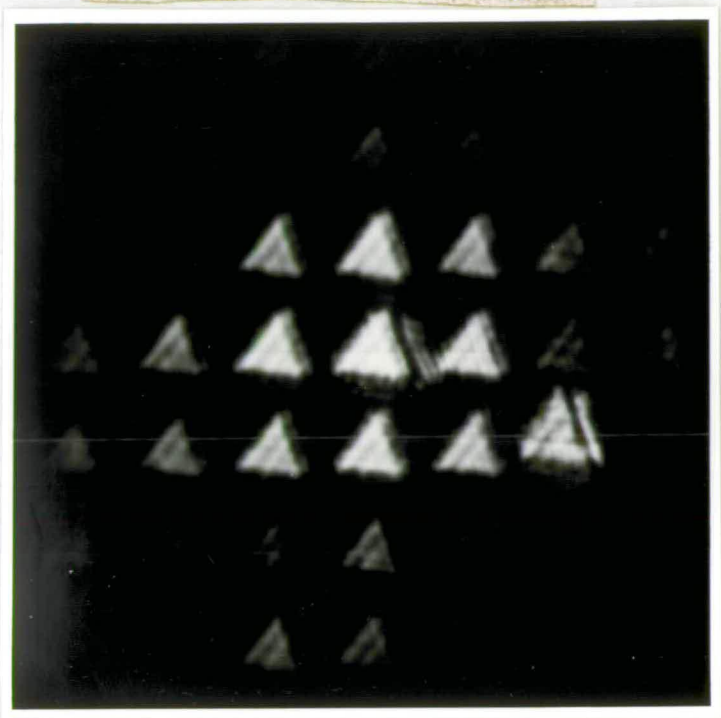

(b) Filtered images.

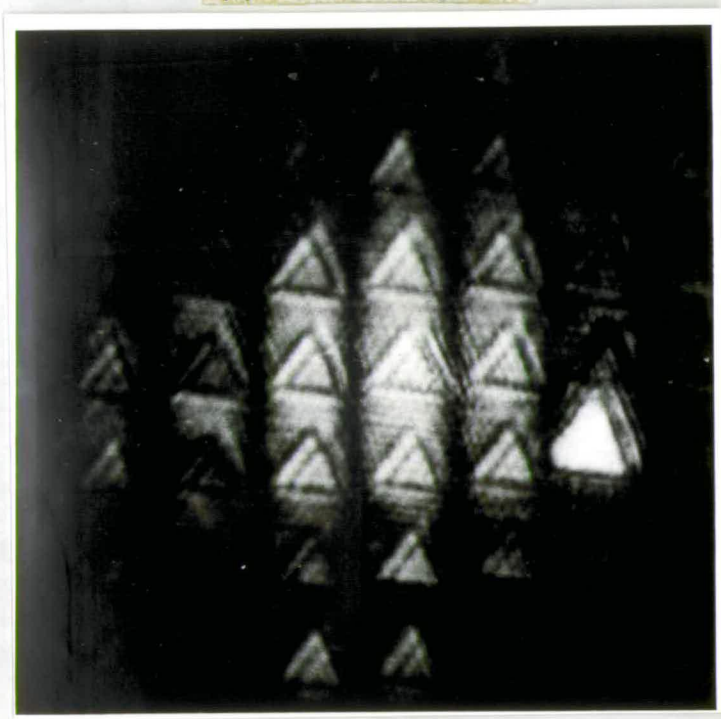

Fig. 5.6 Edge-enhancement by binary phase spatial filtering: A phase modulating SLM in the Fourier plane is used to change the phase of the low spatial frequency components of a triangular object by π radians.

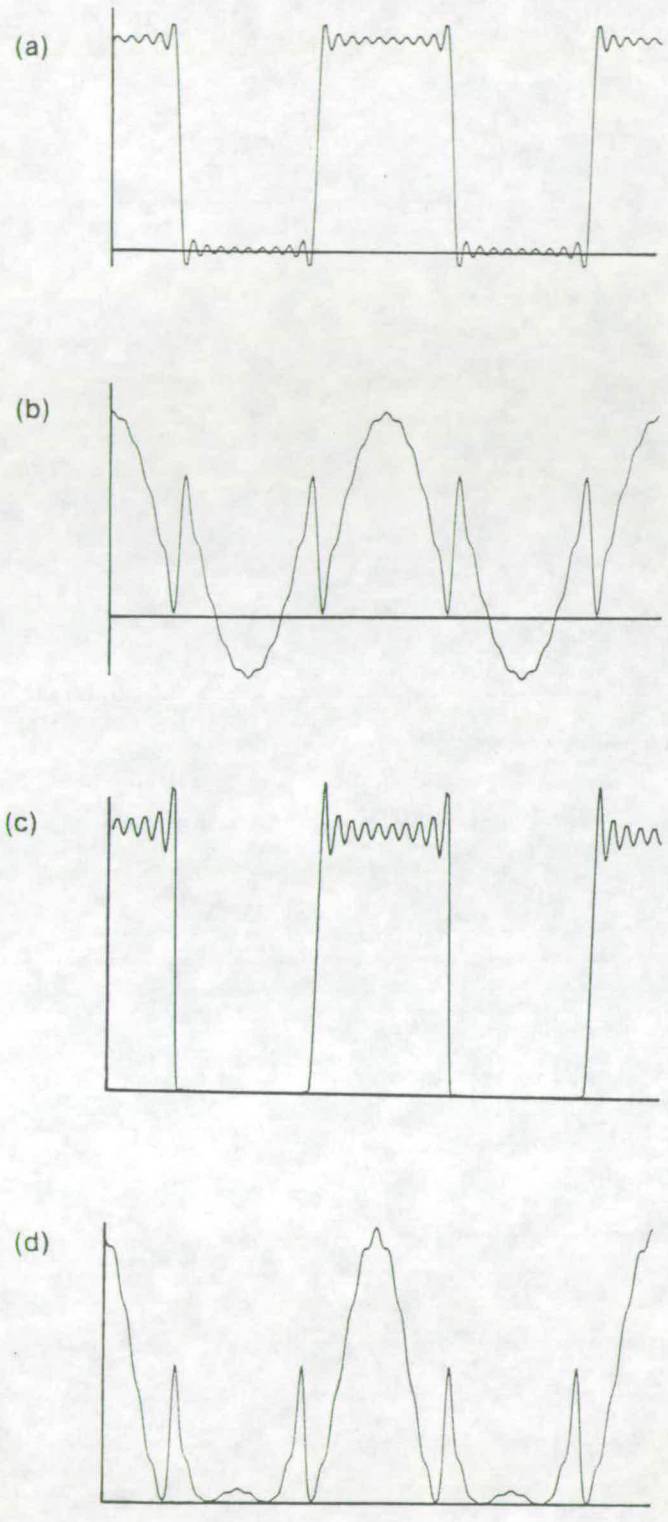

Fig 5.7 Simulation of binary phase edge-enhancement

detailed in section 1.2.1. The method involves calculating the FT of the "target object", discarding the amplitude information and thresholding the phase to 0 or π radians. Horner quantifies the vast improvement of these filters over the analogous matched filter. Flannery et al. show the striking results obtained in using a 48x48 Light-Mod SLM. Despite the very low resolution of the FIB SLM it has been attempted to demonstrate this application here.

The target object used was a square. This was chosen because it is extremely simple to calculate and programme the SLM pattern. The FT of a square object is a sinc(x).sinc(y) distribution. Applying the prescription described above gives a filter pattern with square regions of constant phase on a square array as shown in Fig. 5.8.

Various objects were used: a square, a letter "D" and a letter "Z" and these same objects rotated through 45°. The images of all of these are illustrated in Fig. 5.9 (a) to (f). They are easily identified from the unfiltered image due to reflections from the SLM glass.

At first sight these appear impressive. The images from the square are most intense, as are the images from the objects in the "correct" orientation. However much work has still to be done to validate this application.

The major problem that must be addressed is to make the total transmitted intensity of each object the same. The square has the greatest transmitting area so the high intensity of its images is to be expected. It is sensible to arrange that the objects all be of the same approximate size so the best solution to this problem is to control the amount of illumination of each object. It was observed that rotating the object caused it to translate across the illumination field which is not uniform. A further necessary improvement is either to make the illumination more uniform or to ensure that the object does not translate. The use of a Dove prism (image rotating prism) did not help as it causes the Fourier transform to shift across the SLM.

A further problem arises from consideration of the effects of pixelation and finite array size on image intensity during rotation. Most of the intensity in the FT of a square object is confined to the x and y axes. The effect of rotating this through 45° on a square array is to increase the distance between samples in the Fourier plane by the square root of 2, therefore

Notes on Fig. 5.9 (a)-(f).

These photographs illustrate the results of the binary phase correlator experiment described in section 5.5. The phase modulating SLM in the Fourier plane is programmed for the entire experiment with the pattern illustrated in Fig. 5.8. The photographs show the images observed for each of six different binary-amplitude objects. These notes clarify what is to be observed in these images.

Two main features are contained in each photograph. The more important is the replicated image (the correlation). The other is the single unfiltered image seen in the bottom left corner of the photograph caused by reflection from the SLM glass.

There are two general trends present which suggest that correlations are indeed observed:

Firstly, for the square objects, the intensity is confined to one particular region of each replication (the correlation spot). For the other objects, the intensity is distributed in a more even way over the entire replication. This shows the potential for pattern recognition.

Secondly, as explained in chapter one (page 10) the discarding of the amplitude of the filter pattern is similar to edge-enhancing the target object. Thus correlations with an edge-enhanced square are expected. Each correlation has the general features to be expected from correlation of the object with an edge-only square. For example, for the solid square object of Fig. (a), the result of the correlation process can be crudely predicted to have the form shown below. The diagram shows one quadrant of the amplitude pattern obtained by correlating an edge-only and a solid square. By thresholding this pattern at various levels, it is possible to identify features present in some of the replicated images. For example, thresholding at a high level, say 10, leaves a cross shaped pattern. Such features can be identified in many of the replications in the upper part of the image. Thresholding at lower levels, say 5, leaves a square without its corners. Many of the replications are squares with "faded" corners.

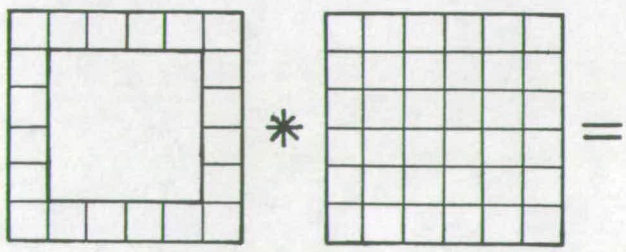

1	2	3	4	5	6
2	3	4	5	6	8
3	4	5	6	7	10
4	5	6	7	8	12
5	6	7	8	9	14
6	8	10	12	14	20

insert

0	π	0	π	π	0	π	0
π	0	π	0	0	π	0	π
0	π	0	π	π	0	π	0
π	0	π	0	0	π	0	π
π	0	π	0	0	π	0	π
0	π	0	π	π	0	π	0
π	0	π	0	0	π	0	π
0	π	0	π	π	0	π	0

Fig 5.8 Filter pattern for square object

Fig 5.9 Correlations of square target with various objects

(See supplementary notes on preceding page)

(a) square

(b) rotated square

0	π	0	π	π	0	π	0
π	0	π	0	0	π	0	π
0	π	0	π	π	0	π	0
π	0	π	0	0	π	0	π
π	0	π	0	0	π	0	π
0	π	0	π	π	0	π	0
π	0	π	0	0	π	0	π
0	π	0	π	π	0	π	0

Fig 5.8 Filter pattern for square object

Fig 5.9 Correlations of square target with various objects

(See supplementary notes on preceding page)

(a) square

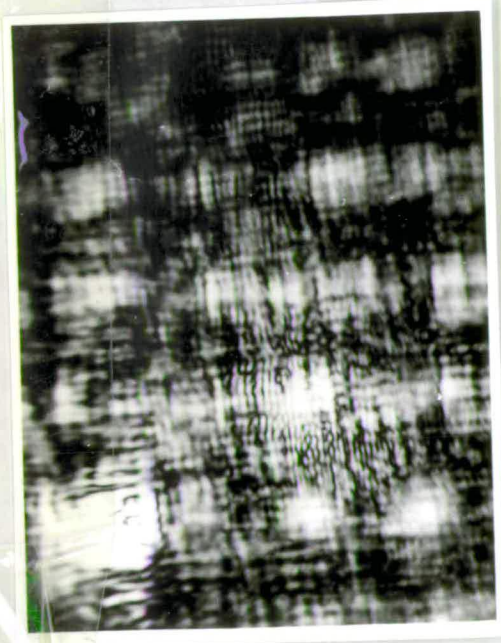

(b) rotated square

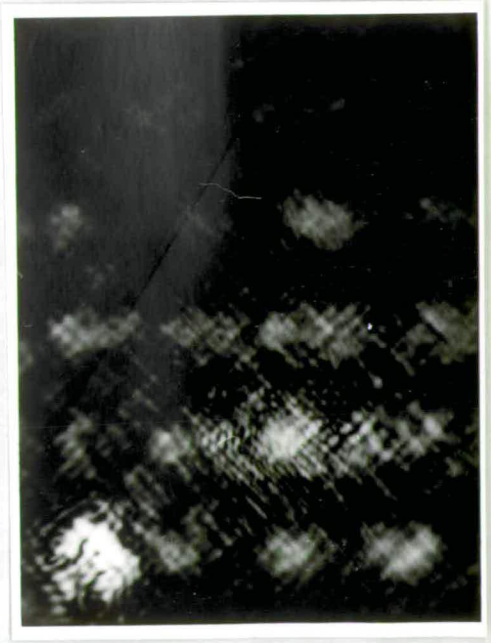

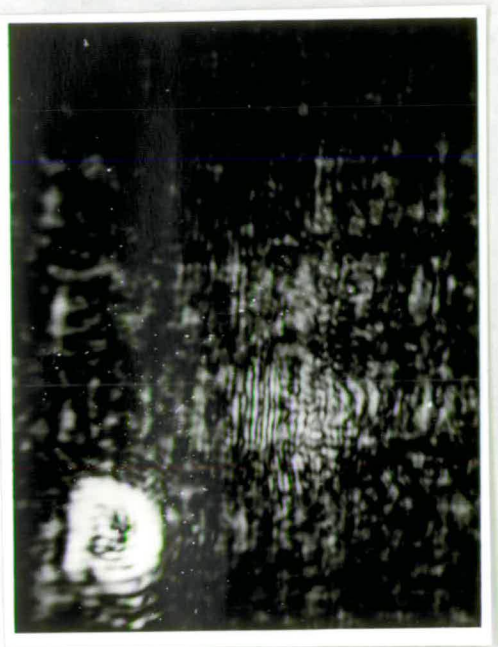

(c) "D"

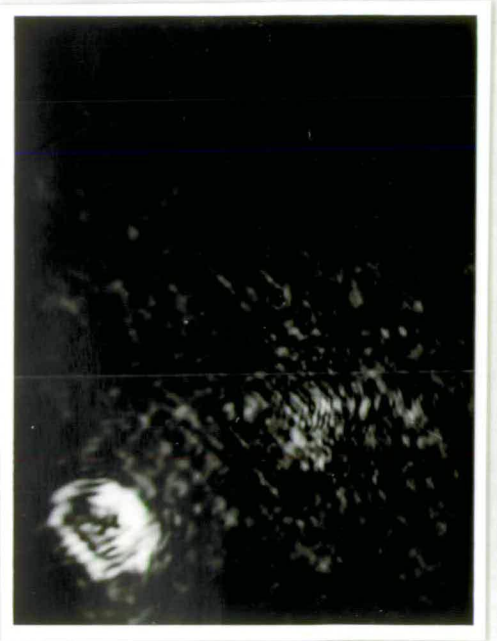

(d) rotated "D"

(e) "Z"

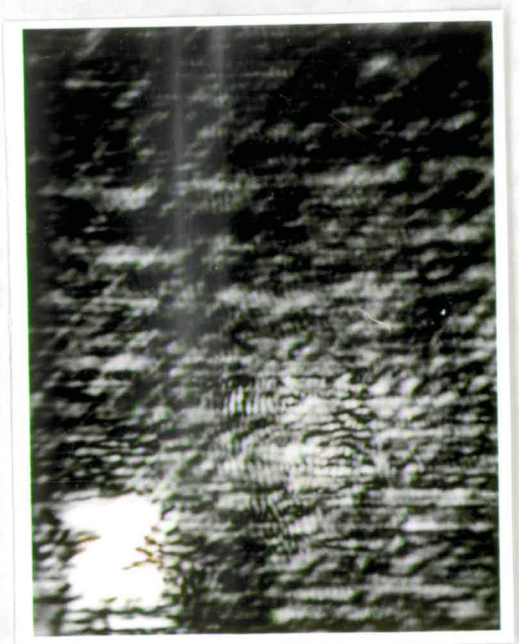

(f) "rotated "Z"

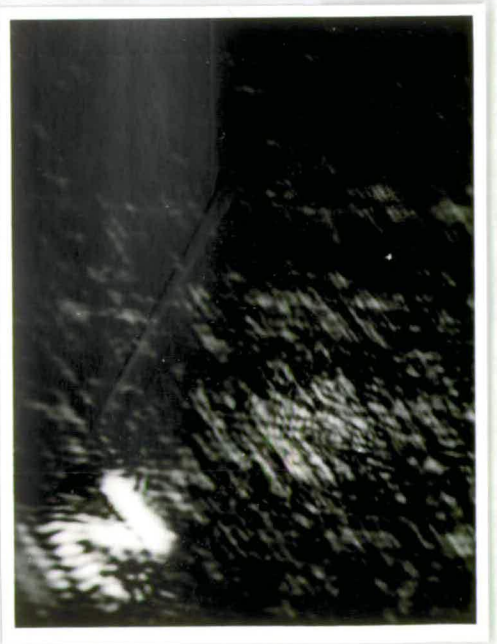

Chapter 6

Discussion of Experimental Results

In this final chapter, it is intended to discuss some of the experimental results relating to the phase modulating spatial light modulators described in chapters three and four. Firstly, the observed operational characteristics of the two SLMs will be summarised. Secondly, possible device improvements will be noted. These will mostly be acheivable in the near future with relatively little further work. However some improvements requiring significant research will also be mentioned. Finally, the relative strengths and weaknesses of the liquid crystal and deformable mirror techniques will be compared.

6.1. SLM performance summaries.

6.1.1. The deformable mirror SLM.

All of the basic principles of operation of the deformable mirror spatial light modulator were demonstrated in chapter three where Schlieren filtering techniques were employed to show the devices in use as phase modulators. Although the drive chip was designed for addressing liquid crystals , it does not seem to have been adversely affected by this particular application. The static memory elements in each pixel, which are necessary for dc operation of the device, have been shown to deform the mirrors as required. All deformable mirror SLMs working with thin, pixellated mirrors described in the literature have switching speeds in the region of 1µs or even faster and so it

making the transmitted intensity less. The overall size of the SLM along the diagonal is longer, and higher frequencies of the FT can be transmitted complicating the matter further. This effect could be investigated easily by using a backplane in place of an SLM. Finally using a higher resolution array would improve results greatly. This would allow the use of an object having several different features. This cannot be done with the 16x16 device as arranging that the replicated images do not overlap allows very little high spatial frequency information onto the array.

5.6. Summary

In this chapter the FIB SLM has been demonstrated in a number of varied applications. In some cases, the results could be improved with a device of a greater resolution. An improvement of the understanding of the driving voltages applied to the liquid crystal to permit accurate setting of the phase would be invaluable. The poor uniformity and low contrast of the SLM, and the reduction of the reflection of light from the cover glass would also be important areas for improvement in the future.

In summary, the versatility of the FIB SLM and of phase modulating SLMs in general has been proven.

Chapter 6

Discussion of Experimental Results

In this final chapter, it is intended to discuss some of the experimental results relating to the phase modulating spatial light modulators described in chapters three and four. Firstly, the observed operational characteristics of the two SLMs will be summarised. Secondly, possible device improvements will be noted. These will mostly be acheivable in the near future with relatively little further work. However some improvements requiring significant research will also be mentioned. Finally, the relative strengths and weaknesses of the liquid crystal and deformable mirror techniques will be compared.

6.1. SLM performance summaries.

6.1.1. The deformable mirror SLM.

All of the basic principles of operation of the deformable mirror spatial light modulator were demonstrated in chapter three where Schlieren filtering techniques were employed to show the devices in use as phase modulators. Although the drive chip was designed for addressing liquid crystals , it does not seem to have been adversely affected by this particular application. The static memory elements in each pixel, which are necessary for dc operation of the device, have been shown to deform the mirrors as required. All deformable mirror SLMs working with thin, pixellated mirrors described in the literature have switching speeds in the region of 1μs or even faster and so it

can be expected that ultimately this device will have comparable speed.

The work described in chapter three shows that there is a single area in which the device is currently lacking. This is the quality of the mirrors. Their optical quality is satisfactory but they are mechanically unpredictable. This is manifest in gross defects such as tears in the mirror and in the great variation in the mirror tension which causes fabrication problems and response non-uniformities. Conclusions have been reached about possible improvements that can be made in this respect.

6.1.2. The FIB liquid crystal SLM.

The birefringence of liquid crystals has been used in chapter four to produce a SLM capable of both phase and amplitude modulation. Measurements made from test-cells have given upper bounds on the switching times of 10ms "ON" and 20ms "OFF". A lower bound on the contrast ratio of 100 was also measured from these test cells. These parameters were not measured from the SLMs themselves although it can be expected that this would yield faster switching times but lower contrast. This is because of power dissipation in the electronic circuitry. This effect is faster than many other effects in nematic liquid crystals due to the small molecular reorientations required and the high molecular torques involved. Because the light modulation effect in very strongly related to the LC layer thickness, the question of the uniformity of the SLMs is important. However, as it has proven advantageous for other reasons to operate the SLMs in the voltage regime where birefringence is low, this is not a great problem. Given this condition, it appears likely from experimental observation that it is technologically feasible to produce cells of adequate thickness uniformity.

6.2. Suggestions for device improvements and future research.

6.2.1. The deformable mirror SLM.

As was noted in section 6.1.1, the major effort that must now go into this project is in improving the production of the deformable mirrors. Thoroughly investigating the possible mirror materials and coating techniques to optimise

the mechanical and optical properties of the mirrors would be a substantial project. However it is likely that significant improvements to both the fabrication technique and to the device characteristics could result from the design of an extra mask level for the chip. This could be done relatively quickly and would define a spacer layer featuring air-channels through the spacer and supporting "pillars" in the active region of the pixel.

A more advanced silicon backplane has now been produced and used to produce LC SLMs by McKnight et al. [1988]. This array has 50x50 pixels on a 74µm spacing and is a suitable basis for a higher resolution SLM.

The groundwork for development of an photo-cathode addressed deformable mirror device similar to the PEMLM has been conducted as a part of this project. This could be brought to a conclusion in several ways. Possibly the most attractive project would be to develop the system described at the end of chapter three. This incorporates a laterally conducting face-plate into a vacuum photo-diode which would permit many light modulating media to be examined including some which are otherwise incompatible with vacuum such as liquid crystals.

6.2.2. The FIB liquid crystal SLM.

The liquid crystal device described in chapter four could be improved by a further investigation of the FIB effect. This may involve more test-cell work to ascertain the conditions for best uniformity, contrast and speed. It is likely that there will be a "trade-off" in these factors so some compromise may be required. Other liquid crystals could be examined to find a more suitable material for this application.

It should be clear from the preceding work that in moving from test-cells to SLMs there are factors introduced which need attention. For example, because of voltage drops across transistors, the signal generated on the pixel electrodes does not precisely correspond to the input voltages. It would therefore be necessary to undertake a calibration of this. A very important matter is the acquisition of a knowledge of the phase of light reflected from the circuitry of the SLM. This is generally a very complicated matter as the thickness and birefringence of the LC varies considerably in this region.

Although the device is very useful without this knowledge, it would be very important for an experimental examination of the theory of phase-modulating devices.

Another worthwhile refinement would be the production of the spacer by photolithographic techniques resulting in greater uniformity and reproducibility. the use of the 50x50 array already mentioned in section 6.2.1 is a further important improvement for the near future.

6.3. Comparison of liquid crystals and deformable mirrors for phase modulation.

If this comparison were based purely upon the experimental results obtained during the course of this research, then the LC device would probably be attributed a great number of advantages over the deformable mirror device. This is due, to a large extent, to the much more widespread use and more extensive development of LC technologies. However to make a valid comparison of the two devices, it is necessary to consider also the projected performance of the light modulation techniques and the work of other researchers.

The criterion regarding which it is possible to make the greatest distinction is probably the response time. The switching speed of nematic liquid crystals is often quoted as a one of their major drawbacks. In the effect used in this project, the switching speed has been measured to be of the order of a few milliseconds. It is unreasonable to expect this to improve to the extent of competing with the µs switching times reported for deformable mirrors. The deciding factor on this point is the intended application. LCs can certainly be operated at television framing rates which is adequate for many uses.

The reflection of light from the cover glass of the LC device cannot be eliminated completely when it is being used as a phase modulator. This introduces a significant amount of noise into images or, viewed in another way, reduces the efficiency or contrast of the device. Note that although the deformable mirror SLM has no cover glass, an analogous effect due to light being reflected from the circuitry would be noticed if the reflectance of the mirror were too low.

One of the major advantages of the LC device is its potential for use to modulate amplitude in addition to phase. The deformable mirror device is intrinsically a phase modulator. This versatility is useful for device characterisation and will be useful for many applications. Examined from the point of view of obtaining a pure phase modulation this aspect of the device could in fact be seen as a disadvantage. In general, it is the specific application under consideration which dictates the relevance of this fact.

The last important distinction between the two devices is the effect of the non-addressable parts of the array. For the DM device, the mirror in this region is not expected to deform much. The phase of the light reflected from this region will not be variable. Secondly, it can be expected that the value of this phase will be near to the value for an undeformed pixel and near to the mean phase. This means that the intensity observed in the image plane after Schlieren filtering will be low for inactive areas and unaddressed pixels, and will follow a simple Bessel function for the addressed pixel. This is attractive for some applications such as display and would simplify work examining the phase-modulation theories. However, as has already been remarked in section 6.2.2, the phase of the light reflected from the inactive parts of the LC SLM is not easily quantified.

In most other respects, neither device has a clear advantage. Both devices can potentially produce multiple π radians of phase change and, if not restricted by binary drive circuitry, can produce a "grey-scale". The resolution of both devices is determined primarily by the array spacing however will be fundamentally limited at some point. For LCs, the limit is reached when the pixel dimension becomes comparable to the LC layer thickness and fringing of the electric field becomes noticeable. For the deformable mirrors, producing a π phase change from a pixel smaller than a critical size will lead to large strains in the mirror and result in rapid degradation.

6.4. Conclusion.

In this final chapter, the work on constructing and assessing the two spatial light modulators has been summarised and the devices have been compared. Thus the objectives of the project as specified in chapter one have been completed.

I. Light transmission by a birefringent plate

Fig. A1.1 shows a plate of birefringent material whose optical axis is defined by the vector $\underline{D}$. Let us suppose that it is illuminated with light linearly polarised at a direction θ to the optical axis and that the transmitted light is analysed by a second polariser at an angle ϕ to the optical axis.

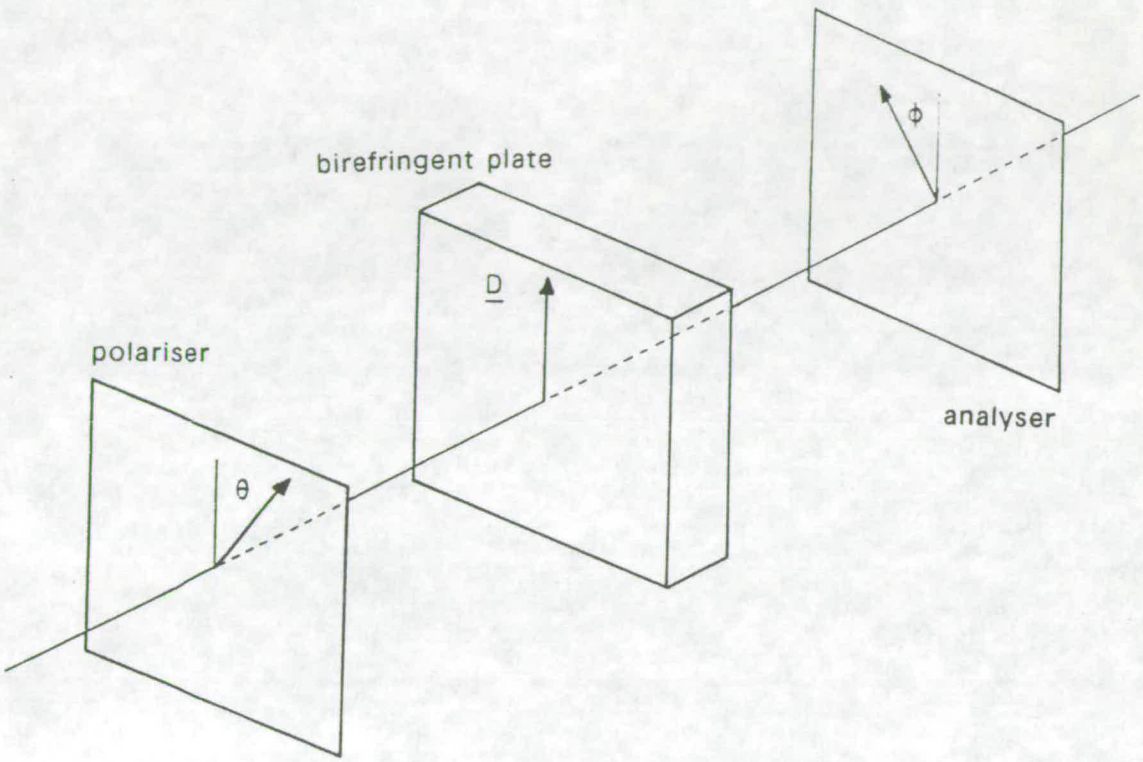

Fig A1.1 Light transmission by a birefringent plate

If the amplitude of the light transmitted by the first polariser is U_o then its components resolved parallel and perpendicular to the optical axis, ($U_{parallel}$ and $U_{perpendicular}$), are given by:

$$U_{parallel} = U_o \cos\theta \text{ and} \qquad \text{(A1.1a)}$$

$$U_{perpendicular} = U_o \sin\theta. \qquad \text{(A1.1b)}$$

The effect of the cell is to retard the phase of the parallel component by an amount δ. The components of polarised light leaving the cell can now be

repesented by $U'_{parallel}$ and $U'_{perpendicular}$ where

$$U'_{parallel} = U_o \cos\theta e^{i\delta} \tag{A1.2a}$$

$$U'_{perpendicular} = U_o \sin\theta \tag{A1.2b}$$

The analyser will transmit those components of $U'_{parallel}$ and $U'_{perpendicular}$ which are parallel to its polarising direction defined by ϕ.

The magnitude of the transmitted electric vector, U', is thus given by

$$U' = U'_{parallel}\cos\phi + U'_{perpendicular}\sin\phi$$

$$= U_o(\cos\theta\cos\phi e^{i\delta} + \sin\theta\sin\phi) \tag{A1.3}$$

and the intensity I observed in a plane beyond the analyser is given by

$$I = | U' |^2$$

$$= U_o^2 \ (1 + \cos2\theta\cos2\phi + \cos\delta\sin2\theta\sin2\phi)/2 \tag{A1.4}$$

In the case of either polariser being parallel or perpendicular to the director (i.e. θ or ϕ = 0° or 90°) then the birefringence dependent term becomes zero and the cell appears isotropic exhibiting Malus' law behaviour for rotation of the other polaroid.

In the case of one polariser being at 45° (or 135°) i.e. the cos terms vanish and the sine terms = ±1 then the birefringence independent term becomes zero and intensity modulation by changing δ is possible.

Here $I = U_o^2 \ (1 + \cos\delta\sin2\phi)/2$ (A1.5)

(For θ = 45°)

If the birefringence and the resulting phase change is varied then light and dark fringes are observed corresponding to $\cos\delta$ = +1 and −1 respectively. The contrast of these fringes is maximum (infinite) for $\sin2\phi = \pm1$.

Thus high contrast intensity modulation is observed for incident light polarised at 45° to the director observed through an analyser at 45° or 135° (crossed or parallel)

The intensity observed in this case is

$$I = U_o^2 \cos^2(\delta/2) \qquad \text{(A1.6a)}$$

for uncrossed polaroids and

$$I = U_o^2 \sin^2(\delta/2) \qquad \text{(A1.6b)}$$

for crossed polaroids.

II. The LCIC chip

A considerable amount of the experimental work in this work concerned with SLM development has been based on the LCIC (liquid-crystal integrated-circuit) chip. This chip was designed and used to drive a guest-host LC SLM in the Applied Optics group at Edinburgh by Underwood [1987] as part of a PhD project. Evaluation of the chip has been published by Underwood et al. [1986]. In this appendix the features of the chip relevant to this project will be presented.

Electronics

The chip is built using a standard 5 micron nMOS process in the Edinburgh Microfabrication Facility. It has 16x16 pixels in a square array. Each pixel has the novel feature of a static memory element dispensing with any requirement for dynamic refreshing of data and resulting in a more stable voltage signal to the LC. The content of the pixel memory circuit is combined with a universal clock signal by an exclusive NOR gate (XNOR). The output of this gate is fed directly to a large metal pad. This pad has the double function of an electrode to control the LC voltage and of a high optical quality mirror to reflect the transmitted light. The mirror voltage can be seen from the truth table, Fig. A2.1, to be a square wave taking values of zero volts and positive rail voltage, V_{DD}. This is in phase or in anti-phase with the clock signal depending as the memory logic value is 1 or 0. This allows an ac voltage signal to be applied to the LC layer by the application of a clock signal to the counter electrode. The pixel array is addressed by 16 row data lines and 16 column enable lines. When an enable input is held "high" the data is passed into the pixel memories of that column where they are stored. The electronic inputs to the chip are thus the 32 addressing lines, a clock input, the positive rail voltage V_{DD}, the earth and the silicon substrate voltage. The chip is packaged in a standard 40 pin IC holder so there are in fact four unconnected pins.

Addressing the chip can be done in a variety of ways but the simplest way is to manually connect the addressing lines to zero or V_{DD} volts as required. A microcomputer controlled interface circuit is being developed.

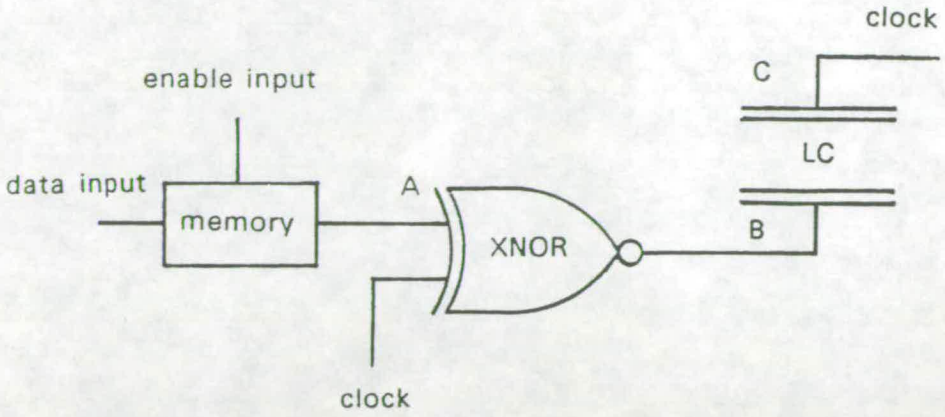

A Ck B C	LC voltage
0 0 1 0 0 1 0 1	+/-V_{DD}
1 0 0 0 1 1 1 1	0

Fig A2.1 Pixel functional diagram and truth table

Fig A2.2 Block plan of LCIC

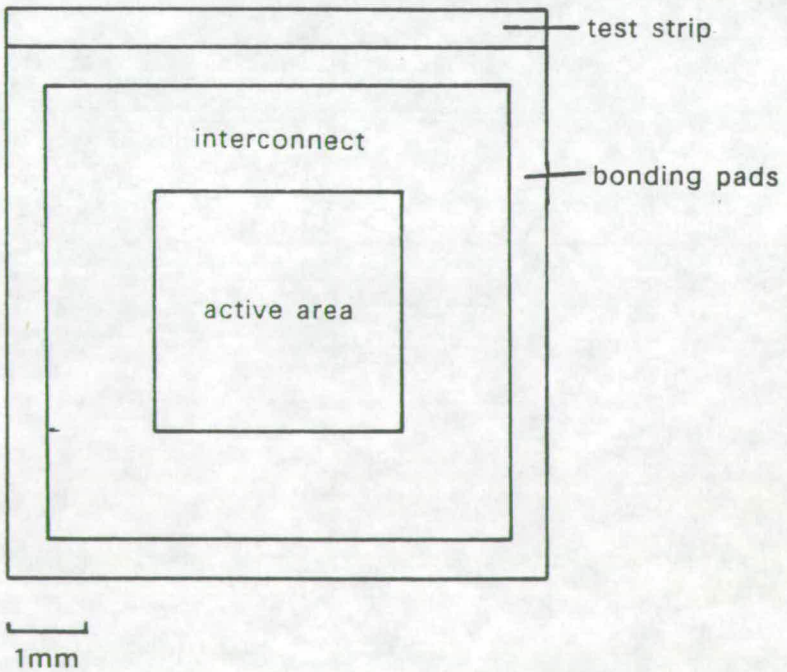

Electronic testing

The IC was tested by Underwood for values of V_{DD} between 5V and 15V. This is important to allow freedom in adapting the chip for a variety of light modulation effects. It should be remembered that the voltage values observed on the electrode are not exactly the chip drive voltages. This is due to voltage drops across the transistors. The fall and rise times of the pixel electrodes were found to be 0.03µs and 0.2µs respectively at 5 volts. Thus the chip will cope with nematic liquid crystals which switch in milliseconds. When using it to drive faster modulating media, the limitation may be the electronic switching time.

Topography of the chip

For the purposes of fabricating SLMs on this silicon backplane it is important to have a good understanding of the dimensions of the chip. This is invaluable for the developmant of light modulating mechanisms and for mechanical tolerancing in the fabrication itself. Fig A2.2 shows a block plan of the layout of the whole IC.

The outer edge of the die contains the bonding pads to which fine gold wires are welded to make electrical contact. The region between these contains the interconnecting conductors to the active part of the chip which is $3.2 \times 3.2 mm^2$ in area. The die is mounted in a standard 40 pin IC holder. It should be noted that the chip is recessed below the level of the top surface of the holder which influences the techniques of SLM construction.

At a lower level, the dimensions of the pixel are important. The pixel mirror has an area of $100 \times 100 \mu m^2$ within the pixel of $200 \times 200 \mu m^2$. The remainder of the area is taken up by the driving circuitry. The pixel mirror itself is optically flat, but the circuitry results in height variations of about 0.6 µm above the mirror level.

Anderson RH, "Edge enhancement of coherent magnetooptic images", *Appl. Opt.*, **25**, (1986), 976-982.

Arfken G, "Mathematical methods for physicists", Pub. Academic press, (1970).

Baillie WL, "Developments of reflection mode liquid crystal light valves using $Bi_{12}SiO_{20}$ as the photoconductor", *IEE Proc. J*, **134**, (1987), 326-332.

Blinov LM, "Electro-optical and magneto-optical properties of liquid crystals", Pub. John Wiley and Sons, (1983).

Bracewell RN, "The Fourier transform and its applications", Pub. McGraw-Hill, (1978).

Bradshaw MJ, "Liquid crystal devices", *Phys. Educ.*, **18**, (1983), 20-26.

Brooks RE, "Micromechanical light modulators for data transfer and processing", *Proc. SPIE*, **465**, (1984), 46-54.

Casasent D, "Spatial light modulators", *Proc. IEEE*, **65**, (1977), 143-157.

Castellano JA, "Surface anchoring of liquid crystal molecules on various substrates", *Mol. Cryst. Liq. Cryst.*, **94**, (1983), 33-41.

Cathey WT, "Optical information processing and holography", Pub. John Wiley and Sons, (1974).

Clark MG, Harrison KJ and Raynes EP, "Liquid crystal materials and devices", *Phys. Technol.*, **11**, (1980), 232-240.

de Gennes PG, "The Physics of Liquid Crystals", Pub. Pergammon Press, (1975).

Efron U, Grinberg J, Braatz PO, Little MJ, Reif PG and Schwartz RN, "The silicon liquid crystal light valve", *J. Appl. Phys.*, **57**, (1985), 1356-1368.

Farhat NH, Psaltis D, Aliuzio P and Paek E, "Optical implementation of the

Hopfield model", *Appl. Opt.*, **24**, (1985), 1469-1475.

Fisher AD, Ling LC and Lee JN, "A high performance photo-emitter membrane spatial light modulator", *Proc. SPIE*, **465**, (1984), 36-45.

Fisher AD, "A review of spatial light modulators", technical digest, OSA meeting on "Optical Computing", (1985).

Fisher AD and Lee JN, "The current state of two-dimensional spatial light modulator technology", *Proc. SPIE*, **634**, (1986), 352-371.

Fisher AD, Ling LC, Lee JN and Fukuda RC, "Photoemitter membrane light modulator", *Opt. Eng.*, **25**, (1986), 261-268.

Flannery DL, Biernacki AM, Loomis JS and Cartwright SL, "Real-time coherent correlator using binary magnetooptic spatial light modulators at input and Fourier planes", *App. Opt.*, **25**, (1986), 466.

Gibson DG, Aldridge N, Brown MB, Levenston AG and White H, "Automatic recognition and tracking of targets from visible or thermal imagery, using optical processing", *Proc. SPIE*, **492**, (1984), 165-174.

Goodman JW, "Introduction to Fourier optics", Pub. McGraw Hill, (1968).

Goodman LA, "Liquid crystal displays", *J. Vac. Sci. Technol.*, **10**, (1973), 804-823.

Grinberg J, Jacobson A, Bleha W, Miller L, Fraas L, Boswell D, Myer G and Cobleigh UT, "A new real-time non-coherent to coherent light image converter - the hybrid field effect liquid crystal light valve", *Opt. Eng.*, **14**, (1975), 217-225.

Hopfield JJ, "Neural networks and physical systems with emergent collaborative computational capabilities", *Proc. Natl. Acad. Sci. USA*, **79**, (1982), 2554-2558.

Horner JL and Bartelt HO, "Two-bit correlation", *App. Opt.*, **24**, (1985), 2889-2893.

Lakatos AI, "Photoelectric induced elastomer deformation in PVK-TNF type

γ-RUTICON", *J. Appl. Phys.*, **45**, (1974), 4857-4868.

Latham SG and Owen MP, "A silicon liquid-crystal spatial light modulator", *GEC J. Res.*, **4**, (1986), 219-222.

Ling LC, Fisher AD, Lee JN and Fukuda RC, "Operation of the photo-emitter membrane spatial light modulator", *Proc. SPIE*, **567**, (1985), 121-131.

McKnight DJ, Vass DG and Sillitto RM, "Development of a spatial light modulator: a randomly addressed liquid-crystal-over-nMOS array", "Spatial light modulators and applications", 1988 technical digest series, **8**, (1988), 151-154.

Neff JA, "Major initiatives for optical computing", *Opt. Eng.*, **26**, (1987), 002-009.

Paek EG and Psaltis D, "Optical associative memory using Fourier transform holograms", *Opt. Eng.*, **26**, (1987), 428-433.

Pape DR, "An optically addressed membrane spatial light modulator", *Proc. SPIE*, **465**, (1984), 17-22.

Pape DR and Hornbeck LJ, "Characteristics of the deformable mirror device for optical information processing", *Opt. Eng.*, **22**, (1983), 675-681.

Petersen KE, "Micromechanical light modulator array fabricated on silicon", *Appl. Phys. Letts.*, **31**, (1977), 521-523.

Preston K, "The membrane light modulator and its application in optical computers", *Opt. Act.*, **16**, (1969), 579-585.

Psaltis D and Farhat N, "Optical information processing based on an associative memory model of neural nets with thresholding and feedback", *Opt. Lett.*, **10**, (1985), 98-100.

Rolsma PB, Lee JN and Oh T-K, "Experimental investigation of photoemitter membrane spatial light modulator performance limit", "Spatial light modulators and applications", 1988 technical digest series, **8**, (1988), 179-182.

Ross WE, Psaltis D, and Anderson RH, "Two-dimensional magneto-optic

spatial light modulators for signal processing", *Opt. Eng.*, **22**, (1983), 485-490.

Sheridon NK, "The ruticon family of erasable image recording devices", *Trans. IEEE*, **ED 19**, (1972), 1003-1010.

Sheridon NK and Berkovitz MA, "Coherent optical processing capabilities of the Ruticon", *Proc. Electro-optical Sys. Des. Conf.*, (1975), 475-480.

Somers LE, in "Advances in electronic and electron physics", Pub. Academic Press, Vol 33A, (1973), 493-510.

Sommer AH, "Photoemissive materials", Pub. Krieger, New York, (1980).

Tanida J and Ichioka Y, "Optical logic array processor using shadowgrams", *J. Opt. Soc. Am.*, **73**, (1983), 800-809.

Thompson BJ, "Hybrid processing systems - an assessment", *Proc. IEEE*, **65**, (1977), 62-76.

Underwood I, Vass DG and Sillitto RM, "Evaluation of an nMOS VSLI array for an adaptive liquid crystal spatial light modulator", *IEE Proc. J (Optoelectronics)*, **133**, (1986), 77-82.

Underwood I, "An nMOS addressed liquid crystal spatial light modulator", PhD. Thesis, University of Edinburgh, (1987).

Vander Lugt A, "Coherent Optical Processing", *Proc IEEE*, **62**, (1974), 1300-1319.

Vass DG, Dougal RC, Weir K and MacGregor AR, "Light transmission through twisted nematic liquid crystal cells", *Proc. SPIE*, **651**, (1986), 112-119.

Vohl P, Nisenson P and Oliver DS, "Real-time incoherent-to-coherent optical converter", *Trans. IEEE*, **ED-20**, (1973), 1032-1037.

Wallace DJ, "Neural network models: a physicist's primer", Proc. 32nd Scottish Summer School in Physics, (1987), 168-210.

Warde C, Weiss AM, Fisher AD and Thackara JI, "Optical information processing characteristics of the microchannel spatial light modulator" *App. Opt.*, **20**, (1981), 2066-2074.

Warde C and Thackara J, "Operating modes of the microchannel spatial light modulator", *Opt. Eng.*, **22**, (1983), 695-703.

Weigelt J, "Binary logic by spatial filtering", *Opt. Eng.*, **26**, (1987), 28-33.

Welkovsky MS, Efron U, Byles W, and Goodwin NW, "Status of the Hughes charge-coupled-device-addressed liquid crystal light valve", *Opt. Eng.*, **26**, (1987), 414-417.

Willson PH, "Pixelated spatial light modulators used as spatial filters in the Fourier transform plane of an optical system", Annual PhD report, (1987), Dept. of Physics, Univ. of Edinburgh, (unpublished).

Wu S-T, Efron U and Hess LD, "Birefringence measurements of liquid crystals", *App. Opt.*, **23**, (1984), 3911-3915.

Young M, "Low-cost LCD video display for optical processing", *App. Opt.*, **25**, (1986), 1024-1026.

Publications

Some of the results contained in this thesis were presented at the IEE colloquium on Optical Techniques for Information Processing in London 1987 and published as

Vass DG, Sillitto RM, Underwood I, McKnight DJ, Willson PH and Ranshaw MJ, "Progress in developing VLSI based Spatial Light Modulators", *IEE Colloquium Digest 1987/105.*

This paper is reproduced overleaf.

Two unpublished papers were presented at the IoP optical group meeting at Heriot Watt university, 18th May 1988, entitled

McKnight DJ, Ranshaw MJ, Underwood I ,Vass DG, and Willson PH, "Experiments with electronically addressed SLM arrays."

and

Fancey NE, Ranshaw MJ, Sillitto RM, Sillitto W, and Willson PH, "Imagery of sampled objects with pixellated Fourier plane filters."

A presentation will be made at the ICO Topical Meeting on Optical Computing in Toulon, France, August 1988 and published as

Ranshaw MJ, Vass DG and Sillitto RM, "Phase or amplitude modulation by birefringence in a liquid-crystal spatial light modulator", *Proc. SPIE,* **963,** (1988).

A summary of this is included in the thesis.

Presented at IEE Colloquium on Optical Techniques for Information Processing, London 1987, IEE Digest 1987/105.

PROGRESS IN DEVELOPING VLSI BASED SPATIAL LIGHT MODULATORS

D.G. Vass, R.M. Sillitto, I. Underwood, D.J. McKnight, P.H. Willson and M.J. Ranshaw.

Introduction

The development of high quality spatial light modulators (SLMs) is essential for the realisation of real-time optical information processing systems and optical computers. In particular for those systems where the information is carried by coherent light, the 2-D SLM must impose precisely controlled amplitude and phase modulations on the coherent light beam. In this contribution we discuss the development of VLSI nMOS arrays as the pixel-addressing components in devices, and describe amplitude-only and phase-only SLMs which may be constructed using these nMOS arrays.

Prototype 16x16 pixel liquid-crystal-over-silicon SLM

A 16 x 16 pixel array on a 7 x 7 mm^2 silicon chip has been designed using the VLSI design and mask-making facilities at the Rutherford-Appleton Laboratory (RAL) and fabricated using the 6 µm nMOS process at the Edinburgh Microfabrication Facility (EMF). The pixels are spaced 200 µm apart and each carries a metal pad, insulated from the silicon substrate by an oxide layer, which acts both as an output electrode and as a mirror. The pixel mirrors 110 x 110 μm^2 are flat to within ± 25 nm as judged by white light interferograms obtained using a LINNICK interferometer at Imperial College. A prototype SLM has been fabricated using a guest-host liquid-crystal mixture on the surface of the silicon as the light modulating medium. The VLSI array is addressed as a static random access memory (1 bit deep), and the liquid crystal above each pixel mirror activated to absorb or transmit light according to whether the datum stored in the array element is a logic '0' or a logic '1'. An assessment of the electrical performance of the VLSI array has already been published[1], and the use of the SLM as a binary-amplitude filter in the Fourier plane of a coherent optical processor is being investigated[2].

Development of a 128 x 128 pixel liquid-crystal-over-silicon SLM

Following the successful testing of the 16 x 16 prototype SLM, research has been initiated to fabricate a 128 x 128 nMOS array using a more compact integrated circuit technology. A schematic diagram of the circuitry associated with each pixel in the array is shown in figure 1. A 128 bit data word is applied via shift registers to the 128 inputs of the rows of the pixel array and a sequence of read/hold pulses is applied to each of the 128 column inputs, again by means of shift registers. In this way a logic signal is loaded into each pixel circuit and the datum stored as a voltage level at the node D, figure 1. The voltage signal fed to the mirror electrode to activate the overlying liquid-crystal layer is derived by mixing a universal clock signal with the logic signal at node D. The complement of this clock signal, $\overline{clock}$, is fed to the transparent counter electrode which encapsulates the liquid crystal on top of the IC. With this arrangement, as indicated in the truth table of figure 1, the liquid

The Authors are with the Physics Department, Edinburgh University. Mayfield Road, Edinburgh. EH9 3JZ.

crystal experiences an alternating electric field when the voltage level at node D is nominally +5V, whereas no field is generated when the voltage level is zero.

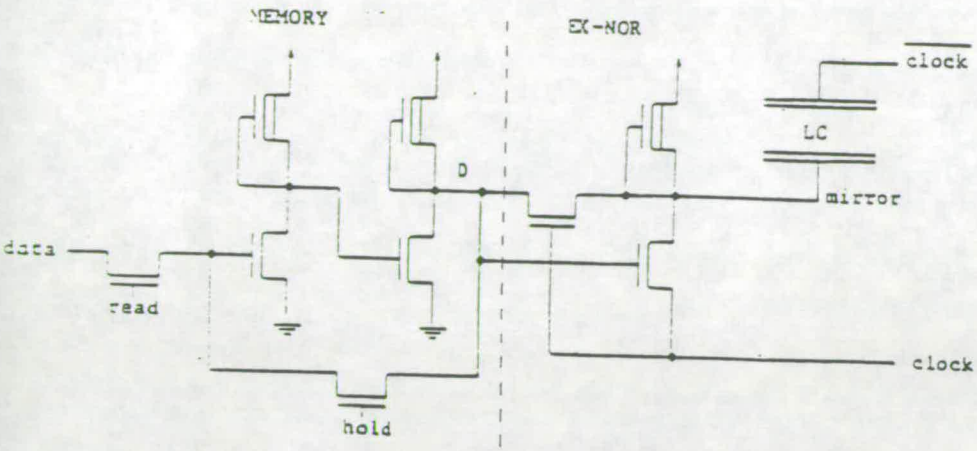

D	ck	mirror	$\overline{ck}$	LC
0	0	1	1	OFF
0	1	0	0	OFF
1	0	0	1	ON
1	1	1	0	ON

Figure 1.

The layouts for a 12 level mask set carrying test structures for this second generation SLM have been produced, and X10 reticles procured through the Silicon Brokerage at RAL. The fabrication of wafers is well advanced using the 1.5 µm nMOS process being developed at the EMF. A block diagram showing the disposition of test structures on the 1 x 1 cm^2 IC surface is given in figure 2; as indicated a 50 x 50 array is included in the top left hand quadrant for test purposes. This array has mirrors of area 45 x 44 μm^2 with the mirror centres 74 µm apart, which means that the mirror surfaces cover just over 33% of the area of the array.

It is intended to construct a SLM for use as a binary-amplitude filter by establishing a 45° twisted nematic arrangement, as described by Grinberg[3], on the surface of the chip. Measurements of the intensity of light reflected from test cells, constructed to simulate the operation of the reflective SLM, show that contrast ratios > 10^3 between the intensities reflected in the ON and OFF states may be obtained. Also the spurious reflections from the glass/ITO/liquid crystal interfaces, which degraded the performance of the guest-host liquid crystal arrangement used with the 16 x 16 pixel SLM[2], may be rejected using the 45° twisted nematic scheme.

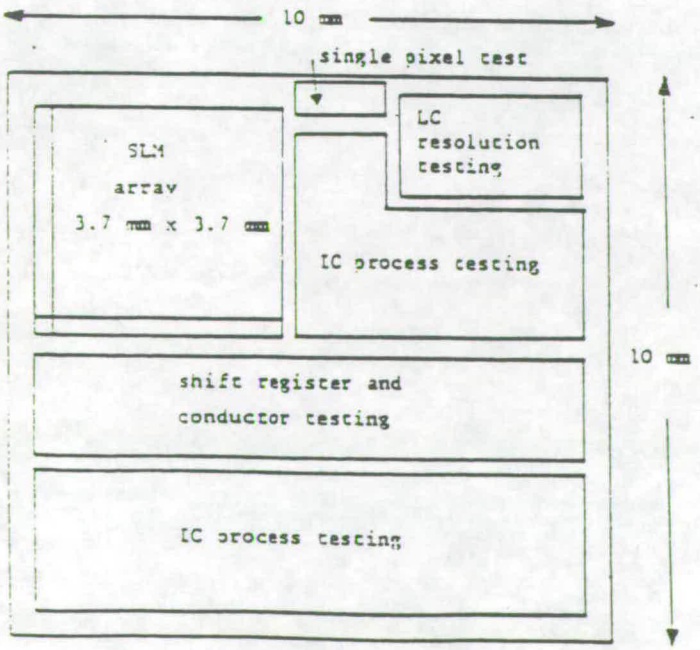

Figure 2.

Development of a deformable-mirror-over-silicon SLM

A phase modulating SLM may be constructed using a deformable mirror to control the lengths of the optical paths travelled by coherent light through the device, as described by Pape and Hornbeck[4]. The imagewise deflection of a deformable mirror may be accomplished using a modified version of either one of the VLSI arrays described above. The structure of a typical deformable-mirror device based on a VLSI array is illustrated in figure 3. An insulating layer of photoresist - 3 μm thick is deposited on the surface of the wafer and "wells" formed in the insulator by etching away the photoresist above the metal electrodes. A thin membrane of nitrocellulose 300-400 nm thick is formed and a layer of aluminium - 30 nm thick evaporated onto one surface. This thin, reflecting, electrically conducting membrane is then stretched across the surface of the integrated circuit and covers each of the "wells" as indicated in figure 3. A static voltage V_m is applied to the aluminium mirror on the membrane and, by applying a steady clock signal to the pixel array, a voltage V_p is applied to the pixel electrode: V_m = 25 V; V_p = 0V or 5V. The local potential difference $(V_m - V_p)$ between each pixel electrode and the aluminium mirror determines the deformation profile of the membrane which is deflected into the well from its equilibrium position. The maximum deflection D of the deformed mirror is given approximately by $D = K(V_m - V_p)^2$, where K is a constant whose value depends on the pixel geometry and the elastic properties of the membrane. The change ΔD in the maximum deflection caused by a change of pixel voltage ΔV_p is given, therefore, by $\Delta D = K\,\Delta V_p(2V_m - \Delta V_p)$. Obviously the dynamic range of the device may be tuned by adjusting the bias voltage V_m.

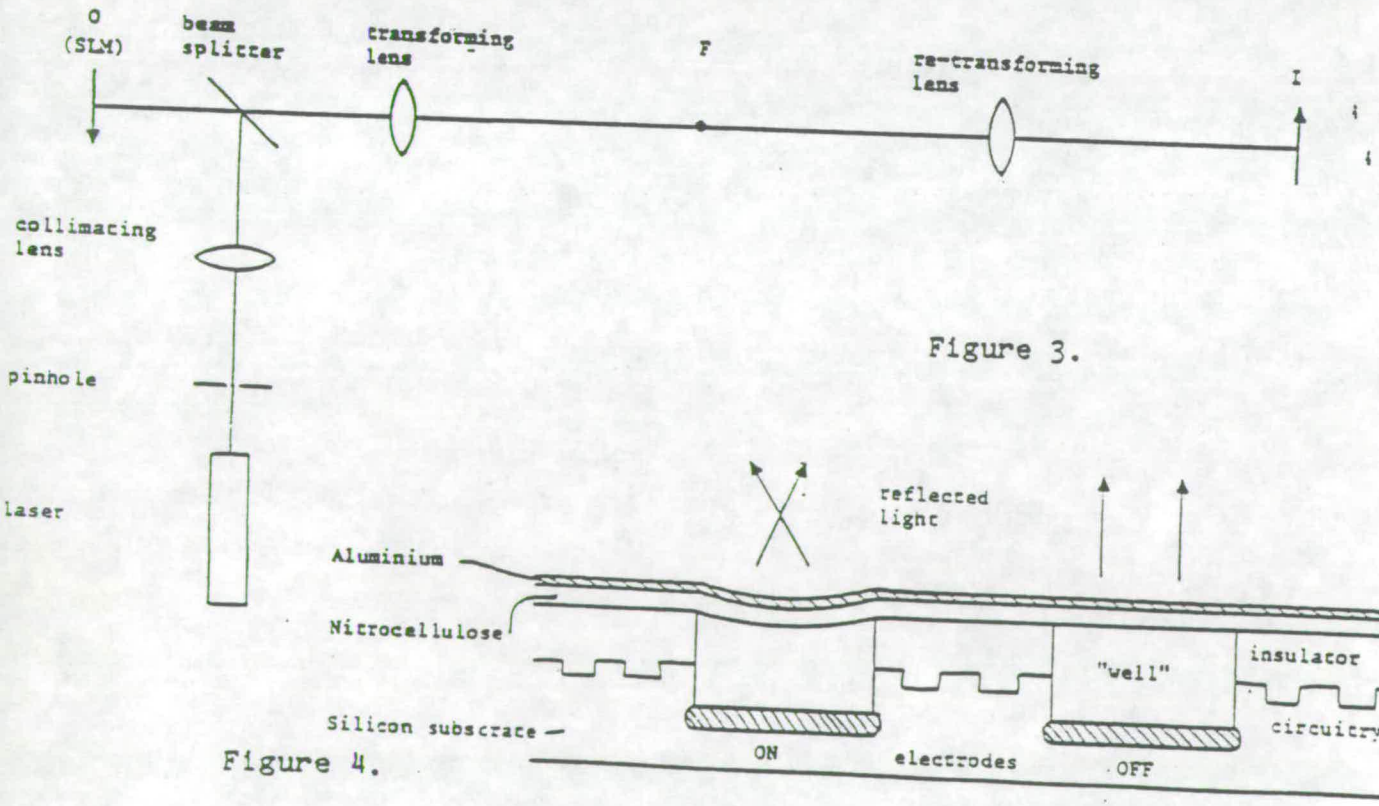

Figure 3.

Figure 4.

In order to render visible the phase variations imposed on a coherent light beam by the deformable-mirror SLM under test, the SLM is mounted in the input plane O of the Schlieren type optical processing system shown in figure 4. A plane, parallel beam of monochromatic coherent light is

incident on the SLM, and the Fourier transform of the light reflected from its surface formed in the Fourier plane F by the transforming lens. A filtered image of the light is formed in the output plane I by the re-transforming lens. For a perfectly flat mirror most of the light in the Fourier plane is confined to a spot on the axis, where a stop is placed. Any deformation of the mirror causes the light to by-pass the stop and to form in the output plane a visible "image" of the deformed region of the mirror.

The basic principles of operation have been checked using the 16 x 16 pixel array as the backplane. Further work is in progress to improve the metalisation of the membrane, and the tensioning of the membrane over the surface of the integrated circuit.

Conclusion

VLSI circuits, carrying pixellated mirror structures with on-board static memory to support independent addressing of each pixel, are providing versatile backplanes for SLM development. nMOS arrays are capable of operating at frequencies above 1 MHz, and with currently used processing technology statically-addressed pixels with minimum dimensions of ~ 75 x 75 μm^2 are attainable. As the microelectronics industry develops robust sub-micron fabrication processes, smaller pixel structures will become available. We are also considering the fabrication of binary phase only modulators by controlling the refractive index variations in parallel nematic structures above the silicon backplane.

Acknowledgements

The support received from SERC for this project and for research studentships is gratefully acknowledged, as is the supplementary support from the Dewar Fund, Edinburgh University. We wish to thank Mr. A. Kurzfeld, RAL, and Professor J.M. Robertson, EMF, and the staff of both institutions for their generous assistance. We are also grateful to Professor C.J. Dainty for granting us access to the LINNICK interferometer at Imperial College. The work on the 128 x 128 liquid-crystal-over-silicon SLM is being carried out in association with STL Ltd., Harlow. Finally we record our appreciation of the encouragement, helpful advice and technical assistance from our colleagues in the Physics Department.

References

1. UNDERWOOD, I., VASS, D.G. and SILLITTO, R.M.: "Evaluation of an nMOS VLSI array for an adaptive liquid-crystal spatial light modulator", IEE Proc. J.: Opto-electronics, Vol. 133, pp 77-82, 1983.

2. UNDERWOOD, I., WILLSON, P.H., SILLITTO, R.M. and VASS, D.G.: "An adaptive Fourier optical processor", Proc. SPIE, Vol. 860, paper 01, 1987.

3. GRINBERG, J., JACOBSEN, A., BLEHA, W., MILLER, L., FRAAS, L., BOSWELL, D., MYER, G.: "A new real-time Non-coherent-to-coherent light image converter. The hybrid field effect liquid crystal light valve", Hughes Reserach Labs., Opt. Eng., Vol. 14, pp 217-225, 1975.

4. PAPE, D.R. AND HORNBECK, L.J.: "Characteristics of the deformable mirror device for optical information processing", Opt. Eng., Vol. 22, pp 675-681, 1983.

Phase or amplitude modulation by birefringence in a liquid-crystal spatial light modulator.

M.J. Ranshaw, D.G. Vass and R.M. Sillitto,
Department of Physics, University of Edinburgh,
Mayfield Road, Edinburgh. EH9 3JZ. U.K.

Introduction

We describe an electronically-addressed liquid-crystal SLM. The device consists of a parallel nematic LC above a VLSI backplane and uses the field-induced birefringence effect[1]). By suitable polariser / analyser combinations, the device can be configured as either an amplitude or phase modulator.

The SLM structure

The prototype array[2]) used to drive the device has 16 x 16 pixels spaced 200μm apart on a square array. Each pixel has a static memory element which determines the electronic state of a 100 x 100 μm^2 electrode / mirror. The 12μm liquid crystal layer (BDH E7) is contained between the drive chip and a counter-electrode of indium tin oxide coated glass. The LC is secured in the homogeneous configuration by obliquely evaporated magnesium fluoride layers on the chip and counter-electrode surfaces. Each pixel thus acts as a variably birefringent plate whose extraordinary refractive index depends on the applied peak to peak voltage.

A consequence of using nMOS circuitry is that the logic "1" value of the electrode voltage (~ V_{DD}) is restricted to be above about 3.5 V. This requires using an off-set wave train on the counter-electrode to obtain the required a.c. voltages across the LC. The electronic circuitry, truth table and voltage drive signals are illustrated in fig.1.

Amplitude modulation

The SLM can be operated as an amplitude modulator by placing it between crossed polaroids at 45° to the optic axis of the LC layer. In this case a phase difference δ is introduced between the e- and o-components reflected from each pixel having a LC layer thickness d such that

$$\delta = \frac{4\pi\, d}{\lambda} \left(n_e(V) - n_o\right).$$

The transmitted intensity is given by $I = I_o \cos^2\left(\frac{\delta}{2}\right)$.

The pixel acts as a binary amplitude filter by arranging that $\delta = 2m\pi$ for a logic value 0 and $\delta = (2m+1)\pi$ for a logic value 1; m is a small integer. Preferably m = 0 to reduce the effect of cell thickness non-uniformities.

Figure 2(a) shows a SLM imaged in coherent light and programmed with a high pass filter pattern. We will present results of simple binary amplitude filtering operations by the device.

Phase modulation

The SLM can also be operated as a pure phase-modulator by arranging

that the incident light is polarised parallel to the extraordinary refractive index of the LC. Any change induced in this refractive index manifests itself as a phase change of the transmitted light.

Figure 2(b)shows the SLM programmed with phase differences of π radians between alternate columns of the array. Figure 2(c) shows the optical Fourier Transform of this phase grating, with the expected spatial frequency component associated with the columns twice that associated with the rows.

Binary phase correlator [3]

The device has been used successfully as a phase only filter in the Fourier plane of a coherent optical correlator. We will present results of this application.

References

1. Wu S-T, Efron U., Hess L.D., Applied Optics 23, 3911-3915, 1984.
2. Underwood I., Vass D.G., Sillitto R.M., IEE Proc. J. Optoelectronics 133, 77-82, 1986.
3. Horner J.L., Bartelt H.O., Applied Optics 24, 2889-2893, 1985.

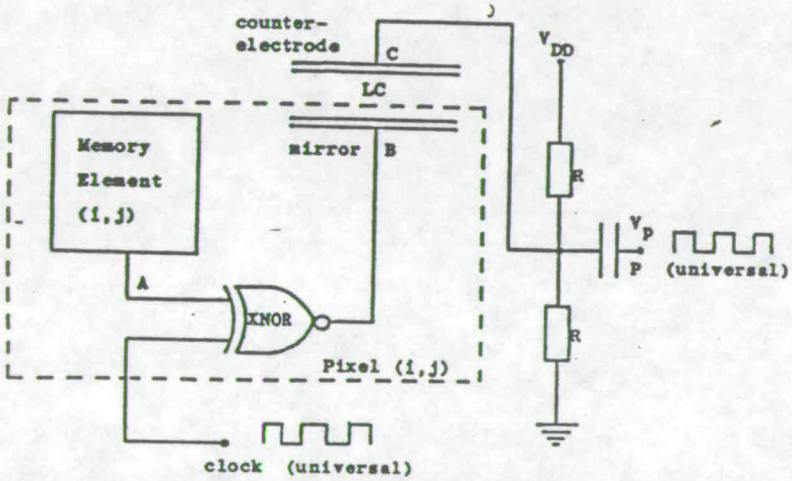

Fig. 1

	LOGIC TRUTH TABLE			NODE VOLTAGES			L.C. VOLTAGE
	A	clock	B	B	P	C	
'OFF'	0	0	1	V_{DD}	0	$\frac{1}{2}(V_{DD}-V_p)$	$\pm \frac{1}{2}(V_{DD}+V_p)$
	0	1	0	0	V_p	$\frac{1}{2}(V_{DD}+V_p)$	
'ON'	1	0	0	0	0	$\frac{1}{2}(V_{DD}-V_p)$	$\pm \frac{1}{2}(V_{DD}-V_p)$
	1	1	1	V_{DD}	V_p	$\frac{1}{2}(V_{DD}+V_p)$	

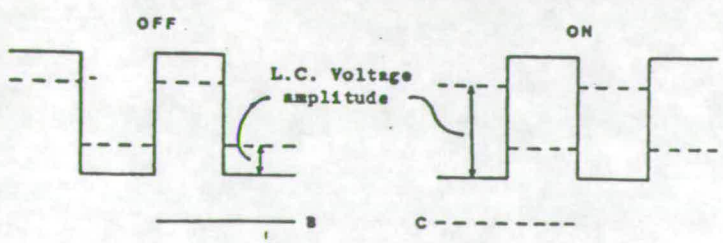

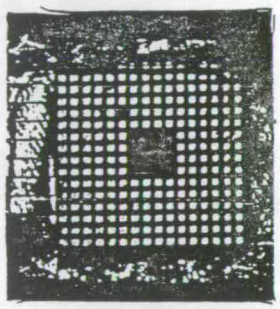

Fig.2a

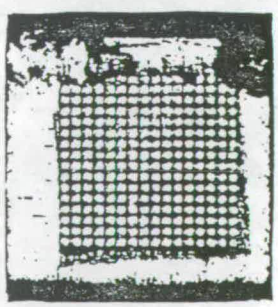

Fig.2b

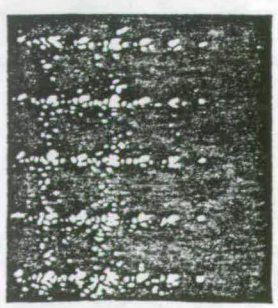

Fig.2c